Covalent Attachment of Fibronectin to 316L Stainless Steel Using Amine and Carboxylic Acid Alkanethiol Self-Assembled Monolayers: Applications for Coronary Artery Stents

---

Jeffrey A. Harvey

Department of Chemical Engineering
McGill University, Montreal, Canada
August 2009

A thesis submitted in partial fulfillment of the requirements of the degree of Masters in Engineering

Abstract

Background: Metallic stent implantation is currently the minimally invasive procedure of choice for the treatment of blocked coronary arteries. However, stent implantation can cause vascular trauma and denude a monolayer of cells from the vascular wall called the endothelium. This event initiates an exaggerated response to injury whereby smooth muscle cells (SMC) proliferate inward causing re-closure of the artery in a process known as in-stent restenosis.

Hypothesis: It has been shown that rapid re-endothelization of the artery after stent induced trauma decreases the severity of SMC proliferation considerably. By covalently tethering a cell adhesion protein, fibronectin (FN), to a stent via linking self-assembled monolayers (SAMs) it is believed that FN will increase the rate of endothelial cell attachment to the stent. This may result in the formation of a functional and confluent endothelial layer around the stent, thereby suppressing restenosis.

Results: A novel electrochemical method for monolayer self-assembly was developed in this work. Alkanethiol SAMs of carbon length 10 with NH_2, COOH, and CH_3 surface exposed functionality were attached to 316L stainless steel, which is the major stent material. The SAMs were reasonably ordered, demonstrated desired surface chemistry and were stable after rigorous rinsing and sonication tests validating their robustness for use in biomedical applications. FN was covalently attached to SAMs in two ways (1) to NH_2-terminated SAMs via glutaraldehyde and (2) to COOH-terminated SAMs through n-hydroxysuccinimide (NHS) and 1-ethyl-3-{3dimethyl aminopropyl] carbodiimide (EDC). FN demonstrated stronger attachment to the surface than non-covalently bound FN which was easily removed under sonication in 0.1 M NaOH. The FN coated surfaces demonstrated augmented endothelial cell attachment compared to bare 316LSS surfaces *in vitro*.

The surface-immobilized FN and SAMs properties were examined using polarization modulation infrared reflection absorption spectroscopy (PM-IRRAS) contact angle goniometry and cyclic voltammetry. This novel electrochemical method of SAM immobilization and protein attachment may also be expanded to other types of drugs/proteins and a variety of biomedical applications.

Résumé

Historique: L'utilisation des stents métalliques est présentement la procédure la plus préconisée afin de contrer les symptômes des maladies coronariennes. Cependant, cette technique peut causer des traumas vasculaires en retirant de l'artère une couche monocellulaire nommée endothélium. Cet événement cause une prolifération des cellules des muscles mous. Un processus nommé stent resténose est alors enclenché où l'artère se met à se refermer en réponse à au trauma.

Hypothèse : Il a été démontré que la re-endothélisation rapide de l'artère peut diminuer la resténose de façon significative. Afin de réaliser ce processus, nous proposons de créer un lien covalent entre la fibronectine et le stent en acier inoxydable. Les couches unitaires auto-assemblées sont utilisées en tant que lien chimique dans le but d'attacher la FN à l'acier inoxydable. La FN a pour rôle d'augmenter le nombre de liens créés entre les cellules endothéliales retrouvées sur le stent et d'atténuer la resténose.

Résultats : Une nouvelle méthode électrochimique a été mise au point durant cette recherche afin d'assembler les couches unitaires sur l'acier inoxydable. Les couches unitaires –thiol avec une chaîne de 10 carbones, du NH_2, COOH et CH_3 ont été créées. Les couches unitaires étaient bien ordonnées et ont démontrées une organisation chimique désirée. Ces films ont démontré une bonne stabilité même après avoir été exposés à la sonication validant ainsi leur durabilité pour des fins d'utilisation dans le domaine biomédicale. Un lien covalent a alors été créé de deux façons entre la fibronectine et les couches unitaires auto-assemblées : (1) les couches unitaires NH_2 ont été liées grâce au glutaraldéhyde (2) les couches unitaires COOH ont été liées en utilisant le N-hydroxysuccinimide (NHS) et le 1-ethyl-3-(3dimethyl aminopropyl) carbodiimide (EDC). Les méthodes décrites ci-haut ont permis à la fibronectine de se lier plus solidement à la surface de l'acier inoxydable comparativement à la fibronectine absorbée dont les liens ont été facilement brisés par 0.1 M de NaOH. La fibronectine liée de façon covalente a

démontré un plus grand taux d'attachement de cellules endothéliales en comparaison avec une surface régulière d'acier inoxydable in vitro. Ces films furent examinés à l'aide de la méthode de PM-IRRAS, de goniométrie d'angle de contact et de la voltamétrie cyclique. Cette méthode pourrait aussi être utilisée afin de lier d'autre types de protéines, des anticorps et certains médicaments.

Acknowledgements

I would like to thank my supervisor, Dr. Sasha Omanovic, for entrusting me with this excellent project. He has provided me with the freedom to explore, while always being available for consultation. He is an excellent researcher and friend.

My sincerest thanks goes to everyone in our the electrochemistry lab; Nadia Afara, Irshad Ali, Khawtar Ahmed, Cecillia Lee, Ziad Bou-Saleh, Hesam Dadafarin, Saad Ghareba, Arash Sharhyari, and Marie-Elise Viger, for their excellent discussion and companionship during my stay here.

As well, I am very appreciative of the technical staff for keeping the work place safe, providing technical training and machining my samples. Thanks go to Frank Caporuscio, Lou Cusmich, Gerald Lepkyi, and Ranjan Roy.

Thanks to summer students Marine Bolarin and Julie Guy from France. They were very dedicated. Their research was very helpful with my project.

Biochemist Andreas work was integral for completing *in vitro* cell tests. His expertise was much appreciated.

I would like to thank my grandparents George and Helen Streb, and Chick and Rosa Harvey for helping support my education. Thanks to my parents Dan and Joan who were always supportive and caring. I would not have been able to do half the things I have done without them. Also I should mention my sister and brother, Sarah Jane and Chris who I always look up to.

Also thanks to my girlfriend Julie St-Jean for the wonderful times we have had together during our stay in Montreal. Her understanding was incredible. If it was not for her, I'd probably have thrown my thesis and then myself into the St. Lawrence River.

Table of Contents

List of Figures

List of Tables

CHAPTER 1: INTRODUCTION

Cardiovascular diseases (CVDs) are well established as major causes of illness, disability and death in Canada. In fact, heart attack and stroke take more lives annually then all cancers combined [1]. In 2004, an estimated 80.7 million Americans were diagnosed as having CVD and that same year 1.0 out of every 2.8 deaths were a result of it (866 000 deaths) [2, 3]. The upcoming years are of particular concern in Canada because the population age distribution is changing. Currently 13% of all Canadians are over the age of 65, but Statistics Canada projects that by 2031 that number will increase to a whopping 25% [4]!

Since *age* is one of the most prominent factors on a long list of cardiovascular disease risk factors including; smoking, diabetes, obesity, genetics, inactivity and high blood pressure; the demands placed on medical professionals in hospitals performing interventional cardiovascular surgeries looks only to increase [5, 6]. This means two things, firstly, cardiovascular devices will continue to be in demand for years to come, and secondly to make sure everyone can receive adequate care, initial treatments need to work and they need to last.

Presently, this is not the case. Angioplasty followed by metallic stenting is the minimally invasive procedure of choice for treating atherosclerotic legions in the coronary arteries due to its relatively high success rates, reasonable cost, and length of hospitalization [7]. A stent is a rigid structure that acts as a physical barrier to vascular recoil and increases blood flow through the coronary arteries. Stenting decreases both mortality and morbidity in patients suffering from vascular diseases, but there are deficiencies of this biomaterial *in vivo*.

- Principally, stent implantation causes trauma to the blood exposed vascular wall, thereby denuding the monolayer known as the endothelium. This event can initiate an over exaggerated response to injury where once quiescent smooth muscle cells (SMC) proliferate inward decreasing the vascular

diameter causing in-stent restenosis (>50% diameter reduction). This will require re-intervention.

In brief, this thesis is an investigation into a solution to this critical problem. It is proposed; that by irreversibly binding fibronectin (FN), a protein involved with cell attachment and growth, to a stainless steel stent, in-stent restenosis can be minimized. This is because the FN will improve the stent`s biocompatibility and increase the rate of stent endothelization. Rapid re-endothelialization of the stent and surrounding vasculature has been shown to have an anti-proliferate effects on SMCs [8]. And without SMC growth, in-stent restenosis does not occur.

To irreversibly attach FN to a steel surface so that it is not removed by blood sheer stress, a chemical link must be made between FN and the surface. Functionalized alkanethiol self-assembled monolayers (SAMs) are organic films suitable for this task. SAMs can bind to certain metal surfaces and provide a metal surface with defined surface physicochemistry. In the current project the functionalized SAMs (i.e. SAMs' terminal group) will be an amine or carboxylic acid to link to fibronectin through known peptide chemistry. Although alkanetiol SAMs can easily be formed on some model metal surfaces (gold, copper, silver), their formation on commercial surfaces, such as 316L stainless steel, represents a very challenging task. Thus, this task was also one of the major objectives of the current project.

CHAPTER 2: BACKGROUND AND LITERATURE REVIEW

Background and Literature Review Scope

The principle purpose of this chapter is to familiarize the reader with 3 topics pertinent to this research. Therefore it is organized into 3 sections: (1) self-assembled monolayers and stainless steel (2) cardiovascular diseases and devices (3) fibronectins, integrins and extracellular matrices.

2.1 Self-Assembled Monolayers

2.1.1 Introduction

Self-assembly refers to the spontaneous ordering of matter at the molecular scale. Today, self assembled monolayers, SAMs, are synonyms with alkanethiols ($X\text{-}[CH_2]_n\text{-}SH$, where X=COOH, CH_3, NH_2, OH, etc...) chemisorbing onto gold by a strong sulfur-gold bond. Many other *head groups*, not just sulfur, have been used to chemically bind molecules to metallic surfaces including; phosphonic acids ($-PO_3$) [9-13], carboxylic acids (-COOH) [14-17], amines ($-NH_2$) [18, 19], and siloxanes ($Si(OEth)_3$) [19-21] among others. The possibility of attaching these groups however, is heavily dependant on the substrate chemistry and the deposition environment including; pH, temperature, time and solvent [20]. Electrochemical or chemical pre-treatments may be required to activate the surfaces before molecular assembly [19].

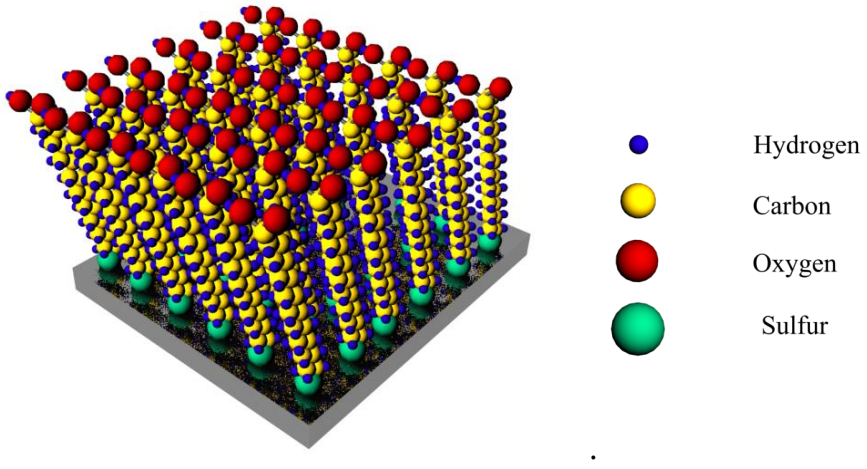

Figure 2.1 A 3D model of a $HS\text{-}C_{18}H_{36}$-COOH highly ordered self-assembled monolayer on a metal substrate.

Some examples of common metallic surfaces that have been studied for the deposition of SAMs are, nickel [20-22], copper [25-27], aluminum [12, 23], titanium [24-26], iron [27, 28], platinum [29], silver [35-37] and gold [30-32]. The simplest way to bind SAMs to a substrate is by immersion of the substrate in millimolar (mM) quantities of the SAM molecule dissolved in a neutral solvent for a certain time until the desired film self-assembles. The ease of this process makes self-assembly very promising for manufacturing and mass production. However, other methods such as vapour deposition [33], aerosol spraying [25, 34], or electrochemical potentiodynamic cycling are advantageous for surfaces when thermodynamic affinity for self-assembly is not favourable: which is the case for stainless steel [15, 17, 21]. SAM modified surfaces have many invaluable uses including; sensors and microelectronics [32, 35-37], controlling cell-surface interactions [24, 38, 39]. reducing friction of surfaces [13, 23, 40], improving corrosion resistance of surfaces [31, 41, 42], and understanding fundamental nanoscale science [43, 44].

2.1.2 Natural Self-Assembled Monolayers: Phases of Assembly

Monolayers of alkanethiols assemble in a stepwise process. Scanning Transmission Microscopy (STM) images can be used to probe the structure of monolayers during these transitions if the surface is flat at the nanoscale [33]. Several authors have demonstrated that before high density structures are formed, a ‘disordered and striped phase’ where the alkanethiols lye horizontally on the surface develops [45, 46]. STM topographical stills of two interesting phases of self assembly are shown in **Figure 2.2**.

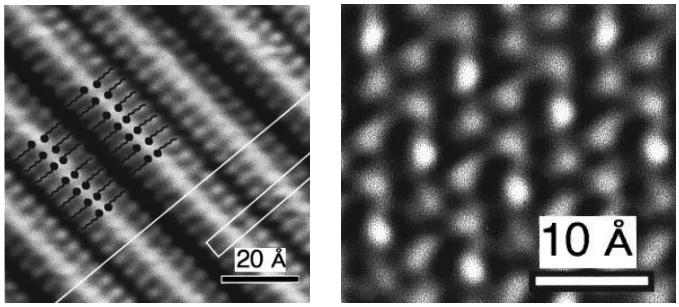

Figure 2.2 Scanning Transmission Microscopy STM image of hexanethiols, C6, on Au(111): (left) preliminary ‘striped phase’ (right) ‘highly aligned vertical phase’. *Adapted from* [47]

The SAM formation process can be explained in the following way (also see Figure **2.3**). **(1)** SAM formation begins with the '*Liquid phase'* where alkanethiols physisorb to the surface. Van der Waals forces between the molecules and the surface cause the molecules to lie parallel to the surface. **(2)** This is preceded by the '*Striped phase'* where chemisorption of the head group, in this case sulfur, to the substrate occurs. Intra-molecular and hydrophobic nature of the molecules force the SAMs to align to minimize energy, with the hydrophobic $-CH_2$ tails touching head to head and the end group, such as e.g. $-CH_3$ (or –COOH, NH_2, -OH, etc), being driven away, much like the phospholipid by-layer of a cell membrane. **(3)** As the number of chemisorbed molecules increases, the SAM begins to pack, but remains somewhat parallel to the surface, known as the '*Advanced Striped phase*'. **(4)** In time, some striped phase remains and some standing up phases begin to appear due to the high density of molecules, forming the '*Disordered phase*'. **(5)** With longer immersion, the '*Standing up phase*' appears and the chain packing density increases. **(6)** Ultimately slight restructuring of the film occurs and the SAM reaches its final well ordered and aligned structure [33, 46].

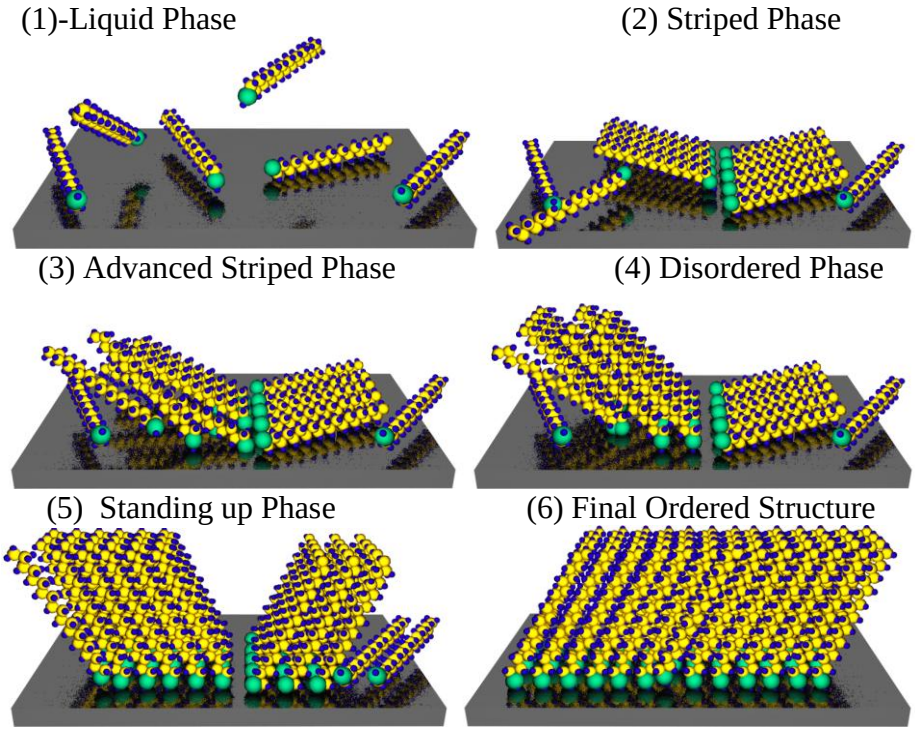

Figure 2.3 Alkanethiol self-assembled monolayers phases of assembly

2.1.3 Self-Assembled Monolayers and Stainless Steel

The formation of SAMs on stainless steel (SS) e.g. the 316L type, is not as trivial is the case on model metal surfaces (Au, Cu, Ag, etc.). The surface of steel is complex and heterogeneous containing predominantly Cr, Fe, Ni, and Mn oxides in multiple oxidation states. The strong affinity for 316L SS to form oxides (passive film) makes it resistant to corrosion. Unfortunately strongly bound oxides make standard thiol assembly through sulfur metallic bonding difficult. Only the head group siloxanes $Si(OEth)_3$ and phosphonates (PO_3) [11] can be used on oxide film surfaces without significant prior modification or driving force. In contrast, carboxylic acid, COOH, and thiols, SH, require pretreatments or electrochemical force to actively drive SAMs onto the steel surface. A summary of the best methods to overcome these difficulties are shown in **Table 2.1**. The table describes which head groups are attached to the steel as well as the groups that are not chemically bound and used to functionalize the surface.

Table 2.1 Pertinent literature of self-assembled monolayers on stainless steel

Author	Type of SS	Method	Head Groups	Functional Groups	Purpose
Shustak et al. [15-17]	316L SS	Electrochemical	COOH	CH_3, NH_2	Protective films fundamental nanoparticles
Gawalt et al. [9, 14, 48]	316L SS	Aerosol spray & solution deposition	COOH, PO_3	COOH, CH_3, OH, NH_2	Fundamental stents/cells
Van Alsten [11]	304	Solution deposition	PO_3	CF, PO_3, CH_3	Protective films
Ruan et al. [19]	316L SS	Electrochemical & solution deposition	SH, NH_2	OH, CH_3	Fundamental
Mahaptro et al. [38, 49, 50]	316L SS	Plasma & solution deposition	SH	COOH, OH, CH_3	Drug immobilization / stents
Zhang et al. [51]	mild steel	Electrochemical	SH	CH_3	Fundamental
Sinapi et al. [52]	316L SS	Solution deposition	$Si(OEth)_3$	CF	Fundamental
Müller [53]	316L SS	Solution deposition	$Si(OEth)_3$	NH_2	Protein immobilization
Minier [54]	316L SS	Solution deposition	$Si(OEth)_3$	NH_2	Protein immobilization
Volmer [27]	Iron	Electrochemical	SH	CH_3	Fundamental

2.1.4 Major Research Groups for SAMs on Stainless Steel

Monolayer films can be made by first reducing a metal working electrode at cathodic potentials, in order to remove the oxide film. Then with the surface activated, by immersing of the metal substrate in a solution of alkanethiols for a certain time. One pertinent example is on iron [9, 32, 33]. As mentioned in **Table 2.1**. Ruan et al. [19] have developed a method that can attach OH and CH_3 terminated thiols to 316L SS in a similar manner to those investigations on iron. The method involves pre-treating 316L SS samples in an electrochemical cell of 1.0 M $HClO_4$ for 20 minutes at -1.2 V_{SCE} to remove the oxide film. After, in an inert environment, the samples are dried and rinsed, and placed in an alkanethiol solution for 3 hours. Some of the drawbacks of this method are the use of corrosive acid which under potential, if uncontrolled, causes the steel to corrode considerably. As well, during the polarization, the acid may be reduced to release undesired chlorine gases.

Some other interesting research in this field has been done by Raman and Gawalt et al. [9, 14, 55]. The team pre-cooled 316L SS samples in an ice bath, then immersed them in a warm tetrahydrofuran solution of mM quantities of various carboxylic acids with COOH, OH, NH_2 or CH_3 terminals at 50^oC for 2 hrs. They found these films to be highly ordered and stable to sonication only after overnight annealing at 120^0C. DRIFT spectroscopy, AFM and contact angle goniometry were used to characterize these films. DRIFT showed that, in fact, the carboxylic acid had bonded to the surface through a stable bidendate COO^- formation. The contact angle measurements showed CH_3 terminated SAMs were very hydrophobic and the charged hydrophilic ends, COOH and NH_2, were consistent with literature. Interesting to note, this method of assembly has been patented with applications for affecting cell attachment on stents [14, 48]. Interestingly, our laboratory has made numerous attempts to replicate these experiments by following the suggested procedure, but we found that the formed SAMs were highly unstable, disordered and yielded poor surface coverage.

Another team with significant work in this field has been Mahaptro et al. [35, 47, 48]. They developed alkanethiols SAMs of CH_3, OH and COOH terminal groups by first treating the 316L SS samples to an oxygen plasma, and then, while still under vacuum immersing the samples in thiol solutions for up to 48 hrs. They were successfully able to attach ibuprofen and pephenazine drugs to OH and COOH terminated SAMs using lipase esterification catalysts as confirmed by FTIR investigations. XPS oxidative and in vitro stability tests showed that the SAMs were oxidized from thiolates to sulfonates within 14 days in phosphate buffer saline exposure, after which the alkanethiols in the form of sulfonates desorbed and simultaneously left the substrate. Therefore drug delivery is limited to short time duration using this method. This team is on the leading edge of attaching drugs to 316L SS stents via self-assembled monolayers. However the use of plasma makes it difficult and for just any lab to use their method and the assembly is time consuming and may possess some scale-up challenges.

A fourth important research group in this field is led by Shustak and Mandler et al. from Jeruselum. This group uses unique electrochemical potendiodynamic polarization techniques to establish a driving force for carboxylic acids (COOH) attachment to 316L SS [15, 16]. They developed CH_3 and NH_2 terminated SAMs using this method. They also demonstrated the possibility of using NH_2 terminated SAMs to electrochemically attach Au and polylactic acid (PLA) nanoparticles to this surface. By using redox probe, hexaaminеruthenium(III) trichloride, $Ru(NH3)_6Cl_3$, and cyclic voltammetry they demonstrated a significant electron transfer blocking effect of palmitic acid films. This group has recently patented their method for stent applications [56].

2.2 Cardiovascular Diseases and Devices

2.2.1 Coronary Artery Physiology

The coronary arteries are primarily composed of endothelial cells (ECs), vascular smooth muscle cells (SMCs), and fibroblasts embedded in a well constructed extracellular protein matrix **Figure 2.4**.

The artery can be separated into concentric layers, the intima, the media and the adventitia [57]. In healthy arteries ECs comprise the intima and are found as a single layer of cells indirect contact with the blood. ECs are particularly important; as they are well known to control the progression of atherosclerosis [58], thrombosis [59], inflammation [60], general homeostasis [61], SMC proliferation [62], and vascular dilation.

The underlying media contains many layers of SMCs. SMCs are the muscle cells that provide vascular tone assisting blood transport. SMC proliferation has a direct role in the processes of hypertension and artery occlusion [63]. The outer most layer in the artery, the adventitia, is mainly composed of elastin and collegans and provides structural support and nutrition to the blood vessel [57].

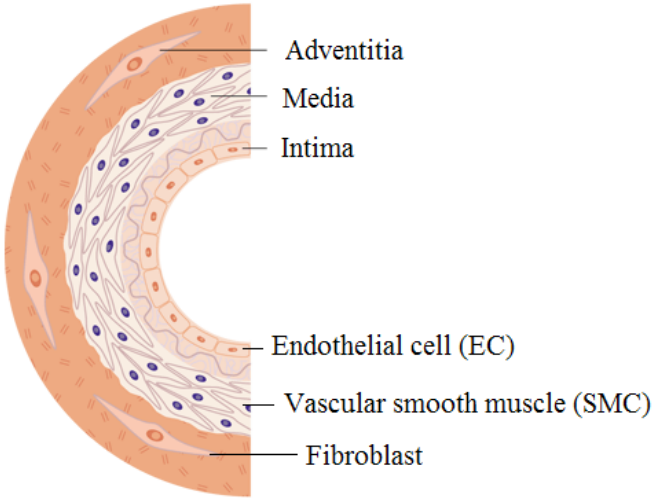

Figure 2.4 Composition of the coronary artery. *Adapted from* [64]

2.2.2 Atherosclerosis

Atherosclerosis is an inflammatory disease affecting the vascular system [6]. The word comes from root words ‘athero’ meaning artery and ‘sclerosis’ meaning ‘paste or gruel.’ It is a local phenomenon where oxidized lipids, cholesterol, and calcified material accumulate within the vascular wall. A number of inflammatory cells penetrate deep within this accumulated mass. The majority are macrophages, and to a lesser extent T-cells and foam cells. These cells are particularly active and trigger inflammation. Covering and protecting this core from the blood stream is a fibrous cap containing smooth muscle cells (SMCs), extra-cellular matrix (ECM) proteins and endothelial cells (ECs) [65].

If the fibrous cap is thick, then this legion is deemed stable, which is true for the majority of plaques. However, a small portion of atherosclerotic legions have weakening caps, and are extremely vulnerable to rupture. Upon rupture the lipid core bursts into the blood stream. This activates platelets, initiating a blood clotting cascade causing the formation of fibrin clot (thrombosis) [66]. This event can lead to heart failure and death. **Figure 2.5** shows the process of atherosclerosis leading to plaque rupture, and possibly to occlusion.

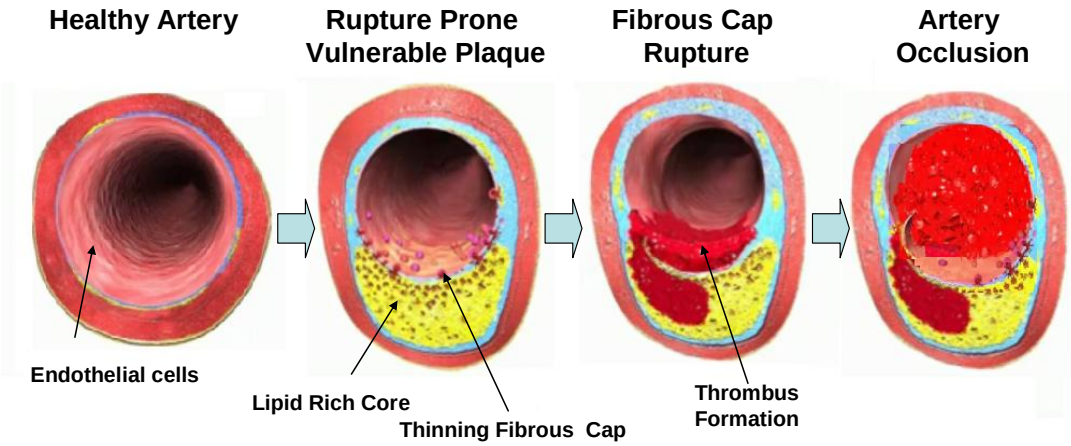

Figure 2.5 Process of plaque rupture in atherosclerotic legion: First, lipid rich plaque builds up in the coronary arteries. As the fibrous cap, the barrier between plaque and blood stream thins, it becomes very sensitive to rupture. When it breaks, the inflamed and lipid rich core is exposed to the blood, where platelets activate forming thrombosis (blot clots). Large thrombus can block blood flow to vital organs, resulting in a stroke or heart attack. *Adapted from* [67]

2.2.2 Stents in Practice

Coronary stents are thin metallic devices usually measuring around 3 mm in diameter and 20-40 mm in length. **Figure 2.6** shows the placement of a metallic stent in the coronary arteries. The procedure is minimially invasive and only requires the use of mild sedatives [68]. A guidewire is first inserted through the skin and into a larger artery, usually in the leg (femoral artery) [68]. The guide wire is transported through the aorta to the coronary arteries and the site of blockage. A flexible catheter containing a collapsed stent and balloon is then placed along the guide wire to the region of interest, **Figure 2.6**. The balloon is filled with saline solution causing pressure buildup for expansion. Depending on the mechanical properties of the stent, the pressure can be in the order of 10 atmospheres or greater and held for (30 seconds to 3 minutes). This causes elastic deformation of the stent which sufficiently expands the artery into place. The balloon is then deflated and retracted, leaving the stent permanently at the site alleviating the blockage and increasing blood flow through the artery [69].

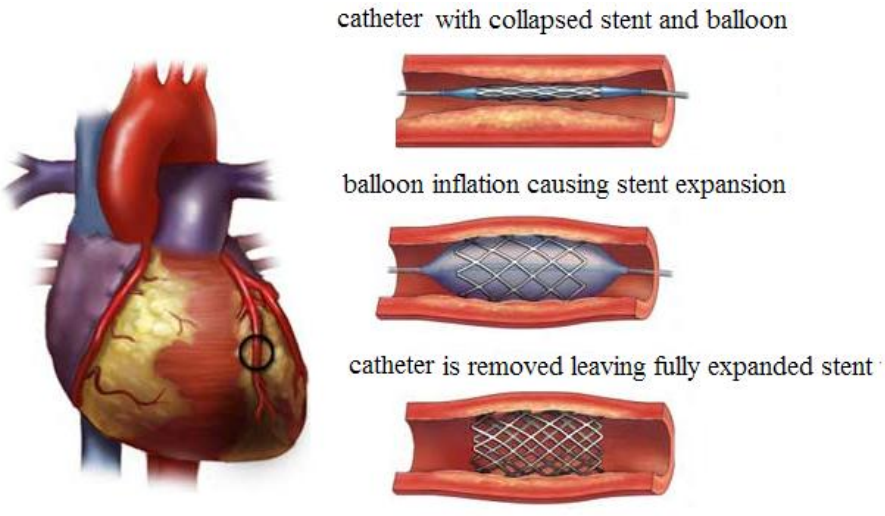

Figure 2.6 Coronary artery stenting procedure. *Adapted from* [69, 70]

To visually demonstrate the benefits of a stent, an angiogram of the coronary arteries of a relative of the thesis author (he received two stents) is shown in **Figure 2.7**. The black arrows point to concerned areas. There is a remarkable increase in blood flow through the coronary arteries after implantation indicated by the dark regions. The patient's physical ability to do exercise and quality of life was significantly improved after receiving the two stents.

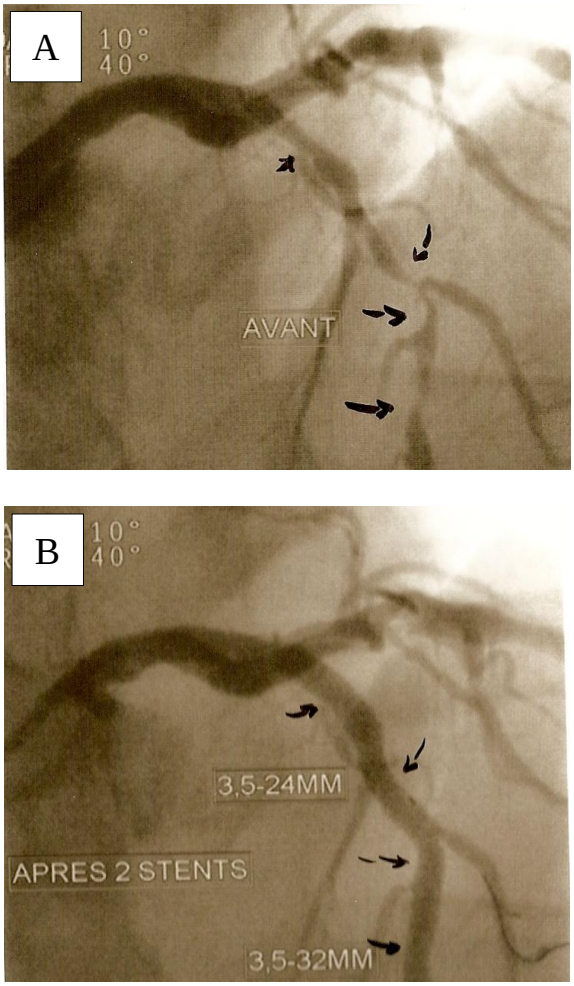

Figure 2.7 Angiogram of a male patient who received 2 bare metal stents in the coronary arteries. The stents both measured 3.5 mm in diameter after expansion. **(A)** before **(B)** after intervention. The black arrows indicate significantly occluded arteries with resistance to blood flow. Dark areas indicate blood.

2.2.3 In-Stent Restenosis Caused by Intimal Hyperplasia

As mentioned previously, restenosis is a significant limitation to current minimally invasive therapy and is defined as a greater than 50% reduction in artery diameter after treatment [71]. It is an aggressive wound healing response of an artery to vascular injury and inflammation [72, 73]. This damage is common after angioplasty, endorectomy, stenting or suturing procedures, which can strip, injure or squash the blood contacting endothelial layer [74]. In clinical practice the balloon pressure used to deploy stents range from 12 to 18 atm. This is high enough to cause significant endothelial trauma [75]. Karas et al. have established a significant correlation between degree of vascular injury and inflammation caused by stent implantation to neointimal thickness [76]. Similarly, Campbell et al. determined that there is a critical legion size for which SMCs will change into proliferate phenotype [77]. Also, it is now well established that inflammation caused by the presence of a foreign object, such as a stent, is in fact a significant factor initiating intimal hyperplasia [78].

To minimize restenosis, it is critical that endothelial cells are present and functioning properly **Figure 2.4**. With the denuded or dysfunctional endothelium, blood proteins and platelets are more likely to aggregate causing inflammation. Not only do endothelial cells provide a non-permeable barrier to protect smooth muscle cells from circulating growth factors, they also release a variety of anti-inflammatory, anti-platelet and anti-proliferation active agents. One agent in particular, nitric oxide (NO) keeps smooth muscle cells in a quiescent and relaxed state [79]. Rapid re-endothelization after injury has shown to be an effective method to reduce restenosis and is the principle theory behind our stent surface design [8].

In terms of the past, historically restenosis was a problem in percutaneous transluminal coronary angioplasty (PTCA) developed in 1977 by Greutzig [80]. PTCA is a procedure similar to stenting, as described in **Section 2.2**, except only the balloon is expanded against the artery wall to increase vascular diameter. The

problem with this procedure is high occurrence of elastic recoiling and unfavourable remodeling of the artery. Similarly this treatment may cause physical trauma to the vascular wall. Restenosis rates of 40-60% after 6 months are not uncommon with PTCA [71, 81, 82].

To eliminate the restenosis and recoiling problems, bare metal stent (BMS) were invented, **Figure 2.6**. In trials comparing directly, restenosis from PTCA vs. BMS, it was determined that BMS had a significantly decreased rate of re-closure compared to just PTCA [83, 84]. Restenosis rates estimated from everyday practice in the US before 1999, appear to be between 10-50% depending on the severity of the legion, skill of the surgeon and health risk factors of the patient [75, 85]. So it is clear, stents show some benefits over PTCA. Still restenosis rates with BMS are much too high

Once again, to improve upon the limitations of current treatments, in this case BMS, drug eluting stents (DESs) were designed. These stents excrete anti-proliferative drugs, limiting cell growth around the stent. Of consequence, the occurrence of restenosis has unequivocally been reduced once again. This evidence was supported by results of a pooled meta-analysis from 38 trials (18,023 patients) with a follow-up to 4 years comparing both sirolimus-eluting and paclitaxel-eluting stents to bare-metal stents. The report was published in the Lancet [85, 86]. The findings support using Sirolimus eluting stents over BMS for the number of revascularization procedures required (p-value of <0.0021). However, there was no difference between DES and BMS in the rate of mortality. This demonstrates that although the use of DES requires less further surgical interventions, there is no difference between receiving a heart attack for patients with either stent type.

2.2.4 Stent Designs Overview

Endovascular stent coatings and materials have been developed in the last few decades to improve the limitations of bare metal stents. Both surface chemistry and physical design of the stent will play a role in its *in vivo* success. This review concentrates only on chemical designs. For an excellent review of the effects of physical stent design refer to Stoeckel et al. [87].

It would be an understatement to suggest surface modification strategies for stents so far have been unoriginal. In fact, researchers have been quite creative. Some have tried to minimize endothelial damage and thrombosis by developing biocompatible coatings, like chitosan, and collagen surfaces. Others suppress neo-intimal growth of SMCs by effecting local cell viability through drug elution and radioactive treatments. New pro-healing approaches, such as the use of antibodies/extracellular matrix proteins, viral vectors and gene therapies attempt to attract endothelial growth on the stent. Whichever design, this area is a current hotbed for active research and development.

Table 2.2 Principle stent designs, categories and examples

Stent Design	Sub-Category	Specific Examples
Biocompatible Coatings	General Treatments	SiC, Carbon, Ti-NOx
	Polymer Coatings	Collagen, Alginic Acid, Chitosan, Phosphorylcholine
Bare Metal Stents	Degradable	Iron, Magnesium
	MRI Active	Platinum-Iridium
	Self-Expanding	Nickel-Titanium
	General Metals	316L SS, Tantalum, Cobalt-Chromium
Drug Eluting and Radioactive	Radioactive	Yttrium 90, Iridium-192
	Drug Eluting	Siroliomus, Heparin, Estradiol Paclitaxel, Nitric Oxide
Pro-Healing Stents	In Vitro Seeding	Endothelial Cell Seeding
	Protein/Antibodies	CD43 Antibody, RGD
	Gene Therapy	Viral Vectors, Plasmids

2.2.5 Bare Metal Stents

The simplest types of stents are made of various metals and alloys. They should have proper mechanical properties, be inexpensive, and induce a reasonable host response. One material may be preferred over the other if it is MRI active, self-expanding or designed to degrade over time. The most common metals/alloys are; 316L stainless steel (316L SS) [88-90], Nitinol (NiTi) [88-90], cobalt-chromium (Co-Cr) [91, 92], tantalum (Ta) [93, 94], platinum-irdium (Pt-Ir) [95, 96] and magnesium alloys (Mg) [97] [98].

2.2.5.1 Stainelss Steel (316L SS): 316L SS is used predominantly over all other alloys simply due to mechanical properties, cost, and respectable corrosion resistance. The fact that 316L SS was the first stent material to be FDA approved and is the material of choice for 7 of 8 FDA approved stents in 2007 makes it the easiest choice for pushing a new coating design to market: less administrative and testing hurdles [99].

2.2.5.2 Nitinol (NiTi): Although pure Titanium has very good biocompatibility and is used extensively in orthopedic implants, it has poor tensile strength and is prone to failure during stent expansion [99]. Therefore Ti is alloyed with nickel (Nitinol). This unique combination has shape memory properties [100]. These stents are compressed while implanted and are designed to expand slightly overtime to match the vascular wall diameter. This eliminates the need for balloon expansion [101]. The shape memory properties of NiTi are shown below in **Figure 2.8**.

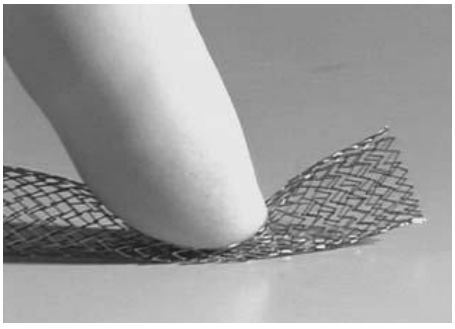

Figure 2.8 Extreme deformation of a (Cordis) SMART Nitinol stent. The form will return after the load is removed [102].

There is concern about nickel allergic reactions. However clinical testing on corrosion, biocompatibility and neo-intimal effects from NiTi show that this material is comparable if not better than 316L SS [103-106].

2.2.5.3 Magnesium: This type of stent is particularly interesting because Mg stents have the possibility of biodegradability. Mg coupons showed low inflammatory response in a rat model and have a suggested degradation half-life of 6 months [97]. A remarkable study by Zartner et al. [107] successfully implanted a Mg degradable stent into the left pulmonary artery of a baby. The degradation process was well tolerated leaving the artery patent. Interestingly, the stent had completely disappeared leaving only a calcium phosphate residual in its place [107]. These stents appear to be safe, as demonstrated in porcine models, and may play a larger role in years to come [108].

2.2.5.4 Gold: The concept of sputtering gold on a stent seems like a potential solution due to its high biocompatibility and extensive use in dental implants. Unfortunately, recent randomized clinical trials show no benefits of gold compared to BMS and some even suggest an increased tendency for stent restenosis [109]. In a large clinical experiment patients were randomly assigned gold (n=367) or uncoated stents (n=364). After one year follow-up event-free survival was significantly less favourable in gold-stent group (62.9% vs 73.9% p=0.001). Similarly vom Dahl et al. showed a gold coated stent had much greater neointimal growth (47±25 vs 41±23 mm^3 p=0.04) [110]. Although not extremely significant, there are no excessive benefits observed so far in gold-stents over stainless steel warranting long term use at the increased cost of gold [111]. However, in the future, gold's affinity for SAMs and the potential for drug/antibody attachment may validate their applicability.

2.2.6 Biocompatible Coatings

2.2.6.1 Ti-NO_x Coated Stents: Chemical vapour deposition by Windecker et al., [112, 113] of Ti-NO_x 500 nm thin films showed very promising results *in vivo* in a porcine model. They attributed a statistically significant decrease in fibrinogen

adsorption and smaller intimal hyperplasia growth compared to BMS. They attributed this to the lower electron conductivity of their ceramic like coating: this work was done in 2001 [112]. In 2005 they took their device to the next level and ran a controlled trial in 87 humans (n=45 Ti-NO_x n=42 BMS) [113]. They showed a 15% restenosis rate in Ti-NO_x vs 44% in BMS as well as a smaller neointimal volume 18±21 mm^3 vs [112]48±28 mm^3 (p=0.0001) and less cardiac events after 6 months (7% vs 27% in BMS group). The limitations of this study are that the long term results have not been published and they used a small subject group: But the results look promising. The coating was also not prone to cracking during stent expansion [113].

2.2.6.2 Carbon Coated Stents: The Carbostent (Sorin Biomedica, Italy) is a balloon expandable 316L SS coated with turbostratic carbon. In three clinical studies using the Carbostent no in-stent thrombosis was observed after 1 year. Nevertheless, in-stent restenosis was significant and observed between 18-25% after 6 months in all trials [121, 125-127]. In comparison, trials against sirolimus DES and BMS of 316L SS, no significant differences in adverse effect and restenosis categories was observed after 1, 6 and 12 months [114, 115]. Ion release from a 316L SS stent was significantly lowered by this diamond like carbon coating [116]. Carbon coating had lower immediate (first 24 hrs) inflammatory response compared to BMS as well [117].

2.2.6.3 Silicon Carbide Coated Stents: It is well established that the thrombus formation requires fibrinogen molecules to transform into fibrin, and this transformation is based on electronic processes of the fibrinogen molecule [118]. It has been shown that electron active surfaces can initiate and amplify this step eg. conduction through bare metals. Therefore semi-conductors such as amorphous silicon-carbide are coated on the stent to improve against thrombus formation even in high risk patients [119]. These films are often coated on Tantalum using plasma deposition [120]. A comparison of platelet adhesion to coated stents vs bare metal showed remarkable decreases in adhesion down to

58.6%, SiC, 32.8% carbon coated, and 7.7%, for heparin coated stents when compared to bare 316L SS [121].

2.2.7 Drug Eluting and Radiotherapy Stents

2.2.7.1 Drug Eluting Stents: were designed to combat the high number of revascularization procedures as a result of in-stent restenosis found in bare metal stents. Biomaterial engineers and pharmacologists have investigated the usefulness of *anti-proliferative* drug coatings on stents and this has been a remarkable example of multidisciplinary cooperation. On these stents, drugs are administered locally diffusing through a biodegradable polymer matrix, usually a few microns thick. The CYPHER sirolimus-eluting stent (Cordis Corp) and TAXUS paclitaxel-eluting stent (Boston Scientific Corp) were the first to be FDA approved for the US market in 2003 and 2004 respectively [75] [122]. They are still extensively used today. **Figure 2.9** shows a scanning electron microscope (SEM) image of a paclitaxel coated stent. The metallic stent is covered with paclitaxel in the poly DL lactid-co-glycolide polymer matrix. A freshly prepared surface is shown in **Figure 2.9** (left). Through controlled time dissolution and bulk erosion of the polymer, paclitaxel is released locally in a phosphate buffer solution, indicated by increased surface roughness (right).

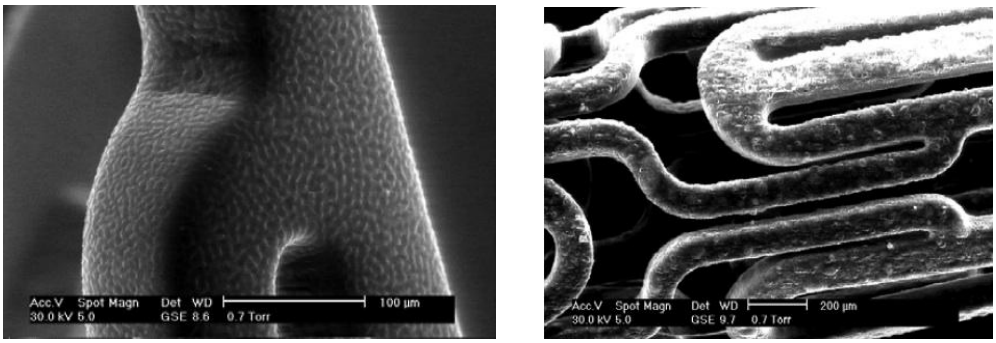

Figure 2.9 SEM image of paclitaxel coated stent (left) before PBS submersion, scale bar 100 µm (right) 37 days after phosphate buffer saline submersion. *Adapted from* [123].

Paclitaxel inhibits proliferation by disrupting microtubules and stopping cell division at the metaphase/anaphase boundary [124]. Similarly, the drug sirolimus inhibits cell cycle protein phosporylation to arrest cell division [125].

The chemical structure of both paclitaxel and sirolimus allows them to be easily taken up by cells. They are both extensively used in cancer treatments. By slowing local cell proliferation at the stent site, these drugs reduce the onset of intimal hyperplasia. Their principle disadvantage is that they are not cell specific and delay proper re-endotheliazation and vascular healing which can increase the chance of thrombosis if anti-coagulant medication is missed.

An abundance of large clinical studies have been conducted on the effects of these DES compared to BMS. The results are now well established. The conclusions from trials between 2003 and 2007 were published in the New England Journal of Medicine and the Journal of American Cardiology [85, 126-129]. The results demonstrate that the need for revascularization procedures is markedly higher for patients receiving BMS. Drug-eluting stents are associated with significant reductions in the rate of target-vessel revascularization among patients with two or three risk factors for restenosis, including diabetes, vessels, < 3 mm, and extensive lesions, >20 mm. So DES should be used preferentially in these situations. However, DESs have a slightly higher risk of in-stent thrombosis after one year compared to BMS. But most interestingly of all, the long term 4 years rates of myocardial infarction do not differ in either group, even though DES have slower healing and less re-endothelization compared to BMS.

2.2.7.2 Radioactive Stents: Brachytherapy as it is called, uses beta or gamma radiation to reduce intimal hyperplasia by actively killing the more radiation sensitive proliferating cells [130]. Radiation therapy was approved by the FDA in 2000 as an alternative treatment for restenosis [131]. Initial investigations with radioactive stents showed promising results after a 6 month follow-up. Unfortunately long-term safety has been an issue. This treatment is severely limited as a stand-alone strategy to CVD because of a few factors. Primarily, achieving an even radiation dosage has been a problem, an event known as the “candy wrapper” or “edge effect” occurs. It causes luminal deterioration in the radiation areas but not at the edges of the stent. This creates undesired fluid dynamics [132]. Secondly a high incidence of late in-stent thrombosis and

myocardial infarction has been documented. The primary attributed cause has been poor re-endothelialzation in radioactive areas [130]. A pro-healing approach is considerably more promising than radioactive treat

2.2.8 Pro-Healing Stents

Rapid and proper endothelialization has been shown to be an effective method for suppressing intimal hyperplasia and is a hot topic in vascular research. Some novel designs include endothelial cell seeding in conjunction with DNA, viral vectors coatings using RGD cell adhesive peptides, or even endothelial cell attracting anti-bodies.

2.2.8.1 Endothelial Seeding with DNA or Viral Vectors: Seeding vascular devices with harvested autologous endothelial cells has been an attractive way for delivering a high local concentration of ECs at the site of injury [133, 134]. However, this method is limited and suffers from the loss of seeded endothelial cells and damage during stent implantation [79, 135]. Still, some have attempted loading the cells with plasmids containing pertinent genes for healing or limiting SMC growth as an option [136]. Two such examples are plasmids coding for vascular endothelial growth factor (VEGF) and viral gene therapy. The problem to date with these methods has been the lengthy surgical interventions in obtaining a large vein or fat tissue from a patient and then extracting the ECs and seeding with the desired compounds. With a consequent delay in therapy and low relevant expression of the recombinant proteins/vectors success has been limited, although Koren et al. suggest considerable progress has been made in this area [137, 138]. Another drawback is the potential biohazards; cytotoxicity and immunological problems associated with this type of gene therapy [137].

2.2.8.2 Organic/Biomimetic Coated Stents: In attempts to camouflage the stent and induce positive cell-material interactions, polysaccharide coatings such as chitosan, alginic acid and hyaluronic acid, cellulose, phosphorylcholine [139], and

heparin [140] have been covalently, physisorbed or electrostatically attached to stent surfaces [141-143]. These coatings have been well characterized but to our knowledge not reached clinical investigations. Both *in vivo* testing of algin and hyaluronic acid showed no significant difference in the blood coagulation cascade.

2.2.8.3 Endothelial Progenitor Cell Capturing Antibodies: Endothelial progenitor cells (EPCs) are cells having the ability to differentiate into endothelial cells (ECs) and can be easily extracted from concentrated whole blood. Infusion of EPCs or statin treatments promoting EPC differentiation has been shown to reduce neointimal growth [144]. By coating the stent with antibodies, anti-CD34, researchers from Toronto Canada et al., have been able to capture circulating EPCs and substantially cover the stent [133]. After 48 hours, a monolayer of ECs was fully developed in a porcine model. After 28 days a significant reduction in neointimal formation was observed [145]. This is a very promising strategy.

The first small scale trial in humans demonstrated the feasibility of this stent [90]. In 2005 the EPC capture stent was assessed in 16 human patients. After nine months follow-up, revascularization was required only in 1 patient. At six-months, the luminal stenosis was significantly improved by the anti-CD34 coated stent compared to stainless steel stents ($15.49 \pm 4.54\%$ vs $23.96 \pm 7.70\%$, $p=0.01$). The stents showed 90% endothelial cell coverage compared to the bare stent which was almost completely devoid of cells [90]. On these stents, the exact strategy to immobilize the anti-CD34 is not discussed in detail, however it appears from their patent, that the antibodies are either embedded or immobilized to a matrix containing synthetic polymers such as polyallylamine, polyethyleneglycol (PEG) or mPEG-N-hydroysuccinimide [146]. These multi-layer polymers are dip coated and dried onto the surface and may incorporate organics such as collagen or other biologically active agents. Their method differs significantly from our immobilization since they are not using the thin self-assembled monolayers to directly immobilize the active agent **Figure 2.10**

demonstrates, through the use of SEM images, the improvement of endothelial cell attachment to an anti-CD34 coated stent compared to an uncoated one.

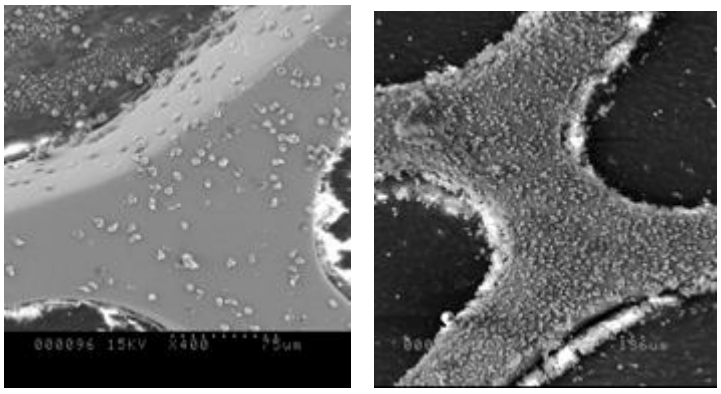

Figure 2.10 SEM of a bare metal stent (left) and anti-CD34 endothelial cell protgenitor (EPC) capture stent after 1 hour implantation in a porcine model. The EPC capture stent demonstrated > 90% EPC coverage. *Adapted from*[147]

2.2.8.4 RGD Coated Stents: The use of arginie-glycine-aspartic acid sequence or RGD oligomers have also shown the advantage of promoting endothelial cell attachment to stent surfaces. This peptide sequence, which is found in fibronectin, but which can also be purchase as a stand peptide has the ability to activate cytoskeleton changes. These positive changes augment a cell's ability to grow and proliferate. Blindt et al. have embedded RGD oligomers within a polymer coated drug eluting stent to induce EPC attachment [144]. The modified stents showed lower neoimtimal growth and reduced rate of restenosis (33 ± 5% cRGD stent vs 54 ± 6% polymer stent) in a porcine model over 12 weeks. In vitro tests showed, in a control experiment, that embedded/ physically adsorbed fibronectin had similar improvements compared to the RGD stent in terms of endothelial cell attachment. In contrast, other researchers have demonstrated that fibronectin has a greater effect on cells than stand alone RGD sequences, due to the need of complimentary synergetic domains [148].

2.3 Fibronectins, Integrins and Extracellular Matrices

2.3.1 The Extracellular Matrix

After discussing various stent technologies, it is important to understand the chemical environment a stent will be placed in, since the ability of ECs and SMCs to function as confluent tissues is integrally dependant on their surrounding microenvironment. A scaffold of specialized proteins form what is known as an extra-cellular matrix (ECM).

The first thing cells do when they make contact with a surface is release ECM proteins to grow on. The composition and conformation of these proteins dictates local cellular processes including proliferation, differentiation, migration, spreading and even death [149-151]. The vascular ECM structure is complex and composed primarily of collagens, elastins, laminins, proteoglycans, and fibronectins [152]. Other low concentration proteins such as von Willebrand factor and vitronectins are also present. [152]. As mentioned before, fibronectin is of particular interest in this project, and it will be discussed in more detail in the following sections.

2.3.2 Fibronectins: Introduction, Structure and Function

Fibronectins (FN) are a family of well-studied and characterized glycoproteins that play a large number of roles in the human body including: wound healing, angiogenesis, and inflammatory responses [39, 151, 153, 154]. They also have profound effects on a cells ability to adhere, proliferate, and spread on surfaces [155-159]. Therefore they are quite interesting to be incorporated for novel implant designs.

Fibronectins are produced from a single gene on the 4^{th} chromosome in humans, and unlike collagen and laminin which are found in most animals such as flies to apes, FNs only appear in vertebrates. Their time course in evolution correlates well with the appearance of organs with endothelial lined vasculature

[155]. There are two principle types of FN when not in fibrillar networks: those existing in soluble state, blood plasma (pFN), and those in insoluble state cellular fibronectin (cFN) [153]. ECs, SMCs and other cell types have the potential to secrete, bind and assemble both pFN and cFN into fibrils and deposit them in the ECM [156]. pFN is secreted from the liver and is the greatest supply of FN in the body [157]. Plasma concentrations of pFN for a healthy individual that have not undergone rapid healing to a source of physical trauma is approximately 300 μg/ml [153].

FNs are heterodimeric proteins consisting of two arms: dimers (**Figure 2.11**). Each dimer is 230 to 270 kDa (1 Da = 1 g/mol) and may or may not be identical. [151] The arms are composed of repeat protein blocks known as *modules*, denoted type I, II and III and in humans the V module (variable length module) [158]. Three different modules can be removed via RNA transcription including two type III modules, EIIIA and EIIIB and subsets of the V module from either dimer or both. This means there can be many variations of FN when two dimer arms are combined [159]. For example, pFN is shorter than cFN and generally does not contain the two type III modules EIIIA and EIIIB. Another difference between cFN and pFN is that, the V module is present on both arms in cFN but only on one arm in pFN. It is thought to be essential for dimer secretion [160].

FN is a unique protein that has the cell binding peptide sequence arginine-glycine-aspartic acid (RGD) on its 10^{th} type III repeat, and in close proximity, on the 9^{th} type III repeat lies the sequence proline-histidine-serine-arginine-asparagine (PHSRN). It is believed the PHSRN motif acts as a synergetic addition to the RGD peptide, enhancing FN's ability to promote cell attachment and cytoskeletal changes. FN also has binding sequences for heparin, fibrin, and collagen, demonstrating it has multiple functions (**Figure 2.11**) [160].

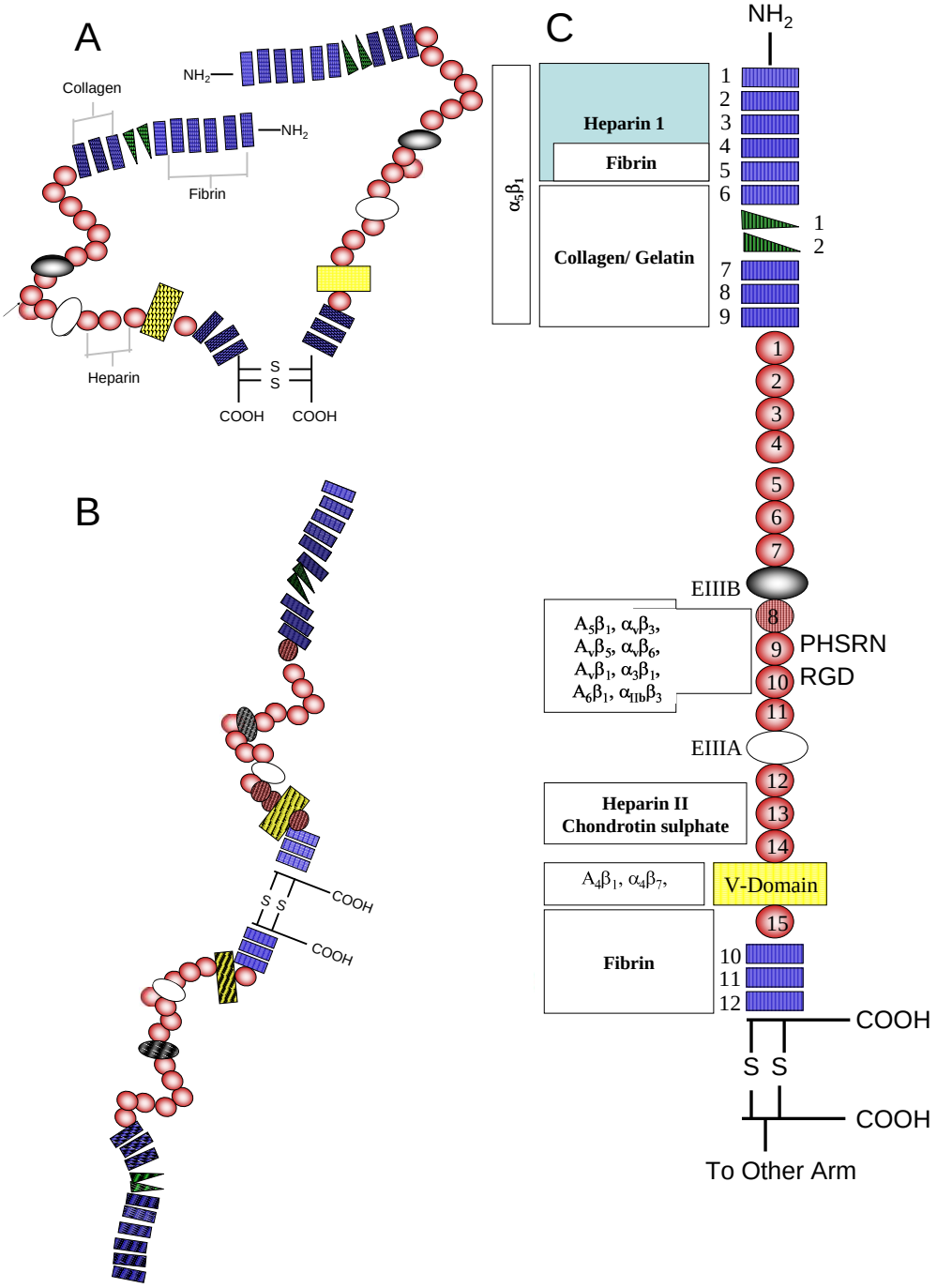

Figure 2.11 Modular representation of fibronectin (FN): (A) Closed arm conformation (B) Open arm conformation. (C) A single dimer arm. (Rectangle) Type I, (Triangles) Type II, and (Circles) Type III domains on FN. The blocks on the left represent which domains each module has binding affinity for. The cryptic cell binding sites, PHSRN and RGD sequences, are found on the Type III 9th and 10th modules respectively. *Adapted from* [161, 162]

2.3.3 Integrins and Fibronectin

Integrins are major cell membrane bound proteins, which attach to extra-cellular matrices and mediate important cell-cell adhesion events [163]. Signals between the ECM and cells integrins affect cell morphology, motility and gene expression [164]. All integrins are αβ heterodimers consisting of an α unit, 120 to 180 kD, and a β unit, 90 to 100 kD attached non-covalently. A few examples of integrins that bind with FN are $\alpha_5\beta_1$ and $\alpha_V\beta_3$ [165].

Now, in terms of FN, at physiological pH and salt concentrations pFN in solution exhibits compact conformation [165]. The compact from is induced by association of the first 5 type I repeats and the first type III repeats from the NH_2-terminals between dimer arms, refer to **Figure 2.11 (C)** [166]. This conformation is hypothesized to hide certain cryptic sites essential for fibril assembly and cell binding and is represented by a closed conformation, as shown in **Figure 2.11 (A)** [167, 168]. However, factors such as increases in pH and ionic strength, variable temperatures, contracting forces of cells, or integrin induced activation, can affect pFN's conformation and induce FN function [169]. Abundant evidence demonstrates FN must be activated before it can form fibrillar networks [160, 167, 170].

As mentioned above, FNs are able to communicate with cells through trans-membrane proteins, integrins which act as a bridge between FN on the cells exterior and the actin cytoskeleton assembly on the cells interior**. Figure 2.12** shows the communication between integrin along the cell membrane and FN on the exterior.

This process is a stepwise event. Firstly FN clings to the cell surface via interactions primarily from the N-terminal 70-kDa region of the protein [171]. This is the same region that is used when the dimer arms are closed in compact formation. Then, tensile forces cause FN to extend, opening up cryptic cell binding sequences, RGD and synergetic sequence PHSRN modules can now bind with cell integrins. The FN molecule in this confirmation now recruits blood

circulating pFN through hemophilic interactions and grows into larger fibrils. As the fibrils grow the network becomes insoluble through an irreversible process [151, 172]. The formation of a large fibrillar matrix causes changes to the actin cytoskeleton within the cytoplasm of the cell which is responsible for positive changes leading to cell/surface attachment and growth.

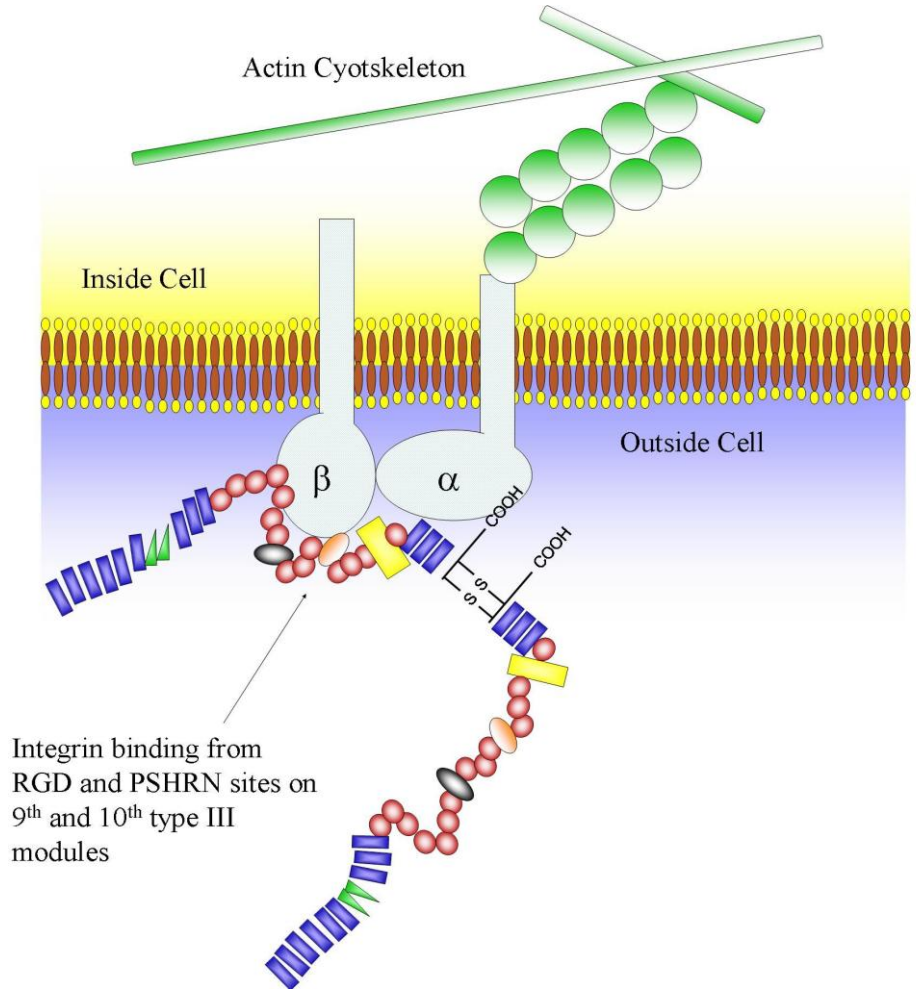

Figure 2.12 Initial step of FN binding to cell membrane bound integrin forming a physical link between FN fibrils of the ECM and cellular cytoskeleton actin filaments. The cytoskeleton changes induced by FN attachment result in enhanced cell proliferation and spreading. *Adapted from* [151, 172]

CHAPTER 3: RESEARCH OBJECTIVES

3.1 Principle Objectives

Fibronectin has been used in various implant applications in order to promote cell/surface interactions. However, in these applications, FN has been only physiosorbed on implant surfaces. In the case of blood-contacting implants, this approach is not desirable, due to the rapid removal of the adsorbed FN under the blood sheer force, leaving the implant surface naked and open to adsorption of undesirable proteins (e.g. fibrinogen). Thus, it is desirable to immobilize FN irreversibly on the implant surface.

Therefore, the final objective of this research is to develop and then optimize a method to irreversibly immobilize fibronectin to a stainless steel surface (stent). The fibronectin will be linked to stainless steel through the use of self-assembled monolayers (SAMs). Then modified substrates will be studied under *in vitro* cell conditions to establish whether endothelical cell attachment is augmented. The intermediate objectives are iterated below in point form.

PHASE I: Develop a method to irreversibly bind functionalized alkanethiol SAMs to 316L SS:

- □ The SAMs must be stable under aggressive environments
- □ The SAMs must display desired chemistry to attach proteins
- □ The procedure should be reproducible, scalable and efficient
- □ If the method is novel, study it to optimize the procedure

PHASE II: Covalently bind proteins bovine serum albumin (BSA) as a model protein and then fibroenctin (FN) to these monolayer films

- □ The proteins must demonstrate great stability on the surface
- □ The procedure must also be reproducible
- □ Study and optimize this procedure

PHASE III: Assess modified substrates affect on cells

- □ Correlate the effects of the FN-modified surface properties on EC attachment

CHAPTER 4: EXPERIMETNAL METHODS AND MATERIALS

4.1 Materials and Sample Preparation

4.1.1 Chemicals

Table 4.1 Chemicals and materials of construction

Chemical	Catalogue Number	Use
Self-Assembled Monolayers		
11-mercapto-undecanoic acid	450561 (Aldrich)	COOH SAM
1-undecanethiol	510467 (Aldrich)	CH_3 SAM
11-Amino-1-undecanethiol	111027-004 (Assemblon)	NH_2 SAM
Solvents, Salts and Acids		
sodium chloride	71381 (Sigma)	corrosion and sonication
sodium hydroxide 5M	SS256B-500 (Fisher)	protein removal
potassium phosphate dibasic	7778770 (Sigma)	phosphate buffer solution
sodium perchlorate	FL020797 (Fisher)	electrolyte
denatured alcohol	A407P-4 (Fisher)	cleaning and solvent
acetic acid	A35-500 (Fisher)	de-carboxylate COOH SAMs
phosphoric acid	A242-500 (Fisher)	"
malonic acid	AC12526-2500 (Acros)	"
citric acid	A940-500 (Fisher)	"
hydrochloric acid	A144-500 (Fisher)	"
sulfuric acid	A510-500 (Fisher)	"
perchloric acid	A2287-LB (Fisher)	"
Protein Binding to Self Assembled Monolayers/ Coupons		
bovine serum albumin (BSA)	A9418 (Sigma)	proof of SAM protein covalent binding
Fibronectin	354008 (BD Bioscience)	increase cell adhesion to 316L SS
1-ethyl-3-[3dimethyl aminopropyl] carbodiimide	3450 (Fluka)	catalyst BSA and FN covalent binding (EDC)
glutaraldehyde	FL080202 (Fisher)	BSA and FN covalent binding (GLU)
n-hydroxysuccinimide	130672 (Sigma)	BSA and FN covalent binding (NHS)
316L stainless steel coupons	9298K131 (McMaster Caar)	machined into 0.5" diameter x 2 mm thick coupons 316L SS
NiCr (nichrome) wire	8880K72 (McMaster Caar)	as electrodes

Chemical	Catalogue Number	Use
Cell Attachment and Proliferation		
quick cell proliferation essay kit	Bioscience (K301-500)	quantifies number of cells in culture
fetal bovine serum	12483 (Gibco)	cell growth agent
penicillin/streptomycin/ glutamine	450-202-EL (Wisent)	cell growth anti-bacteria/virus

4.1.2 316L Stainless Steel Sample Preparation

Identical 316L SS coupons (stent material) 127 mm diameter x 2 mm thickness were used for cell testing, PM-IRRAS investigation and electrochemical measurements. They were machined from a 316L SS rod (9298K131 McMaster Caar).

Table 4.2 Chemical composition of AISI 316L SS (wt%)

Fe	Cr	Ni	K	Mo	Mn
bal	16.22	10.31	0.031	3.2	1.48

Cu	Si	C	Nb	S	Vn
0.57	0.38	0.065	0.034	0.043	-

Before further modification, the samples were polished with 1000, 2400, and 4000 grit SiC paper and rinsed and sonicated with water and denatured alcohol, acetone and chloroform for 10 minutes each to remove any residues from the polishing steps. The samples were dried in ambient air before use. If the SiC residue is not removed its presence is visible by large peaks between 1000 -1100 cm^{-1} in the PM-IRRAS spectra representing Si species which are detrimental to film integrity.

4.2 Methods of Protein Immobilization

4.2.1 Electrochemical Setup for Binding Self-Assembled Monolayers

For SAM deposition, reactions were undertaken in a single compartment 50 mL electrochemical cell. The reference electrode was a saturated caromel electrode in saturated KCl solution, SCE (0.244 V vs standard hydrogen electrode, SHE) [173]. The cell was purged at least 30 min prior to treatment by a gentle stream of argon to remove dissolved oxygen. To cradle the 316L SS samples, NiCr hooks were used as electrical contacts, and a NiCr wire was used as a counter electrode to complete the circuit.

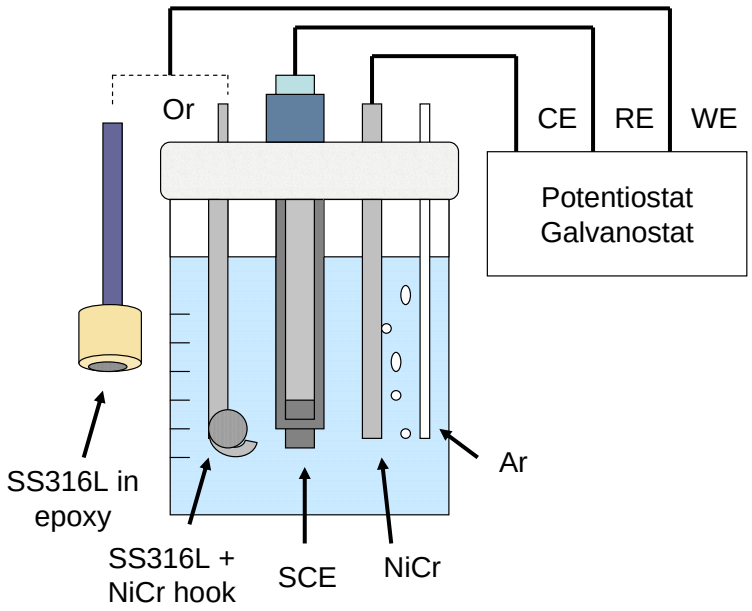

Figure 4.1 Schematic diagram of the setup of electrochemical experiments

The 316L stainless steel surface was using cyclic voltammetry at 100 mVs^{-1} scan rate between 0 and -1.8 V_{SCE}. Several thiols were added to form the desired SAM, The concentrations were as follows; 10 mM 11-mercapto-undecanoic acid for (COOH SAM), 1 mM for 1-undecanethiol (CH_3 SAM) and 1mM for 11-amino-1-undecanethiol (NH_2 SAM). After SAM binding, the coupons were rinsed with deionized water and denatured ethanol before and after 5 minute sonication in ethanol, to remove any physically adsorbed molecules from the surface unless otherwise stated. All PM-IRRAS spectra of SAMs were

developed using this procedure with 25 sweeps unless otherwise mentioned. The potentiostat used for these experiments was an Ecochemie Autolab PGSTAT30 potentiostat/galvanostat equipped with GPES v.4.9.5 software.

Figure 4.2 Ecochemie Autolab PGSTAT30 used for electrochemical measurements

4.2.2 Fibronectin or Bovine Serum Albumin Binding to COOH-terminated SAMs Using 1-Ethyl-3-[3dimethyl aminopropyl] carbodiimide(EDC) and N-hydroxysuccinimide (NHS)

To covalently bind FN or BSA to the 316L SS surface, EDC and NHS chemistry was used. COOH SAMs were first formed using the electrochemical techniques as described above. As discussed later in the thesis, the SAM formation resulted in the arrangement of a SAM-COO^-/Ni complex, thus making the COO^- end group chemically inactive. In order to activate the SAM end group, the substrates were immersed in a weak acid, phosphoric acid, at a pH 1.5 for 30 minutes, and rinsed with deionized water and denatured ethanol several times and dried in ambient air. Then, the modified surfaces were immersed in 15 mM NHS and 75 mM EDC dissolved in deionized water for 2 hrs [35, 174-176].

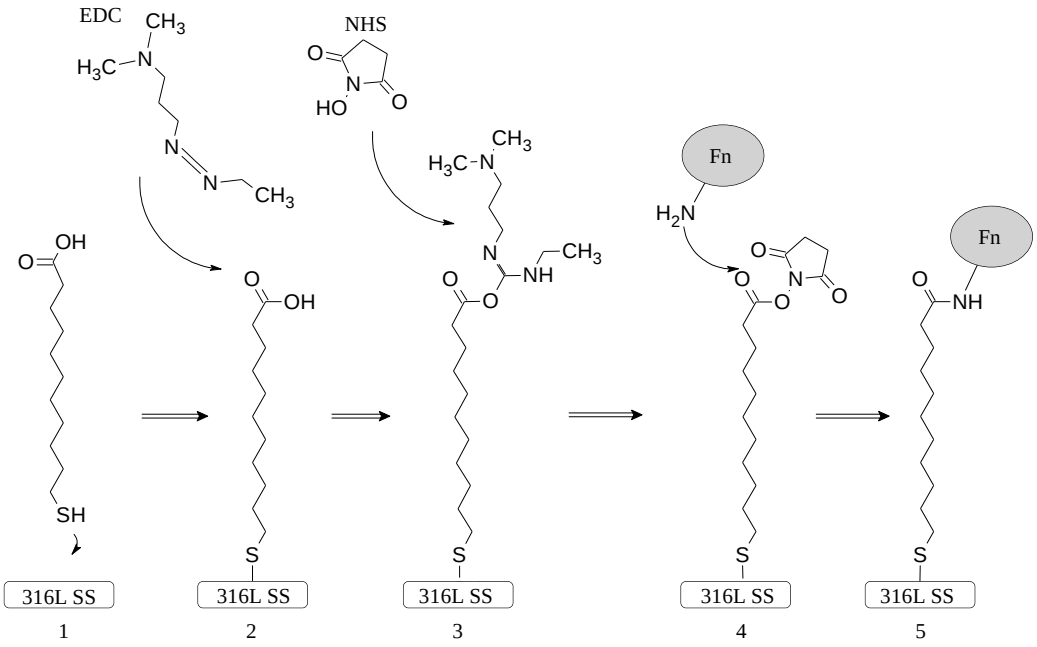

Figure 4.3 Binding fibronectin to 316L SS using 1-Ethyl-3-[3dimethyl aminopropyl] carbodiimide (EDC) and N-hydroxysuccinimide (NHS) on COOH terminated alkanethiols.

After the NHS/EDC immersion, the substrates were rinsed again in the same way and allowed to dry in ambient air. The now NHS ester SAM substrates were placed in a 2 μg/mL FN or BSA solution to immobilize the protein. The protein solution was prepared by first making a 100 mL phosphate buffer stock solution containing 0.05 M KH_2PO_4. The pH was adjusted to 6.0 using 5.0 M NaOH stock. The protein was weighed, then allowed to gently dissolve for 1 hr at room temperature in the phosphate buffer solution. Sonication and vigorous stirring can be detrimental to FN integrity and therefore was not used. The substrates were then incubated overnight in the protein solution to immobilize either FN or BSA to the surface at 4^{o}C. Although the adsorption kinetics may be slower at 4^{o}C, it was determined that this temperature was suitable to lower protein denaturation. The BSA modified substrates were then investigated using PM-IRRAS. However the FN immobilized substrates were further prepared for cell attachment testing.

In the morning, a new phosphate buffer solution, pH 6.0, prepared the same way discussed was made and 2.0 M NaCl was added to it. This solution was used to remove a large portion of physically adsorbed protein from the surface. The FN immobilized coupons were then placed in the 2.0 M NaCl and phosphate buffer solution for 2 hrs to remove any physically adsorbed FN. Then the substrates were rinsed with and stored in a solution of non-saline phosphate buffer 6.0 pH solution until cell testing. Before adding to cell culture media, the substrates were rinsed with deionized water and air dried in air to remove any phosphate buffer residue.

4.2.3 Fibronectin or Bovine Serum Albumin Binding to NH_2-terminated SAMs Using Glutaraldehyde Linking

Binding FN or BSA to the 316L SS surface was also achieved through the NH_2-terminated SAM. The NH-terminated SAMs were formed on the surface in the same way as the COOH-terminated SAM described in **Section 4.2.1.**

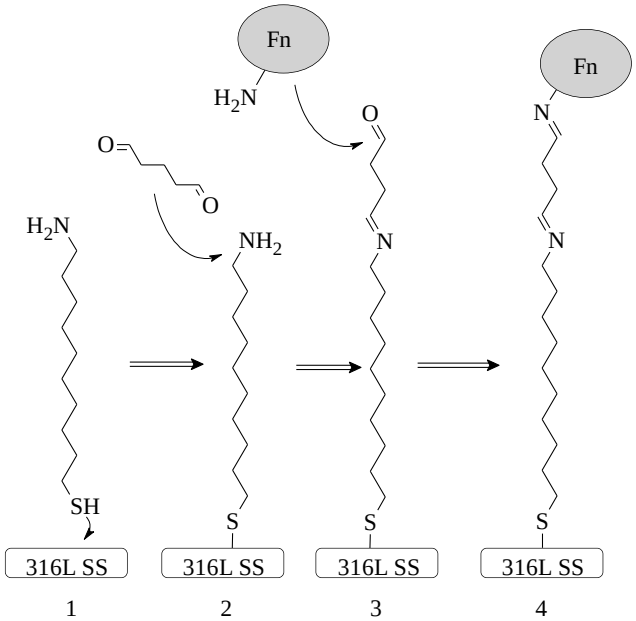

Figure 4.4 Binding fibronectin to 316L SS using glutaraldehyde and NH_2 SAMs

The NH_2-terminated SAM surface was first immersed in a solution of glutaraldhyde (GLU) 20 % v/v for 1 hr, to form a stable imine bond (N=C) between the NH_2 SAM and GLU, **Figure 4.4 step 3**. After this, the samples were sonicated in denatured ethanol for 10 min to remove any non-chemically bound GLU from the surface. The surface was rinsed with dionized water and denatured ethanol and dried in ambient air. FN or BSA was then bound to the free aldehyde group of the NH_2+GLU SAM forming an imide bond. [35, 174-176]. These samples were only investigated using PM-IRRAS and not used in cell attachment experiments.

The protein immobilization on NH_2 SAMs was achieved in a similar manner to the protein immobilization on COOH SAMs. First, a 100 mL phosphate buffer stock solution containing 0.05 M KH_2PO_4 was made. The pH was adjusted to 6.0 using 5.0 M NaOH stock. The protein was weighed to make a final concentration of 2 μg/mL FN or BSA and allowed to gently dissolve for 1 hr at room temperature in the phosphate buffer solution. However, in this case, the NH_2+GLU SAM substrates were placed in a 2 μg/mL FN or BSA solution to immobilize the proteins through reactive aldehyde groups **Figure 4.4 step 4**. The then incubation was conducted overnight in the protein solution to immobilize FN or BSA to the surface at 4^oC and rinsed with deionized water and ethanol and allowed to dry before PM-IRRAS measurements. Similar methods to immobilize proteins the glutaraldehyde modified surfaces have been investigated [32, 37, 54, 177].For more information on binding proteins through glutaraldhyde induced imide bonds refer to these references [32, 37, 54, 177].

4.3 Instrumentation and Chemical Analysis

4.3.1 Polarization Modulation Infrared Reflection Absorption Spectroscopy (PM-IRRAS) Theory

PM-IRRAS is a technique used for detection of thin films, corrosion products and monolayers on reflective surfaces or interfaces. This highly sensitive technique eliminates the need for taking background samples and reduces the effects of atmospheric H_2O and CO_2.

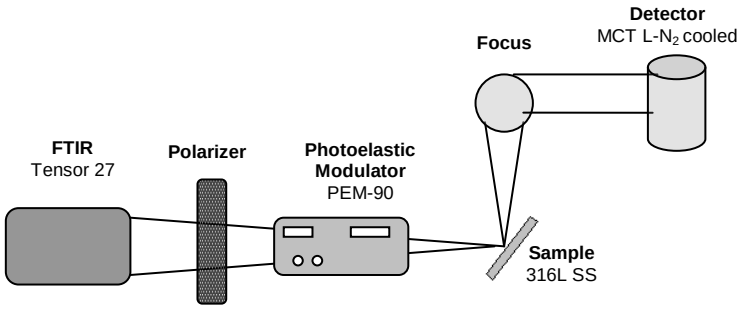

Figure 4.5 PM-IRRAS Schematic

By passing the incident infrared beam through a photoelastic modulator (PEM), **Figure 4.5**, the IR energy can be polarized, ie rather broken into distinct components; a vertical component (P-polarized light) and horizontal component (S-polarized light). When the fused silica in the PEM is compressed, the polarization component parallel to the modulator axis travels faster than the vertical component and when the element is stretched the resulting parallel component is lagged by a lag corresponding to the frequency of compressions. This phenomenon is known as photo-elasticity and causes the time dependant polarization.

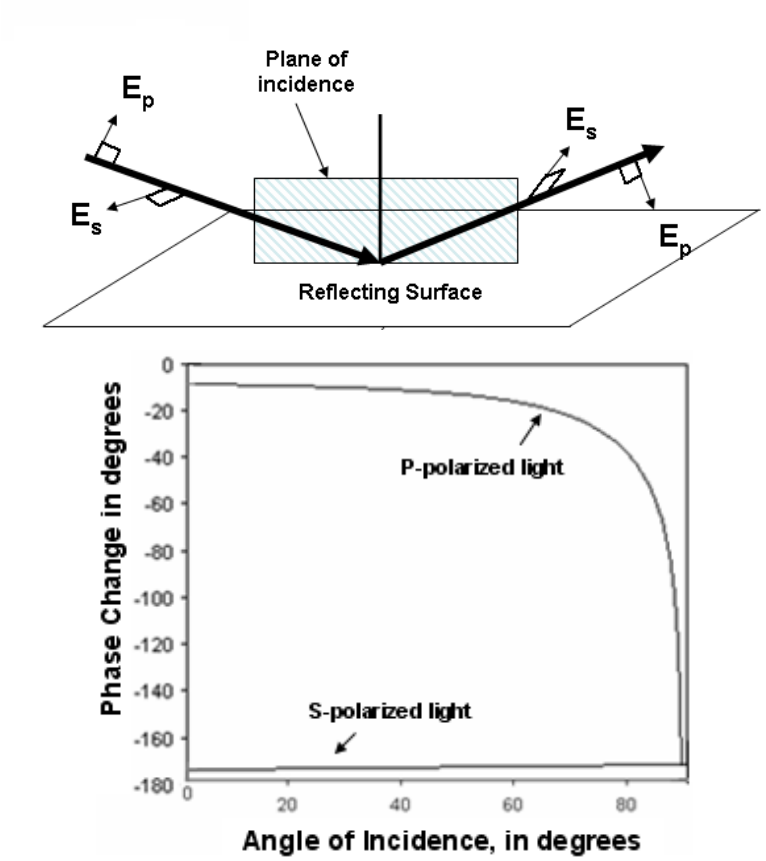

Figure 4.6 (top) schematic of s-polarized light and p-polarized light reflecting off a surface. (bottom) The resulting phase shift as a function of angle of incidence. *Adapted from [178]*.

In **Figure 4.6** (bottom) notice how the phase change of S-polarized light is relatively unaffected by angle of incidence. S-polarized light will always undergo a change in phase of approximately 180^o upon reflection from a surface, effectively canceling out it response to the surface while still absorbing the components in the surrounding.

Conversely P-polarized light perpendicular to the surface is highly affected by the angle of incidence. High angles of incidence between 70-88^o near grazing angle cause phase shifts resulting in complete constructive interference and a combined amplified signal roughly twice the amplitude of the incident beam. Therefore P-polarized light is absorbed by both species in the surrounding and species on the surface. The arithmetic difference over the sum of the intensity

of these two beams will result in the spectra of only what was on the surface and eliminate species in solvent, typically air or D_2O (in situ).

$$\frac{\Delta R}{R} = \frac{2(Is-Ip)}{(Is-Ip)}$$

$\Delta R/R$ is the response to surface. Ip, and Is are the intensity of the P and S polarized light [179].

4.3.2 PM-IRRAS Settings

To increase spectral resolution at a specific region, such as CH_2 stretching or amide region, the photoelastic modulator (Hinds PEM-90) wavenumber was set to either 2900 cm^{-1} or 1600 cm^{-1} respectively. The halfwave retardation was set to $\lambda/2$ or 0.5 for 278 scans at a resolution of 3 cm^{-1}. The angle of the incident beam was 80^o with respect to the surface normal. Aperture setting was 6 mm. Bruker OPUS Spectroscopy software v. 6.7 was used for recording, smoothing, peak picking, baseline corrections and arithmetic manipulations. To obtain clear spectral peaks, the spectrum of the SAM-covered sample was subtracted from a bare and freshly polished 316L SS sample. A liquid nitrogen cooled MCT detector was used in all measurements.

Figure 4.7 PM-IRRAS spectrometer Bruker Optics

4.3.2 Contact Angle Goniometry

Static contact angles were registered using an OCA 20 Goniometer from Dataphysics. The data manipulation was performed by SCA 200 Software at room temperature with 5 μl drop size using deionized water as the solvent. Typically 5 repeat measurements were taken for each surface and the mean and standard deviations were calculated to attain a final contact angle.

4.3.3 Endothelial Cell Attachment

To evaluate the response of modified substrates on human unbiblical vascular endothelial, HUVE, cells, attachment tests were conducted. The three substrates investigated included: Bare 316L SS as a control, COOH-terminated SAMs on 316L SS and FN covalently attached to COOH-terminated SAM_S on 316L SS, COOH and COOH+FN respectively. HUVE cells were incubated in MCDB 131 medium with 10% fetal bovine serum (12483 Gibco) containing 1% penicillin, streptomycin and L-glutamine (Wisent 450-202-EL) for 1,2 and 4 hrs.

After incubation each well was rinsed by pipetting media of 300 μL 3 times to remove any not attached cells. Then, to quantify the cells, 30 μL (9.1% total volume) of the Quick Cell Proliferation Assay Kit (K301-2500) *BD Biosciences* was pipetted into the wells containing the substrate and media and incubated for 2 hrs at 37^{o}C. Afterwards, 10 μL was pipetted from each well and added to a new 96 well-plate and shaken for 1 minute. Absorbances were read using the Beckamn Coulter AD340 Well Plate Reader set to 450 nm [180].

CHAPTER 5: RESULTS AND DISCUSSION- MONOLAYER ASSEMBLY ON STAINLESS STEEL

While the Background and Literature Review Chapter discussed the grand picture of this project; self-assembled monolayers, fibronectin and stents to eliminate restenosis, this chapter develops on the fine details of functionalizing a 316L stainless steel surface. Electrochemical techniques, contact angle goniometry, infrared spectroscopy and scanning electron microscopy were used to identify and understand the surface assembled monolayers at the nanoscale.

5.1 On Monolayer Assembly to 316L stainless steel

As mentioned previously, individual alkane molecules with long chains (usually >C6) under certain conditions can form high density structures that can be used to give metallic surfaces entirely new defined surface chemistry (ex. CH_3, COOH, NH_2 or OH functional groups), **Figure 5.1**. For these films to be of practical use, the individual molecules must be firmly attached to the substrate through a *head group*. This is in contrast to Langmuir-Blodgett films which are not necessarily immobilized to a surface, but rather phyisorbed. In this research, both NH_2 and COOH functionalized 316L SS surfaces 316L SS were made in order to ultimately covalently bind fibronectin to the surfaces. CH_3 terminated SAMs were also developed since they are easily identified by their hydrophobic nature and because the CH_3 terminal is relatively un-reactive making them an ideal model..

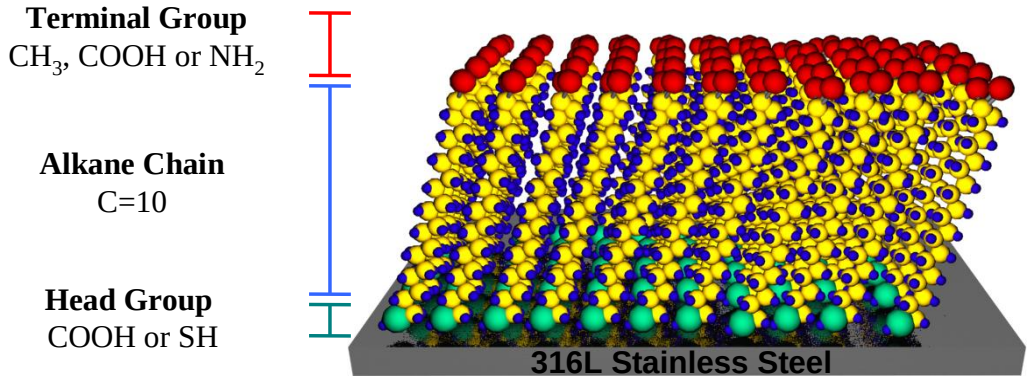

Figure 5.1 Self-assembled monolayer diagram with notation

In addition, forming mixed CH_3- and COOH- and/or NH_2 – terminated binary SAMs could be beneficial since the surface wettability and charge could be regulated this way, as was investigated a college of the thesis author, Nadia Afara [181].

5.1.1 Formation of SAMs on 316L SS Employing Published Methods– Initial Results

Initially it was not considered important what *head group* was used to bind SAMs to the stainless steel surface as long as the method of assembly was controllable, reproducible and stable. Therefore some previously published techniques for monolayer assembly on 316L SS were investigated, with the aim to adapt them for subsequent binding of FN to the surface. These methods are listed in **Table 5.1.**

Table 5.1 Attempted SAM binding procedures to 316L SS from the literature

Authors	Method	Head Group	Functional Group
Shustak et al. [15-17]	Electrochemical	COOH	CH_3, NH_2
Raman et al.[14]	Soaking & annealing	COOH	COOH, CH_3, OH, NH_2
Ruan et al.[19]	Electrochemical & soaking	SH, NH_2	OH, CH_3 ,COOH

X=CH_3, NH_2	X=CH_3, NH_2, OH, COOH	X=CH_3 Y=OH, CH_3
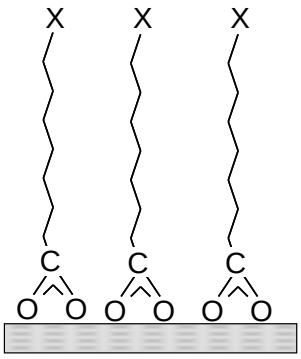	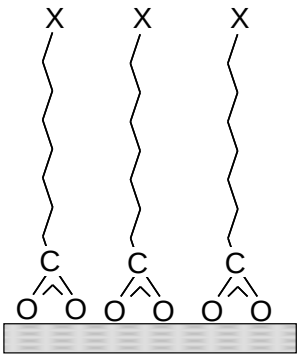	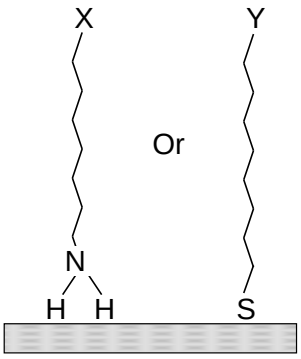
Shustak et al.	Raman et al.	Ruan et al.

As it is shown, both Shustak et al., and Raman et al. developed SAMs onto 316L SS using carboxylic acids in the form of carboxylate surface attachment (COO^-). Both researchers used very different processes (electrochemical vs annealing) but achieved similar outcomes. The details of these procedures are explained in more the Literature Review Chapter.

However, a one-year experimentation with these techniques, by the thesis author or supervised summer students, revealed that no reproducible, stable, reactive and high-surface-coverage SAMs could have been obtained, despite the claims of those authors. The results are briefly discussed:

- **Shustak et al's** method, was studied by summer students Julie Guy and Marine Balorin in the lab. They did have some success in attaching the SAMs, as measured by contact angle goniometry and PM-IRRAS. The contact angle for CH_3 was hydrophobic $97.0^o \pm 1.4$ representative of what is expected for hydrophobic CH_3 films. However, the films when measured by PM-IRRAS (**Figure A.1** available in the appendix) were not as highly ordered as those achieved by the authors themselves.

- **Raman et al.,** This solution deposition, then annealing method to form alkanoic acid SAMs on 316L SS was studied using palmitic acid and 11-amino-decanoic acid (NH_2-$C10H_{22}$-COOH). Some films made using this technique did in fact emulate the PM-IRRAS spectra demonstrated by the authors. However, again, the reproducibility of the films was very poor in a given batch. Also, the health effects of evaporating the required solvent, tetrhydrofuran, even under the fumehood, was concerning. The tetrahydrofuran vapours irritated the throat after transporting the samples from the fumehood to the oven. Care was taken to wear an organics protection mask but with many researchers in the lab it was a safety concern.

- Finally, **Ruan et al.'s** method of establishing thiol monolayers was effective. The authors had made CH_3 and OH-terminated SAMs. But, using their method also worked for COOH thiols (COOH-$C_{10}H_{22}$-SH), the PM-IRRAS spectra is **Figure A.2** available in the appendix. These SAMs displayed a good level or surface ordering and functional groups after overnight solution depositions. This method was quite good for producing one or two samples. The disadvantage of the method however, was the difficulty in employing it to produce large batches with good quality control. It was also very labor intensive, requiring an inert environment and very careful manipulation. Of equal concern was the state of the steel in perchloric acid. It was not uncommon for the steel to begin corroding, forming black textured surface during the oxide removal pretreatment. It is unknown if the authors experienced this phenomenon as well. These corroded surfaces would not be suitable in vivo.

5.1.2 A Novel Discovery: Alkanethiol Self-Assembly Using Potentiodynamic Polarization.

Not being satisfied with results obtained from the methods described above, it was decided to develop a new procedure that may show advantages over those previously studied. From the literature it was clear that thiol SAMs had been formed on other metal surfaces such as copper [182, 183], silver, [184] and nickel [22] by applying controlled potential in an electrochemical cell containing the metal substrate as the working electrode and the alkanethiol molecule in solution. This was motivation enough to attempt electrochemical assembly of alkanethiols on stainless steel.

The thesis author discovered that when a Nichrome (NiCr) wire was used to cradle the stainless steel coupons as the working electrode in electrochemical experiments, SAMs could be formed . It was determined that the NiCr wire was instrumental in SAM binding and if the NiCr electrode was replaced by titanium,

stainless steel or graphite the SAMs would not form. This discovery will be discussed in detail later in the thesis, while in the following sections the electrochemical formation of SAMs will be presented and discussed.

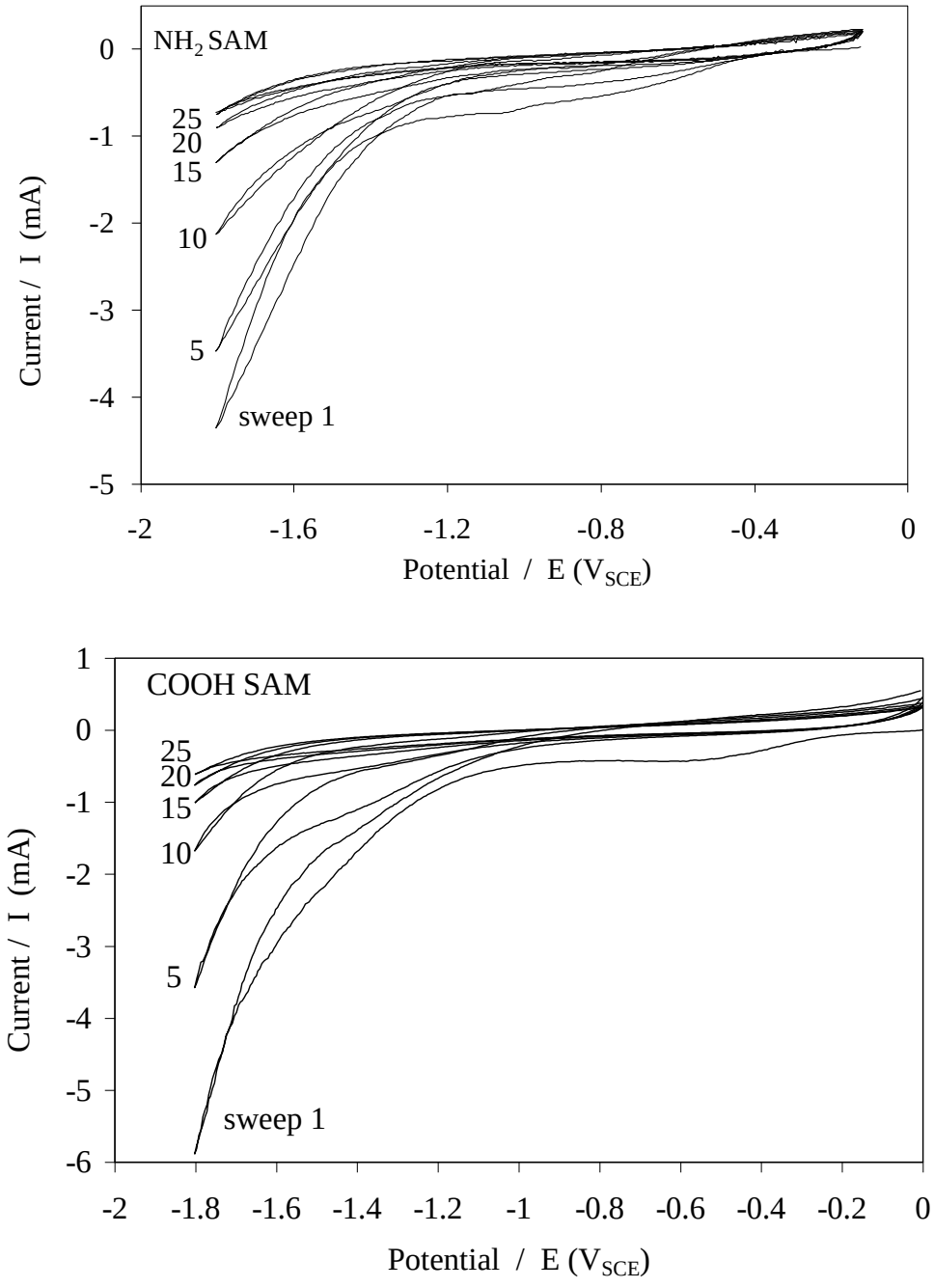

Figure 5.2 First to twenty-fifth cyclic voltammmagram of a 316L stainless steel in a solution of (top) 1 mM 11-amino-undecanethiol (bottom) 10 mM mercapto-undecanoic acid in 0.1 M $NaClO_4$ and denatured ethanol; scan rate, 100 mVs^{-1}.

Figure 5.2 represents the graphical output of the current response vs the applied potential during the SAM assembly, which is also known as a cyclic voltammagram, CV. While monitoring the current response during the potential sweeps, a clear trend in the cathodic region was observed: the current amplitude was decreasing with the number of sweeps. To determine if this effect was a result of alkanethiol assembly on the surface, a control experiment was run, in which the exact same conditions were investigated without any SAM molecules. The result is shown in **Figure 5.3** below**.** As the CV shows, even after 25 sweeps, the CV response remained fairly unchanged, demonstrating that the decreasing current trend in **Figure 5.2** is indeed due to the SAM formation. In this potential region (ca. negative of -1.2V) hydrogen evolution reactions occur. The rate of this reaction, and thus the measured current, depends on the surface area available for the reaction.

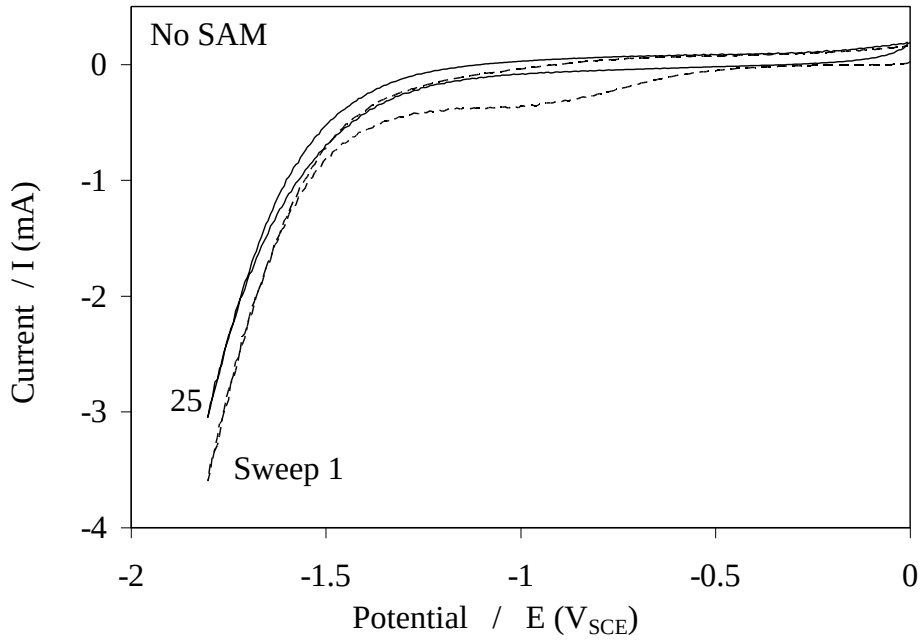

Figure 5.3 Cyclic voltammagram of a 316L SS electrode in 0.1 M $NaClO_4$ and denatured ethanol. ($v=100mVs^{-1}$) No NH_2 SAM or CH_3 SAM molecules are present.

Table 5.2 Alkanethiol current blocking effect during film assembly

Current I / mA At -1.8 VSCE	**No SAM**	**NH_2 SAM**	**COOH SAM**
1st sweep	-3.6	-4.36	-5.89
25th sweep	-3.05	-0.73	-0.60
% difference	15.2	83.3	89.8

Due to the SAM formation on the surface, the surface area available for the hydrogen reaction decreases with each sweep, thus the current density decreased. This is not the case with the control sample (**Figure 6.3**). Therefore the key difference in the CVs in the presence of SAMs compared to the control is that there appears to be a blocking of electron transfer through the 316L SS surface. This is due to the buildup of a non-conductive SAM on the steel surface. The current blocking effects of SAMs are well known [27]. The current blocking effect is summarized in **Table 5.2**.

5.1.3 Effect of Number of Cyclic Sweeps on SAM Formation

To validate that SAMs were being deposited on the 316L SS electrode during these cyclic sweeps PM-IRRAS spectra were used to identify chemical groups of the SAM. It was determined that when the number of sweeps was increased from 1, 5, 10, 15, and 25, the PM-IRRAS peaks between 2917-2930 cm^{-1} and 2845-2856 cm^{-1} continued to rise. This is consistent with the lowering of current in CV measurements with number of scans observed in **Figure 5.4**.

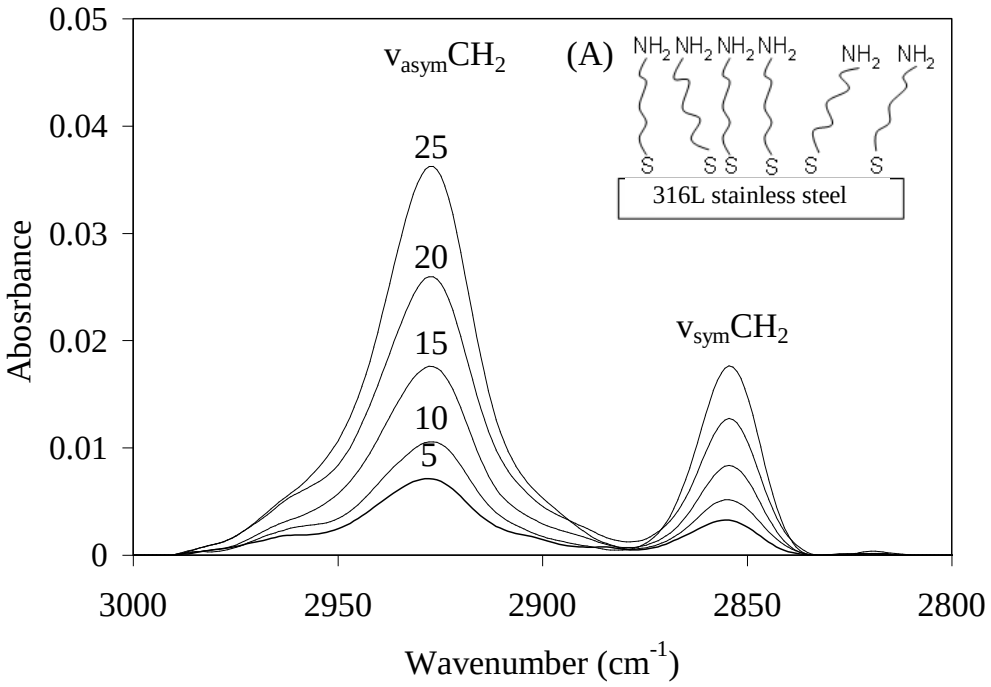

Figure 5.4 PM-IRRAS spectra of an NH_2 SAM made by polarizing a 316L stainless steel coupon in a solution of 1 mM 11-amino-undecanethiol between 0 and -1.8 V_{SCE} in 0.1 M $NaClO_4$ and denatured ethanol; scan rate, 100 mVs^{-1}. Peaks are ≈ 2927 cm^{-1} and 2854 cm^{-1} Inset (A) representation of NH_2 SAM.

These absorbance peaks represent the methylene CH_2 asymmetric ($\nu_{asym}CH_2$) and symmetric ($\nu_{sym}CH_2$) stretching vibrations respectively of the alkane chains. Both the shape and wavenumber of the methylene peaks can be used to identify film structure. The lower the peak wavenumber, moving towards 2917 cm^{-1} $\nu_{asym}CH_2$ and 2850 cm^{-1} $\nu_{sym}CH_2$, the more ordered the film. These films typically had peaks between 2924-2928 cm^{-1} and $\nu_{sym}CH_2$ between 2852-

2855 cm^{-1} therefore the SAM was considered liquid like with random alkane chain packing and gauche defects [185]. A perfectly ordered alkanethiol SAM would give the $v_{asym}CH_2$ peak < 2918 cm^{-1} [9] In general the broader the peak, the less ordered the SAM. Sharp well defined peaks at lower wavenumbers indicate a *trans* conformation in a semi-ordered state [30]. In certain applications, it is desired to have highly ordered films to improve film integrity and homogeneity. However it is not essential to meet the objectives in the current project.

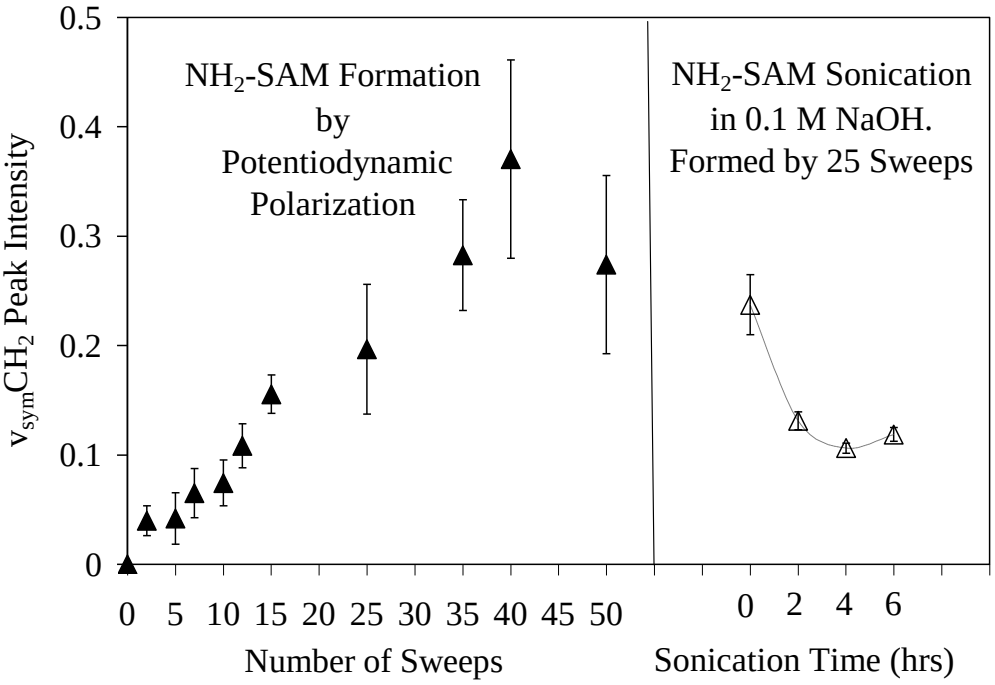

Figure 5.5 (left) Area of $v_{sym}CH_2$ peak intensity as a function of cyclic sweeps on a 316L stainless steel coupon in a solution of 1 mM 11-amino-undecanethiol in 0.1 M $NaClO_4$ and denatured ethanol cycled between 0 and -1.8 V_{SCE}; scan rate, 100 mVs^{-1}. (right) Area of $v_{sym}CH_2$ peak intensity remaining after sonication in 0.1 M NaOH. Each data point is the mean of 3 observations, the error bars are ± the standard deviations from the mean.

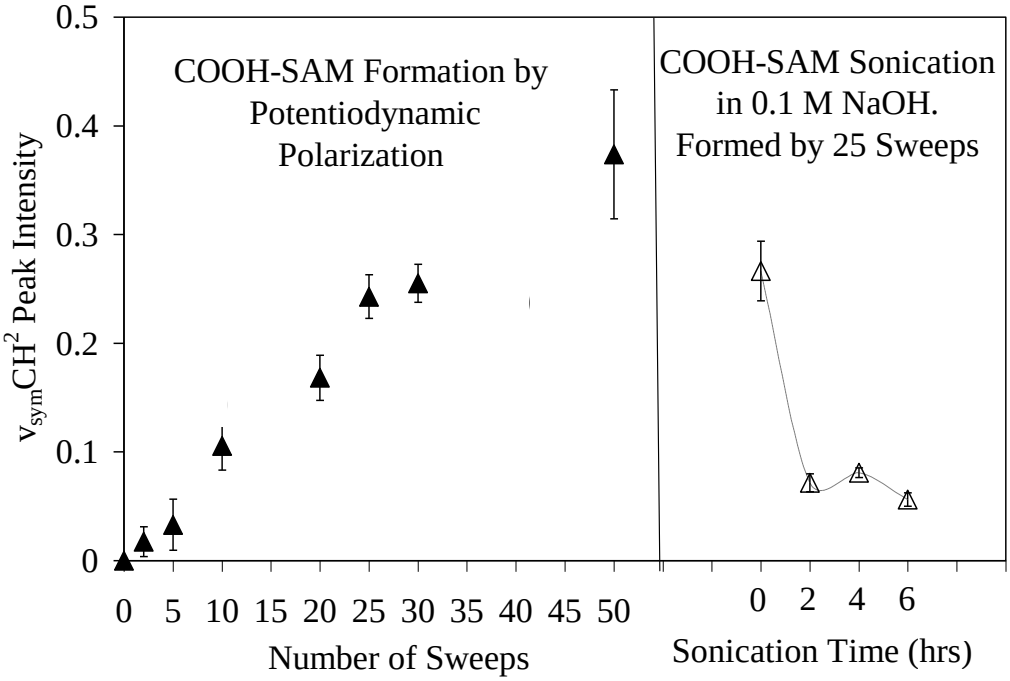

Figure 5.6 (left) Area of $v_{sym}CH_2$ peak intensity as a function of cyclic sweeps on a 316L stainless steel coupon in a solution of 10 mM mercapto-undecanoic acid in 0.1 M $NaClO_4$ and denatured ethanol cycled between 0 and -1.8 V_{SCE}; scan rate, 100 mVs^{-1}. (right) Area of $v_{sym}CH_2$ peak intensity remaining after sonication in 0.1 M NaOH. Each data point is the mean of 3 observations, the error bars are ± the standard deviations from the mean.

Figures 5.5 and **5.6** show the dependence of the $v_{sym}CH_2$ stretching peak intensity on the number of SAM formation sweeps, which is used as an indicator of the quantity of SAMs on the surface. From this result, some very interesting conclusions were made. Typically in monolayer formation, there is a plateau of the intensity as surface coverage reaches a maximum (i.e. saturation) [19, 33]. However, for all COOH and NH_2 SAMs studied, the $_vCH_2$ peak intensity versus the number of scans seems to fit a linear trendrather than a Langmuir-like isotherm type (**Figures 5.5** and **5.6**). Nevertheless, the large standard deviations at higher number of scans (> 25 scans) can be observed, and this is an important observation. Namely, when a critical number of scans was reached, peak variability between sample runs was considerable (as indicated by larger standard deviation bars). This is believed to be a result of formation of SAM *multilayers* on the surface, which seems to be a less controllable process. These multiple layers

were not easily removed by rinsing with water and denatured ethanol. However, they were easily removed by sonication as shown by the right insert on **Figure 5.5** and **6.6**. After 2-6 hrs of sonication in 0.1 M NaOH, SAMs formed after 25 scans still remained tightly bound to the surface, as indicated by the presence of CH_2 stretching vibrations. It was not concluded if a larger number of sweeps (>50) can be used to significantly improve SAMs compared to average 25 sweeps. 25 sweeps was used as an optimal operating parameter, because the SAMs displayed the required durability and it also meant a large number of samples could be made as a consistent batch on the same day for cell testing.

5.1.4 NH_2 and COOH SAM Stability

In order to use self-assembled monolayers effectively as biomedical implant coatings, they must show a large level of stability *in vivo*. Shustak and Mandler et al., [16] Raman & Gawalt et al., [14] and Ruan [19] did not investigate the stability of SAMs on 316L SS in physiological solutions. Gawalt suggested that their monolayers were stable in tetrahydrofuran, water and ethanol after sonication. Ruan only investigated the stability in ambient air up to 24 hrs, and found no oxidized sulfur indicating stable monolayers. Mahaptro on the other hand did investigate the long term strength of his SAMs in phosphate buffer using XPS [38]. He determined that his OH and COOH terminated thiols were stable up to 14 days. Around 21-28 days there was a low response to peaks representing oxidized sulfur and metal thiolate peaks and the SAMs were completely gone. Using his device in a simple phosphate buffer environment is limited to around two weeks. Therefore with the SAMs being developed in this project, it is important to determine how stable they are.

The stability of SAMs formed by the thesis author was tested in three solutions, denatured alcohol (85% ethanol, 15% methanol), 0.1 M NaOH (pH 13), and 0.16 M NaCl, under sonication. These three solutions were chosen because ethanol is a general solvent used to clean samples between stages while building the device and for sterilization of implants; corrosive 0.16 NaCl is used to simulate chloride concentrations found in the human body; and 0.1 M NaOH is used as an extreme alkaline solvent to go beyond conditions that may be experienced in the human body and is well known to remove physically adsorbed proteins. After the sonication, each sample was withdrawn and rinsed with ethanol and reverse osmosis treated water to remove NaCl and NaOH crystals from the surfaces for PM-IRRAS measurement. The results for COOH and NH_2 terminated SAMs are shown in **Figure 6.8.**

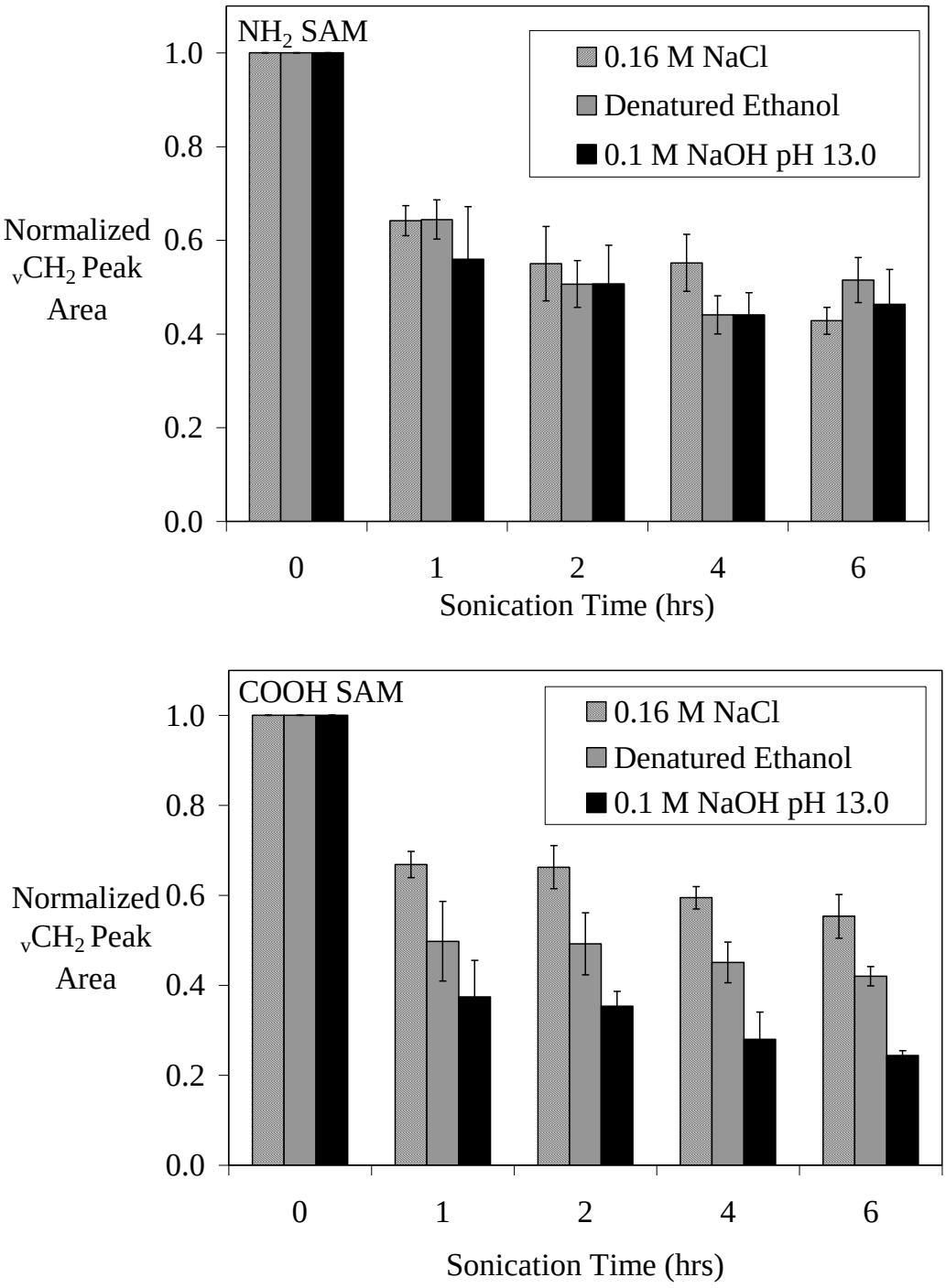

Figure 5.7 Normalized area of $v_{sym}CH_2$ peak after sonication in 0.16 M NaCl, denatured ethanol or 0.1 M NaOH. SAMs were made by 25 sweeps of a 316L stainless steel coupon in a solution of 0.1 M $NaClO_4$ (top) 1mM 11-amino-undecanethiol and (bottom) 10 mM mercapto-undecanoic in denatured enthanol between 0 and -1.8 V_{SCE}; scan rate, 100 mVs^{-1}. Error bars are 95% confidence intervals, n=3.

For the NH_2-terminated SAMs (**Figure 5.7**, top) the trend and SAM quantity remaining after sonication was similar for all the different solvents. This suggests that the solution chemistry was not a determining factor for the stability of NH_2 SAMs. The most destructive parameter was the sonication itself and spontaneous dissolution of non-tightly bound molecules into the solvent. Since alkane stretching remained in all cases it is safe to conclude that most of the SAM molecules are attached to the 316L SS surface covalently. Any physically adsorbed molecules are easily removed by such aggressive treatments.

In the case of the COOH-terminated SAM (**Figure 5.7**, bottom) it seems that after an initial large drop (40-60%) in SAM surface concentration (after 1 hour) the SAM surface amount remains relatively constant, with a much lower rate of SAM detachment over the remaining hours of sonication. This trend was shown for all three sonication solutions.

However, the 0.1 M NaOH seemed to remove a larger amount of SAM from the surface. The explanation for this is that some of the COOH groups could have been bonded to the steel through a COO^- metal carboxylate system and the high alkalinity of the NaOH solution was more successful at "delaminating" the molecules from the surface. In terms of other stability tests, COOH SAMs were also exposed to strong acids for 30 minutes HCl, H_2SO_4, and HNO_3 and still remained secured to the surface, again demonstrating chemical rather than physical attachment to the surface.

It should also be mentioned that the control samples (zero time) in **Figure 5.7** might have some SAM molecules present in the second layer and/or physisorbed on the surface, since these molecules were not removed by 'simple' rinsing. Thus, the drop in actually bond SAM surface amount in the figure is actually be lower then presented.

The most important conclusion of these tests was that the alkanethiol SAMs of COOH and NH_2 termainl groups remained on the surface even after aggressive removal attempts. This validates their robustness at least in the short term, for use as biomedical applications.

5.2 PM-IRRAS of NH_2, COOH and CH_3 Terminated SAMs

The potentiodynamic cycling method discussed above was further investigated using PM-IRRAS. Each of the different terminated SAMs, COOH, NH_2 and CH_3, should display some similar characteristics; they are all long carbon methyene chains (CH_2) followed by a sulfur at one end. Additionally, each SAM can be identified by its unique terminal group using PM-IRRAS.

5.2.1 PM-IRRAS Investigation of NH_2 SAMs

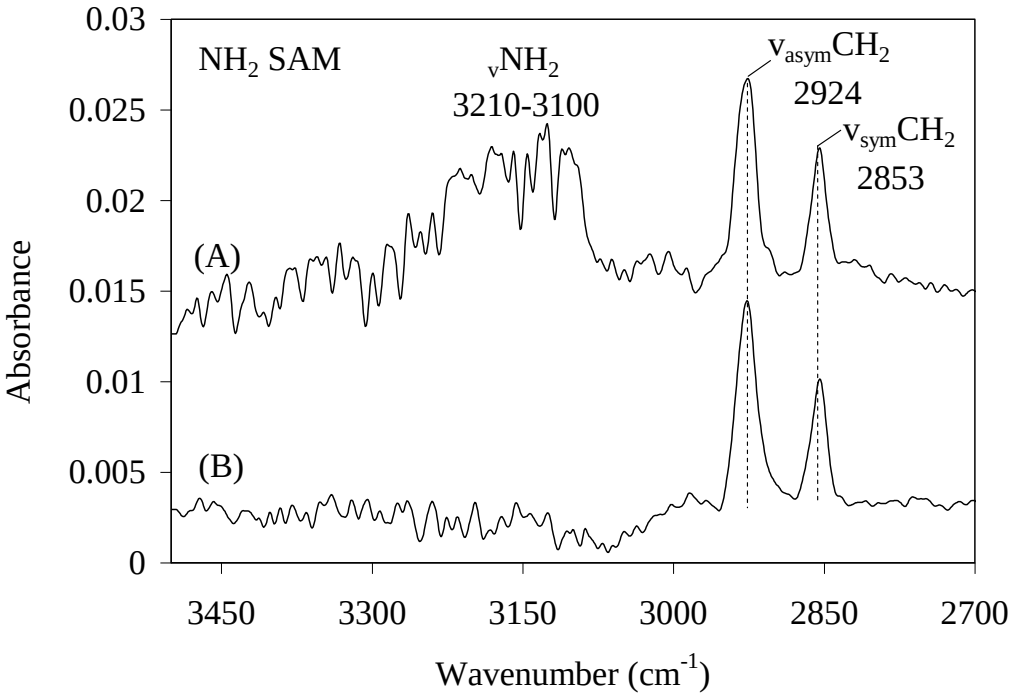

Figure 5.8 PM-IRRAS Spectra of NH_2 SAM. (A) Photoelastic Modulator (PEM) set to 2900 cm^{-1} (B) PEM set to 1600 cm^{-1}

Figure 5.8 shows the IR response of the NH_2 terminated SAM in the higher wavenumber region. No presence of peaks between 3100-3300 cm^{-1}, which represent the N-H stretching of the free amine, was detected although the PEM was set to 2900 cm^{-1}. Many FTIR investigations of NH_2 terminated SAMs have detected N-H stretching in this region [14, 17, 54, 186, 187]. However, as shown in **Figure 5.8** (A) when the PEM was set to 1600 cm^{-1} the peaks were present. This behavior was observed in multiple replicate runs and was therefore not a fluke. Why this N-H vibration was not identified when the PEM was set to 2900 cm^{-1} is unknown.

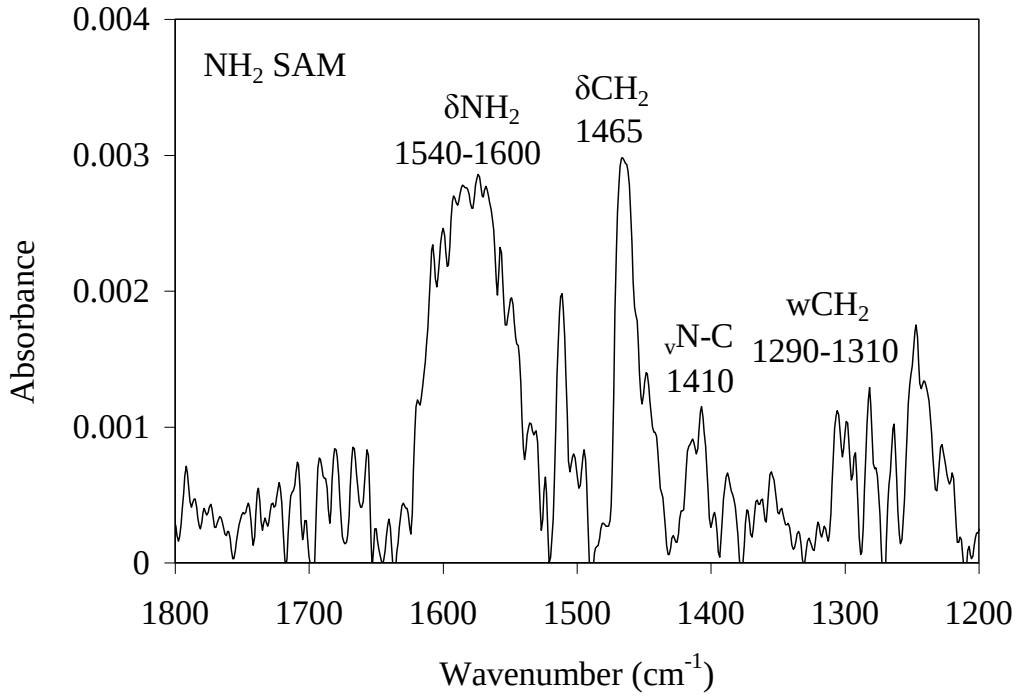

Figure 5.9 1600 cm^{-1} region PM-IRRAS spectra of NH_2 SAM

In the 1600 cm^{-1} region (lower wavenumber) zone, both the amine and methylene groups were identified, **Figure 5.9**. The methylene vibrations were identified by scissoring deformation at 1465 cm^{-1} and methylene wagging between 1290-1310 cm^{-1} [54, 188]. Similarly the amine groups in the form of amide N-H bending and N-H wagging were located. The N-H deformation (δN-H) has suggested locations by a variety of authors, Pradier 1560 cm^{-1}, Minier 1589 cm^{-1}, Toda 1600 cm^{-1}, Frey 1610 cm^{-1} and Arima 1545/1608 cm^{-1} [19, 197-

200]. It seems the peak shown in **Figure 5.9** spans all of those regions and may also depend if the amine is in the charged NH_3^+, or non charge NH_2 state. From this analysis is it evident that the NH_2 SAMs are present on the 316L SS surface is in a desired chemical state.

5.2.2 PM-IRRAS Investigation of CH_3 SAMs

PM-IRRAS spectra of CH_3-terminated SAMs (undecanethiol) 316L SS are presented in **Figure 5.10**.

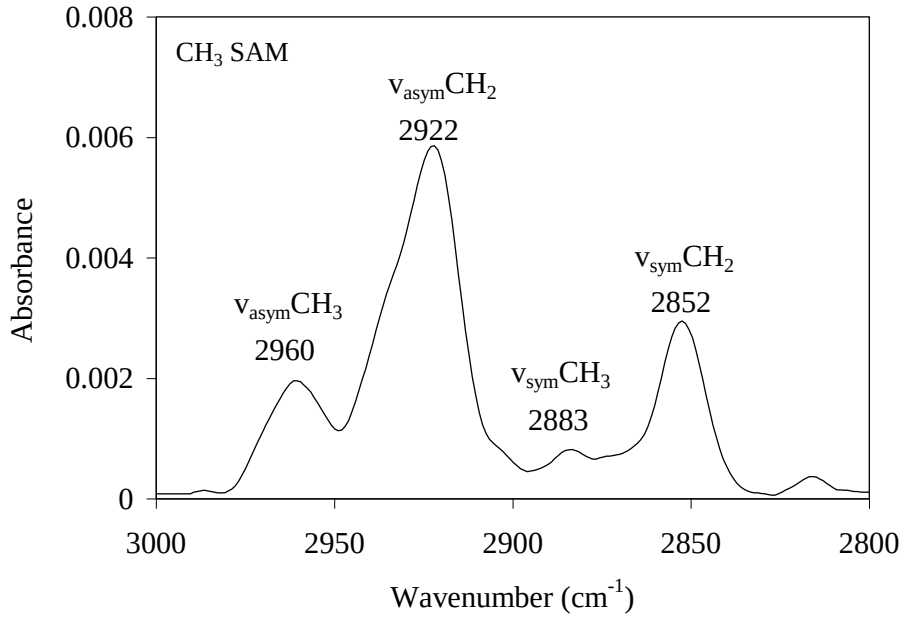

Figure 5.10 2900 cm^{-1} region PM-IRRAS spectra of CH_3 SAM

The detection of both methyl, CH_3 and methylene CH_2 vibrations were identified on the CH_3 SAM surface, and still present after 0.1 M NaOH sonication in **Figure 5.10**. The CH_2 asymmetric and symmetric stretching around 2922 cm^{-1} and 2852 cm^{-1} respectively demonstrated slightly better packing of the CH_3 terminated SAMs compared to the other functionalized SAMs which were commonly found between 2924-2927 cm^{-1}. This may be attributed to fewer repulsion effects of the neutrally charged CH_3 head group and less reactive nature of a CH_3 head group to bind to the surface. The hydrophobic nature of these

molecules may have also contributed to easier packing displacing the polar solvent. The CH_3 groups at 2960 cm^{-1} and 2883 cm^{-1} are evidence that CH_3 is in fact present [25, 35].

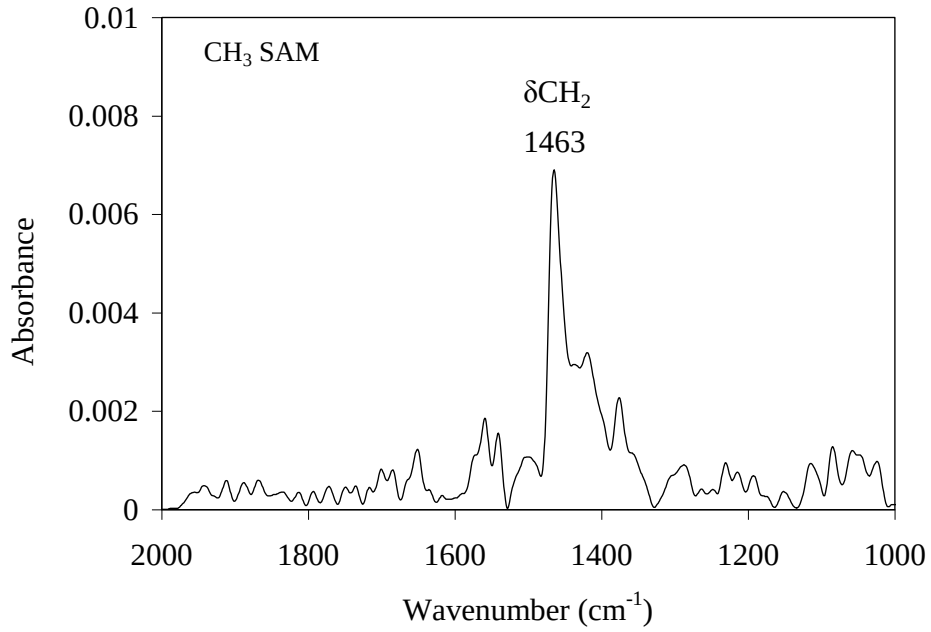

Figure 5.11 1600 cm^{-1} region PM-IRRAS spectra of CH_3 SAM

In the lower wavenumber region, **Figure 5.11**, the methylene deformation at 1463 cm^{-1} was present and no other significant vibrations were identified which is to be expected for CH_3 SAMs.

5.2.3 PM-IRRAS and EDX Investigation of COOH Terminated SAMs

The 2900 cm^{-1} region of the COOH SAM is shown in **Figure 5.12.** The CH_2 vibrations at 2925 cm^{-1} and 2852 cm^{-1} are similar to what was observed with the NH_2 SAMs, indicating slight packing defects in these SAMs.

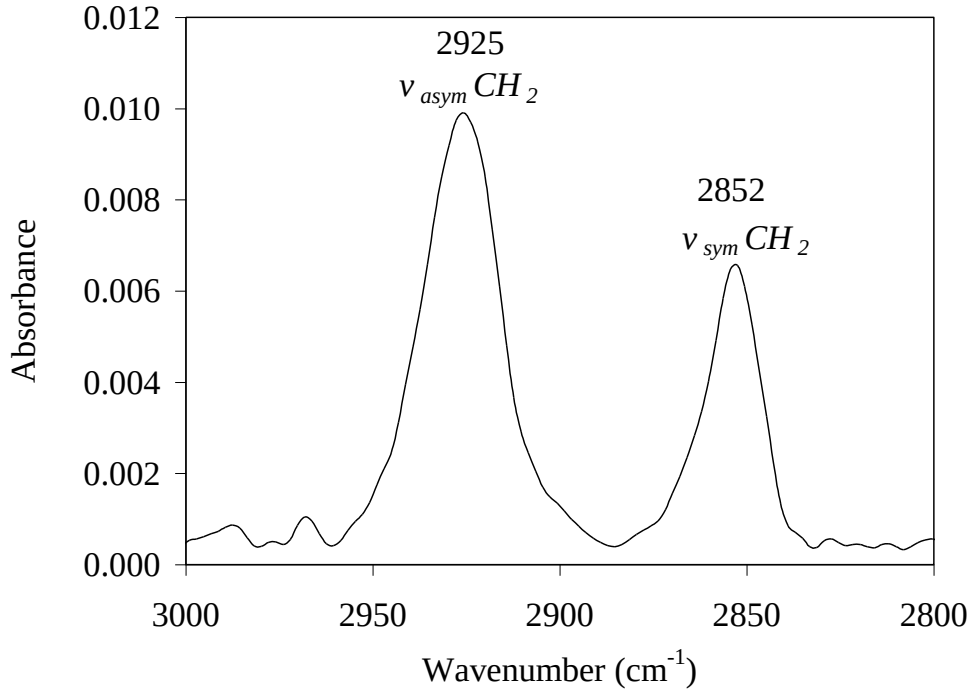

Figure 5.12 2900 cm^{-1} region PM-IRRAS spectra of COOH-terminated SAM

The COOH SAM of 11-mercapto-undecanoic acid was a more complex SAM to work with compared to the other two SAMs. On gold only the thiol (SH) group of a mercapto-undecanoic acid SAM has affinity for the surface. However on stainless steel, COOH has been known to form metal carboxylates with the steel surface in the right conditions [14, 15]. Therefore two groups with possible affinity for the substrate, SH and COOH, must be taken into consideration.

Experimental evidence supports the fact that the new electrochemical binding method developed by the thesis author works through thiol, SH, attachment. Namely, CH_3 SAMs were made and could have only been attached through the SH group (**Figures 5.10** and **5.11**). Similarly, NH_2 SAMs have

comparable binding kinetics to COOH SAMs, which suggests they are complexing to the surface through a similar mechanism. Therefore, it is likely that the COOH SAM attachment through the -SH group is the prominent format. Subsequent binding of n-hydroxysuccumimide (NHS) to COOH SAMs (presented later in the thesis) also evidences that the COOH group is positioned away from the surface, while the SAM is then attached to the 316L SS surface through the sulfur end.

5.2.4 COO-/Metal Complex Formation in COOH-temrinated SAMs

In the case of the COOH SAM, the primary purpose was to use it as a linking molecule to further attach n-hydroxysuccumimide, NHS, then protein which will be demonstrated in the next chapter. However, when experimentation was performed to immobilize NHS, the NHS ester was not forming at all on freshly formed COOH SAMs. This was a puzzle at first, but then made sense after analysis of the PM-IRRAS spectra as shown in **Figure 5.13**. There is no indication for the presence free carboxylic acid (C=O) group represented by the $_{v}$(C=O) peak ≈ 1710 cm^{-1}, which is required for NHS binding. In fact, the PM-IRRAS spectra indicates the existence of metal carboxylate. Namely, the two peak regions in **Figure 5.13**, $v_{asy}(COO^-)$ ≈ 1542-1595 cm^{-1} and $v_{sy}(COO^-)$ ≈ 1410-1448 cm^{-1}. Carboxylates in solution have been well studied using infrared spectroscopy and can be formed in a variety of proposed physical structures, by electron sharing of a metal species and the oxygens from the carboxylic acid moiety (**Figure 5.14**).

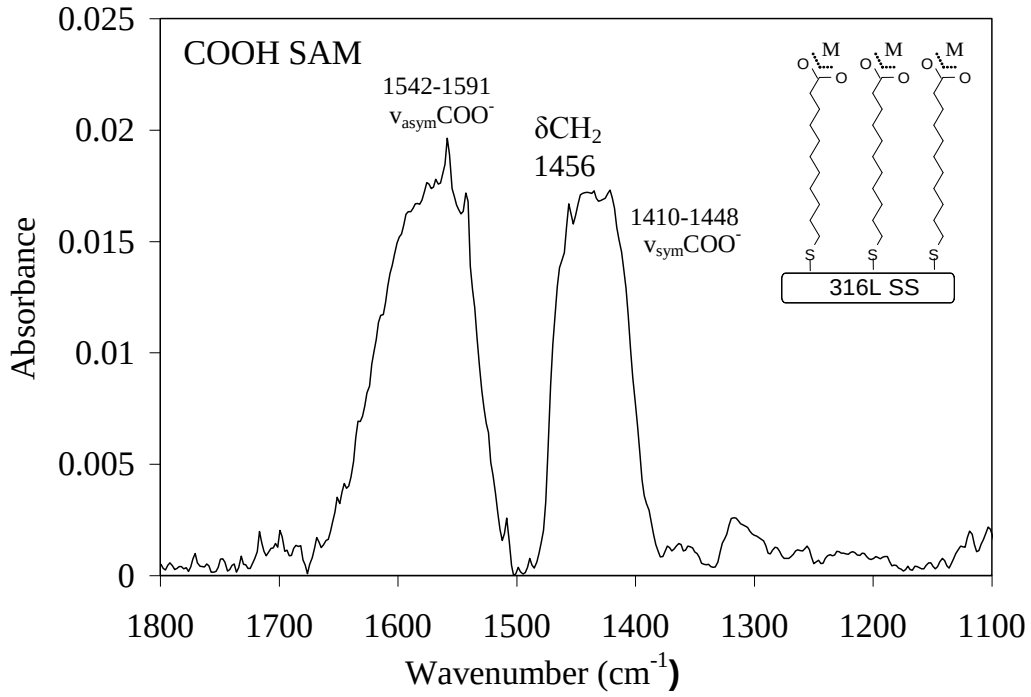

Figure 5.13 1600 cm^{-1} region PM-IRRAS spectra of COO^-/Metal SAM. Inset: representation of the COO^-/Metal SAM. M represents the metal.

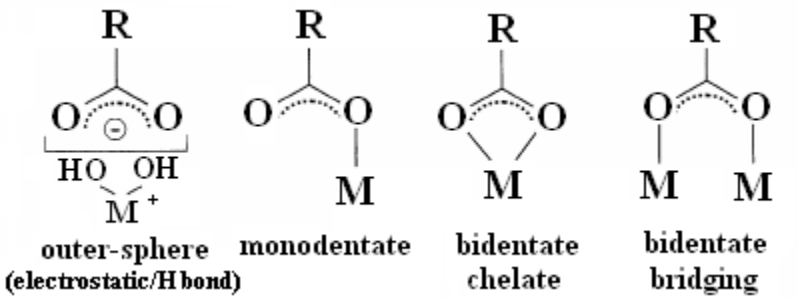

Figure 5.14 Various carboxylate formations (i) outer-sphere (electrostatic/H-bond), (ii) monodentate, (iii) bidentate chelate and (iv) bidentate bridging *Adapted from* [189]

Since it is possible to form carboxylates with any of the following elements, Fe [190], Ni [189] and Cr [191], which were all found in solution after repetitive electrochemical cycling, it is likely the carboxylate SAM was composed of all or some of these species.

Again, since the formation of the COOH SAM was strictly for application of binding proteins/antibodies or drugs, and this was not attainable with freshly-formed COOH SAMs, due to the formation of carboxylates **Figure 5.15** (a), a suitable method had to be developed to destroy the carboxylate/metal complex and produce chemically active COOH groups, while at the same time making sure not to remove the COOH SAM molecules from the surface **Figure 5.15** (b). To the author's knowledge this problem has not been addressed before with self-assembled monolayers.

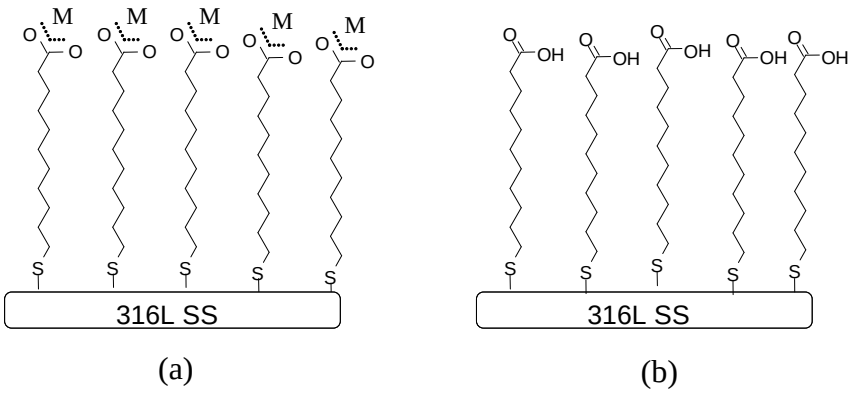

Figure 5.15 Proposed state of COOH SAM (a) undesired carboxylate COOH SAM (b) desired non-carboxltated COOH SAM.

The solution to the problem was to immerse the complexated carboxylate COO^-/Metal SAM into a solution in which the species of the solution would have a thermodynamic tendency to scavenge the metal from the COO^-/Metal SAM surface. It was theorized that weak acids could do this since weak acids, like acetic acid, CH_3COOH, tend to form carboxylates in the presence of metal ions. An example is acetic acid turning into sodium acetate $CH_3COO^-(Na^+)$ in the presence of Na^+ ions. In this case Ni, Fe or Cr ions which were present during the cyclic procedure will act just as the Na^+ ion.

If this theory was valid the following would hold: (1) PM-IRRAS spectra would show a substantial increase in the free $_v$(C=O) group at approximately 1710

cm^{-1} and decrease in the $v_{asym}COO^-$ and $v_{sym}COO^-$ bands, as indicated by the arrows in **Figure 5.16**. (2) With the carboxylic acid group metal-free, it would be possible to undergo chemical reactions such as the n-hydroxylsuccuimide reaction.

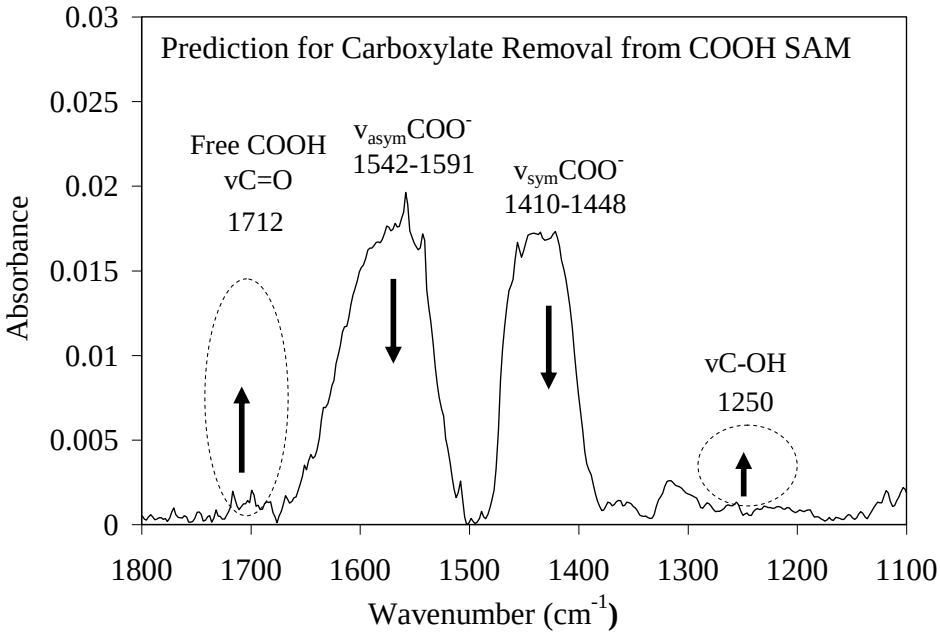

Figure 5.16 1600 cm^{-1} region PM-IRRAS spectra of COO^-/Metal SAM . Arrows represent the predicted peak changes if the Metal from the COO^-/Metal SAM is removed.

The **Figure 5.17** demonstrates that acetic acid was able to cleave some of the metal (M) from the COOH carboxylate. The rise in 1712 cm^{-1} free $_v$(C=O) bond and $_v$(C-OH) at 1250 cm^{-1} with the lowering of the $v_{asym}(COO^-)$ and $v_{sym}(COO^-)$ peaks between 1542-1591 cm^{-1} and 1410-1448 cm^{-1} showed the quantity of COO^- /Metal bonding had lowered significantly and that the first prediction was true. It is important to mention that from sonication stability tests described in **Section 5.1.4**, the sonication of freshly-parepared COOH-terminated SAMs in denatured ethanol, 0.16 M NaCl and 0.1 M NaOH was unable to remove the carboxylate complexes after 6 hrs of sonication. This demonstrates that the metal/carboxylate complex cannot be destroyed simply by brute force.

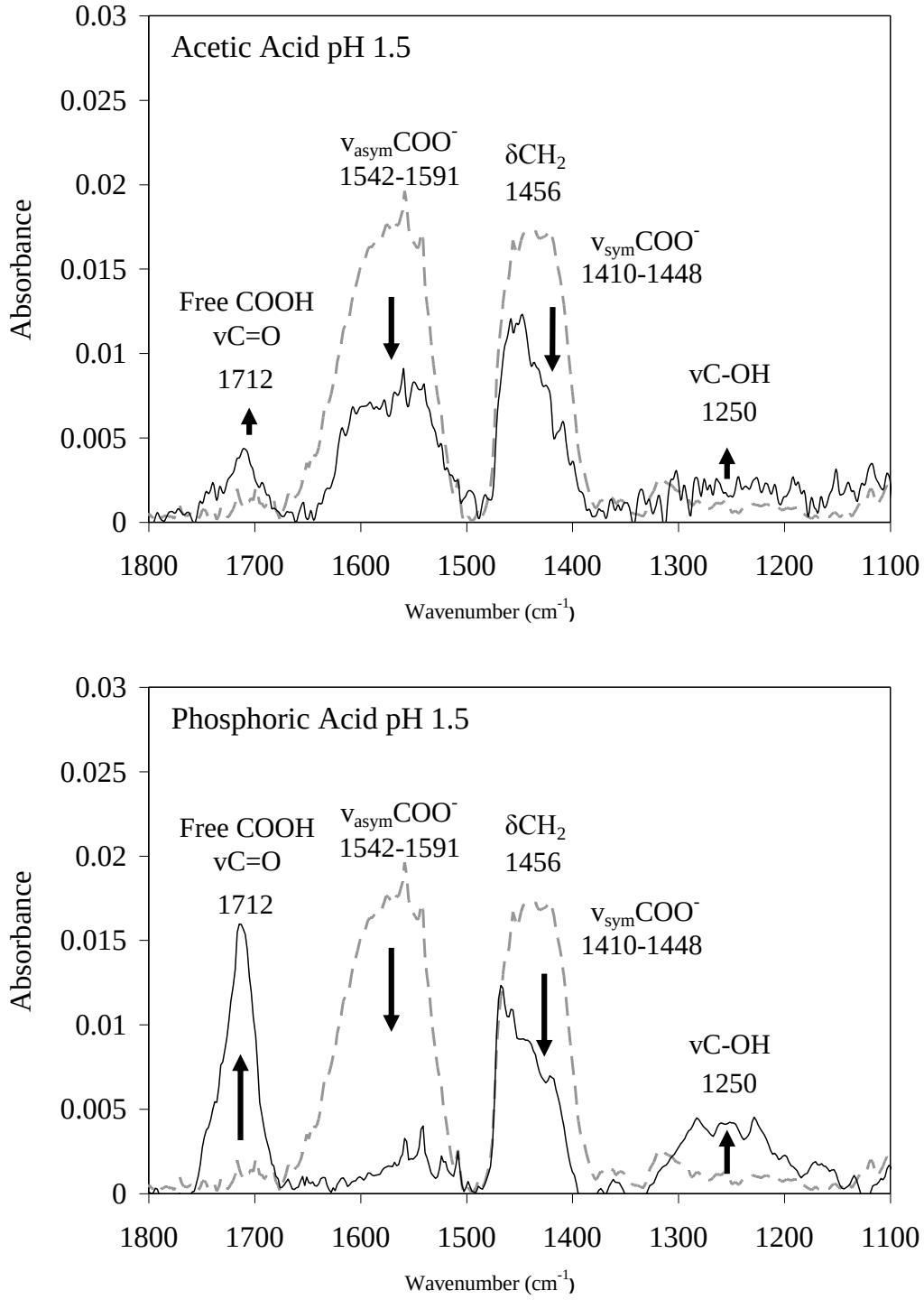

Figure 5.17 1600 cm^{-1} region PM-IRRAS spectra results of metal removal from the COO-/Metal SAM after exposure to (top) acetic acid pH 1.5 (bottom) phosphoric acid pH 1.5 for 30 minutes. Grey and dashed lines are the PM-IRRAS spectra before immersion in the acids. Arrows represent direction of peak change.

The use of phosphoric acid at pH 1.5 was very efficient in removing the COO^-/Metal carboxylate complexes. In fact, phosphoric acid gave the best results among all the investigated acids, and almost completely removed the carboxylate complex (almost no $_v(COO^-)$ peaks were observed after the sample immersion). This result not only shows that phosphoric acid is a good acid to use to remove carboxylates from the surface, but since the COOH SAM is still intact on the surface with intact methylene vibration in the 2900 cm^{-1} and 1456 cm^{-1} regions, the predominant attachment of the COOH-terminated SAM to the 316L SS surface must be through the sulfur group.

Other acids were also studied for the purpose of removing the COO^-/Metal complexes, and the PM-IRRAS spectra are shown in **Figure 5.18**. The strong acids; hydrochloric, nitric and sulfuric acids did not significantly alter the chemical structure of the COOH SAMs that were in the carboxylate state. This was hypothesized to be because strong acids dissociate completely, and therefore would have no inclination to cleave the metal from the COO^-/Metal SAM surface, and associate with Metal. In contrast, the weak acids; acetic, citric, malonic and phosphoric acid do have a tendency to form non-dissociated metal systems in solution, and were therefore able to remove the metal from the SAM surface. The effectiveness of removing the metal from the carboxylated SAMs went in the order: phosphoric (pKa 2.12, 7.21, and 12.32) > citric (pKa 3.14, 4.77 and 6.39) = malonic (pKa 2.83) > and acetic (pKa 4.76) acid.

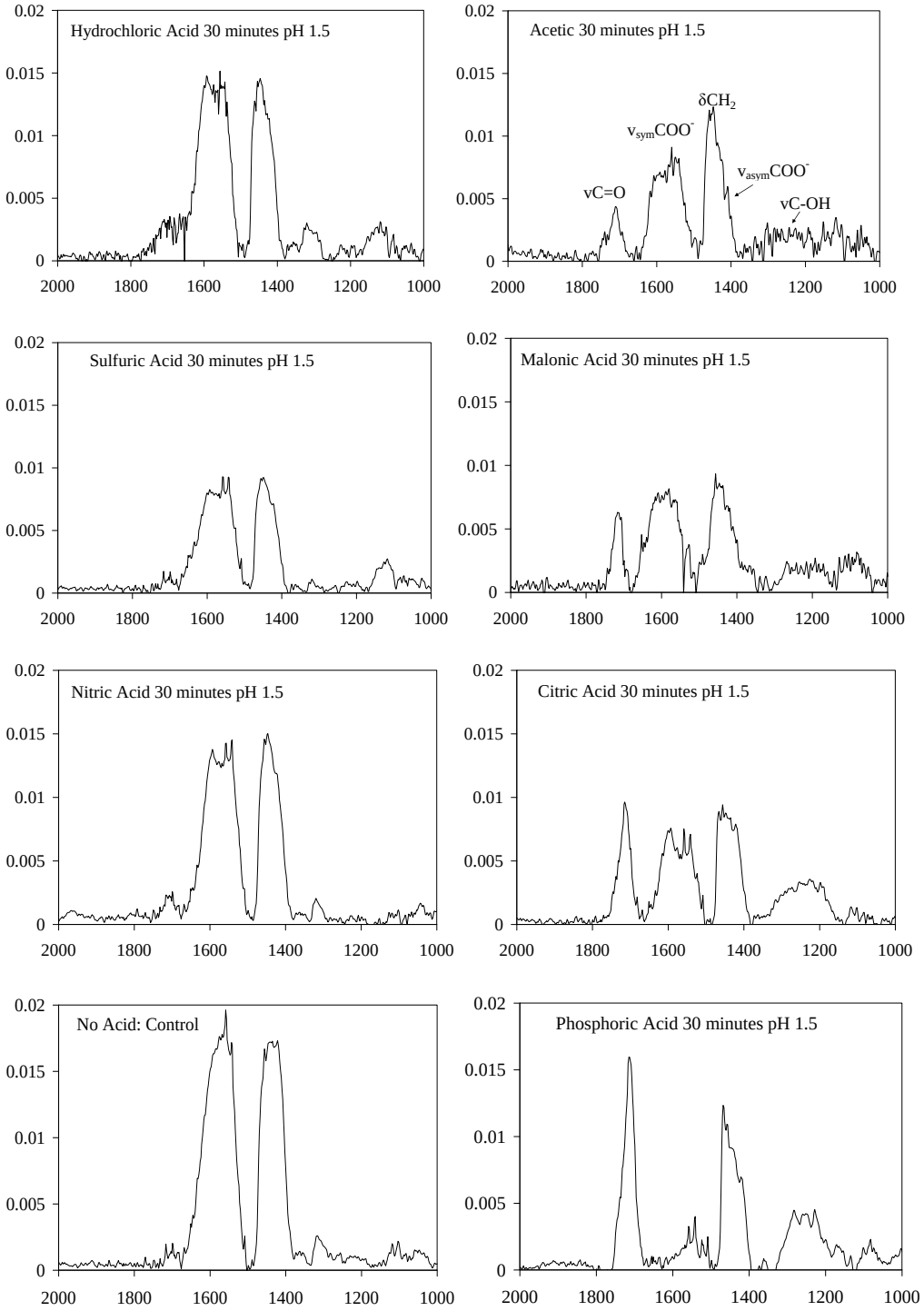

Figure 5.18 1600 cm^{-1} region PM-IRRAS spectra results of metal removal from the COO^-/Metal SAM after exposure to various acids at pH 1.5 for 30 minutes. The control surface was a COOH SAM rinsed with deionized water and denatured ethanol directly after SAM formation.

5.2.5 Contact Angle of NH_2 COOH and CH_3 SAMs

The static contact angle measurements were preformed on the SAMs formed on 316L SS, and the results are presented in **Figure 5.19**, and compared to the literature in **Table 5.3**. This technique can provide useful data on the wettability of the SAM-modified surface.

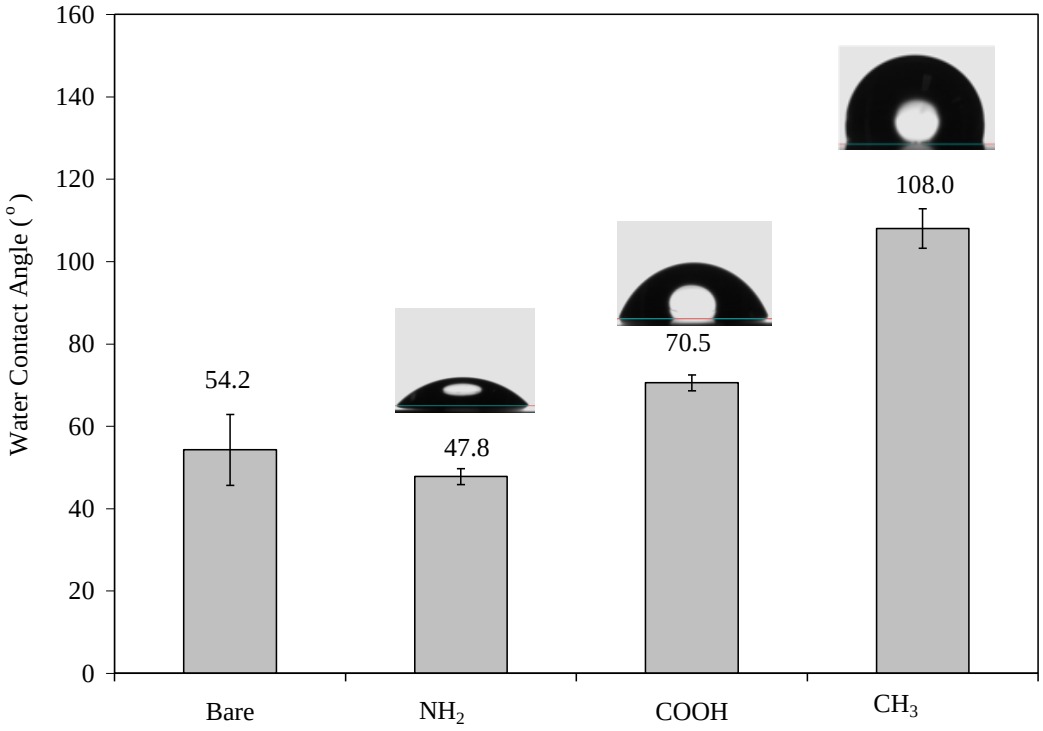

Figure 5.19 Static water contact angle. NH_2, COOH and CH_3 SAMs on 316L stainless steel. Error bars represent ± 1 standard deviation, n=5. Bare is a freshly polished 316L SS.

Table 5.3 Static water contact angle measurements for SAMs on 316L SS (in degrees)

Surface	Harvey 316L SS	Raman 316L SS [14]	Mahaptro 316L SS [38]	Afara Au [181]
Bare 316L SS	54.2 ± 8.6	53.6 ± 3	64 ± 8.8	_
NH_2	47.8 ± 1.9	38 ± 8	_	56.5 ± 3.6
COOH	70.5 ± 1.9	48.6 ± 3	55.4 ± 21.0	51.2 ± 4.3
CH_3	108.0 ± 4.8	104 ± 1	87 ± 18.0	94.7 ± 1.6

NH_2 SAMs decreased the static water contact angle slightly compared to bare 316L SS. Referring to angles measured by Raman et al. and Afara (shown in **Table 5.3**) the angle of $47.8^o \pm 1.9^o$ is somewhere in the middle. NH_2 SAMs created by Mandler had advancing $52^o \pm 3^o$ and reseeding $31^o \pm 3^o$ water contact angles which are in the similar range as measured here [17]. The ability of NH_2 to form hydrogen bonds makes it more hydrophilic. However the methylene groups of the alkane chain of the SAM, if disordered, can be exposed to the surface making the overall surface more hydrophobic. Equally the proportion of charged species NH_3^+ can have an effect on surface wettability.

COOH SAMs were measured directly after electrochemical binding and after 10 minutes of sonication in denatured ethanol to remove surface debris. The measured contact angle $70.5^o \pm 1.9^o$ was quite reproducible, but unexpectedly hydrophobic, when compared to the literature. This unusual behavior is explained by the chelating effects of carboxylate formation of these SAMs that was created during the electrochemical cycling. Due to the COO^- formation and subsequent complexation, rather than the formation of free COOH groups, there was no free OH group to form hydrogen bonds with the water and increase the hydrophilic nature of the surface.

CH_3 SAMs can be easily identified by their contact angle. The contact angle of $108^o \pm 4.8^o$ is consistent with the hydrophobic nature of these SAMs and representative of what is expected from the literature as shown in **Table 6.6**.

5.3 Chapter Summary

For a quick synopsis of what was done in this chapter, the major results on monolayer assembly on stainless steel are summarized below.

i. A novel electrochemical method to bind alkanethiol SAMs of terminal groups NH_2, COOH or CH_3 to a stainless steel surface was developed.

ii. Cyclic voltammagrams during the assembly demonstrated a hydrogen evolution (i.e. surface-) blocking effect of SAMs as the number of cycles increased and the SAMs assembled.

iii. PM-IRRAS spectra supported this observation and showed that indeed the SAM intensity was increasing with each cycle.

iv. Sonication in 0.1 M NaOH, 0.16 M NaCl and ethanol was not capable of destroying the SAMs, demonstrating that the SAMs are tightly bound to the surface.

v. Freshly prepared COOH SAMs were forming undesired carboxylates with a metal (Ni, Cr or Fe). It was discovered that by immersing the complexated metal/COO^- SAM in a solution of weak acids, the removal of the metal and re-construction of –COOH can be done, making the SAM chemically reactive..

Contact angle values of the NH_2 and CH_3 SAMs were similar to the literature. The COOH SAM value was slightly higher than the corresponding literature values, and this may be due to the formation of the metal/carboxylate complex.

CHAPTER 6: RESULTS AND DISCUSSION - PROTEIN IMMOBILIZATION ON STAINLESS STEEL and CELL/SURFACE INTERACTIONS

6.3 Protein Immobilization on 316L SS

In the previous chapter both NH_2 and COOH SAMs were developed onto a 316L stainless steel surface and modified so that they were in a desirable state for protein immobilization. This chapter will literarily build upon the discoveries of the previous chapter and demonstrate how fibronectin (FN) and bovine serum albumin (BSA) were immobilized onto a stainless steel surface.

6.3.1 Glutaraldehyde Modified NH_2 SAMs

One possible way to use NH_2 SAMs as linking molecules is to expose them to a solution of glutaraldehyde, which is a linear alkane five carbon molecule with aldehyde groups (HC=O) at both ends, **Figure 6.1**. The aldehydes readily reacts with free amine groups (NH_2) to form an imine (N=C) bond (**Figure 6.1** step 3). This bond is particularly strong. Once this has occurred, one free aldehyde of the new complex remains exposed to solution and functionalizes the surface. In this state, proteins are particularly susceptible to chemical binding to this 'sticky' surface via the same imine bond reaction through amine groups on the protein (**Figure 6.1** step 4)..

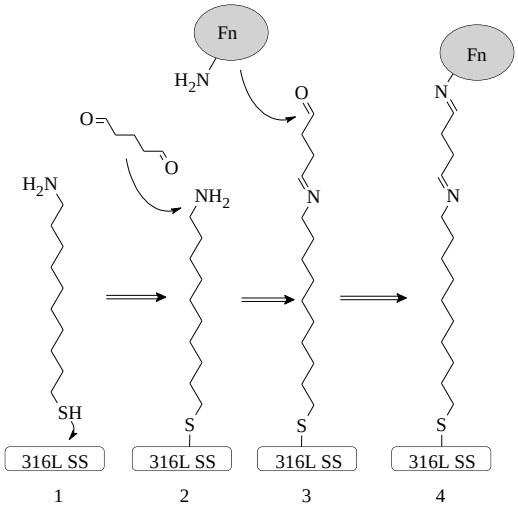

Figure 6.1 Reaction steps for immobilization of fibronectin, FN, using glutaraldehyde and NH_2 SAMs.

The use of glutaraldehyde to link proteins to amine terminated SAMs has been demonstrated many times in the literature [31, 177, 179, 187, 188]. The progress of this reaction in the current project was monitored using PM-IRRAS and was an extremely valuable and quick tool used to identify the surface structures.

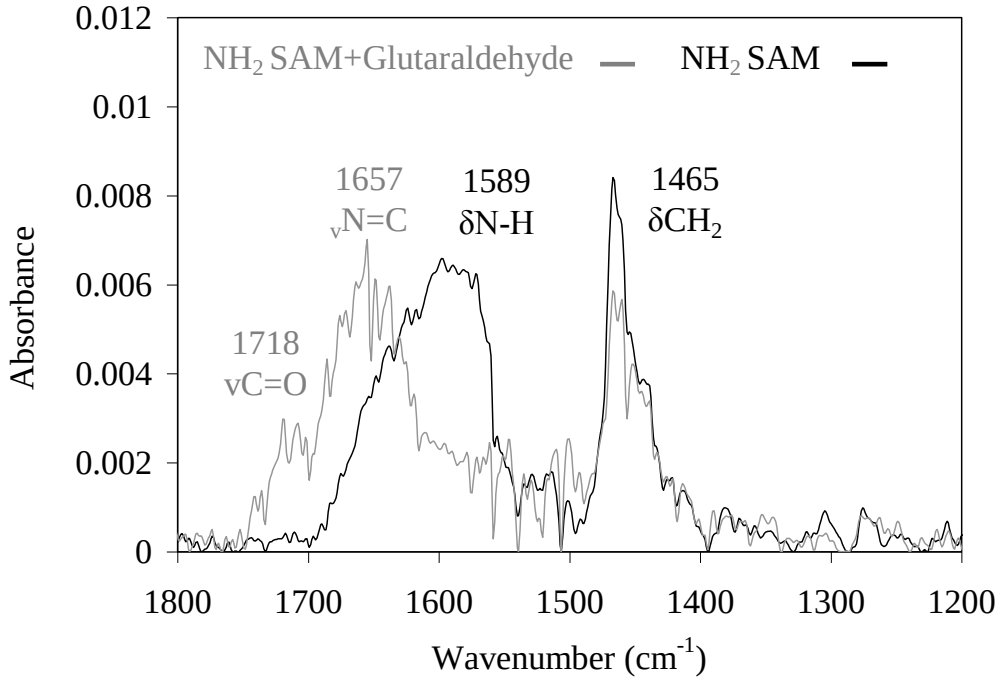

Figure 6.2 1600 cm^{-1} PM-IRRAS spectra of changes to a NH_2 SAM on 316L SS before and after reacting with a 20%v/v solution of glutaraldehyde for 1 hr.

It is clear from **Figure 6.2** that the glutaraldhyde reaction modified most of the free amines of the SAM surface, which were represented by δN-H vibration centered at 1589 cm^{-1}. They were converted to imines, represented by a broad peak of $_{v}N=C$ at 1657 cm^{-1} [192, 193]. It has been suggested to run this reaction in concentrated glutaraldhyde solution to eliminate the glutaraldhyde from bridging itself between multiples amines on the NH_2 SAM using up both alehdyde groups. If glutaraldehyde bridging had occurred there would be no free aldyhde groups at 1718 cm^{-1}. This is not the case, since a large peak at 1718 cm^{-1}, representative of free aldehyde group $_{v}C=O$, is evidently visible. Therefore the surface at this point looks like **Figure 6.1** step 3. This reaction was quite fast

requiring only 1 hr of NH_2 SAM immersion in a 20%v/v solution of glutaraldehyde.

6.3.2 Proof of Covalently Immobilized BSA and FN to NH_2 SAMs

NH_2 SAMs modified with glutaraldhyde were then incubated in BSA and FN solutions, to form the structure presented in **Figure 6.1** step 4. The PM-IRRAS spectra demonstrating the presence of the proteins is shownin **Figure 6.3**.

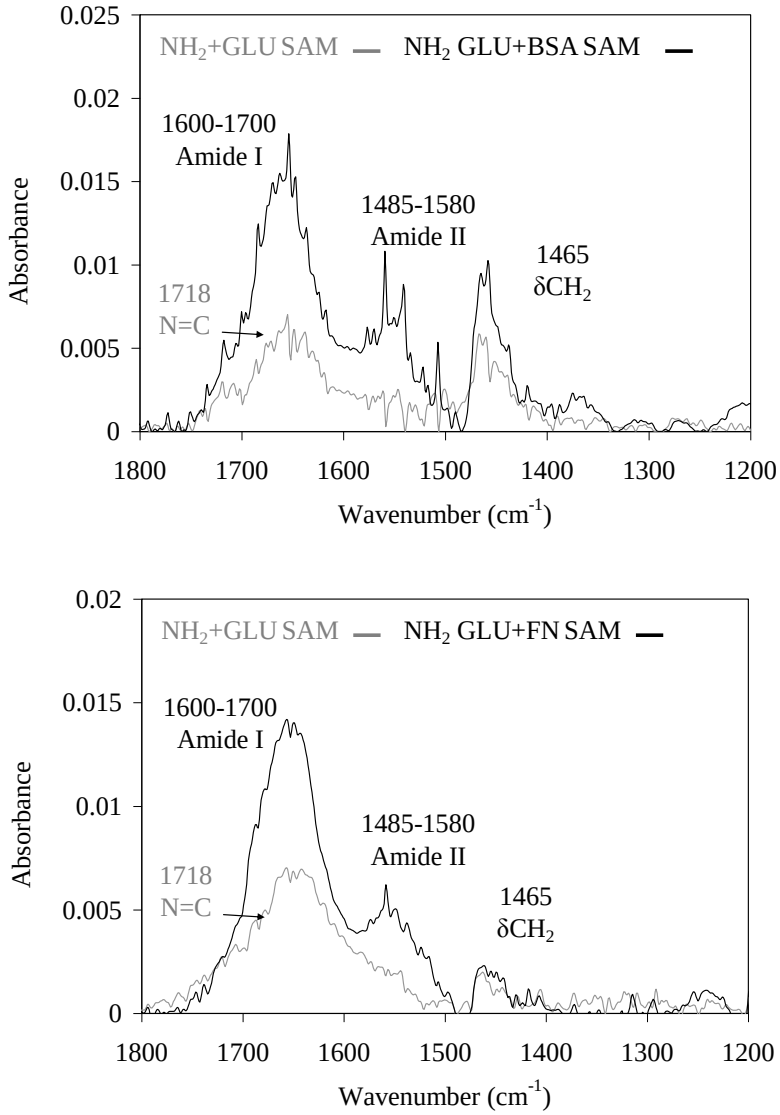

Figure 6.3 1600 cm^{-1} region PM-IRRAS spectra of BSA (top) and FN (bottom) immobilized onto glutaraldhyde modified NH_2 SAMs.

All proteins can be represented by two peaks known as Amide I ≈ 1600-1700 cm^{-1} and Amide II ≈ 1485-1580 cm^{-1} bands. These bands are attributed to C=O stetching, C-N stretching, in plane N-H bending and some C-N stretching; vibrations which are common in most proteins [194]. These peaks are clearly visible in **Figure 6.3** and indicate the presence of BSA and FN proteins.

A controlled experiment was studied in which two groups of samples were run simultaneously with BSA as the model protein to see if the BSA was really immobilized on the NH_2+GLU SAM surface. The control was an NH_2 SAM which should only have physically adsorbed BSA on the surface. These two samples were sonicated in 0.1 M NaOH for 10 minutes and measured using PM-IRRAS before and after. The results are shown in **Figure 6.4**.

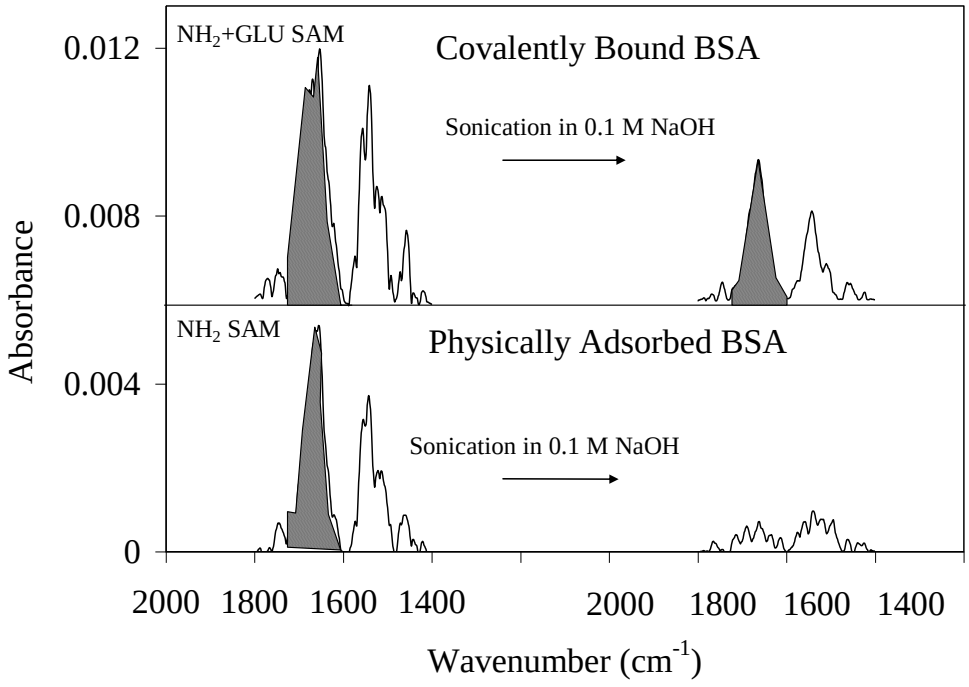

Figure 6.4 1600 cm^{-1} region PM-IRRAS spectra of (BSA) stability after sonication in 0.1 M NaOH. (top) BSA covalently bound to the NH_2+GLU SAM, (bottom) BSA physically adsorbed on the NH_2 SAM. Peaks are Amide I 1600-1700 cm^{-1} (shaded) and Amide II 1485-1580 cm^{-1}.

In both cases the two amide peaks are visible before the sonication, confirming that BSA is indeed present on the surfaces. However, after the

sonication the amide peaks disappeared from the spectra for the physisorbed BSA, indicating that BSA was removed through the sonication. On the other hand, the spectra of the covalently immobilized BSA show the presence of the amide peaks, indicating that the protein remained on this surface. The peaks are smaller than those before the sonication, which is to be expected since not all the BSA will react with the aldehyde groups on the surface and multiple BSA layers may have formed that did not contact the surface directly but were identified by PM-IRRAS. This demonstrated that using NH_2 SAMs with glutaraldhyde linking is a valid method for irreversibly immobilizing proteins onto 316L stainless steel.

6.3.3 N-Hydroxysuccinimide Ester Modified COOH SAMs

As shown in the previous chapter, since carboxylic acid SAMs on 316L SS displayed the desired surface chemistry (free C=O) after acid immersion and the SAMs were determined stable in a range of aggressive environments, they were then further modified to link proteins to the surface just as NH_2 SAMs were. However the procedure is slightly different for COOH SAMs. As shown in the **Figure 6.5,** it was the 1-Ethyl-3-3dimethyl aminopropyl carbodiimide (EDC) and hydroxysuccinimide (NHS) chemistry that was used for protein immobilization. The exact details of this procedure are detailed in the experimental **Section 4.2.2** but shown for reference here.

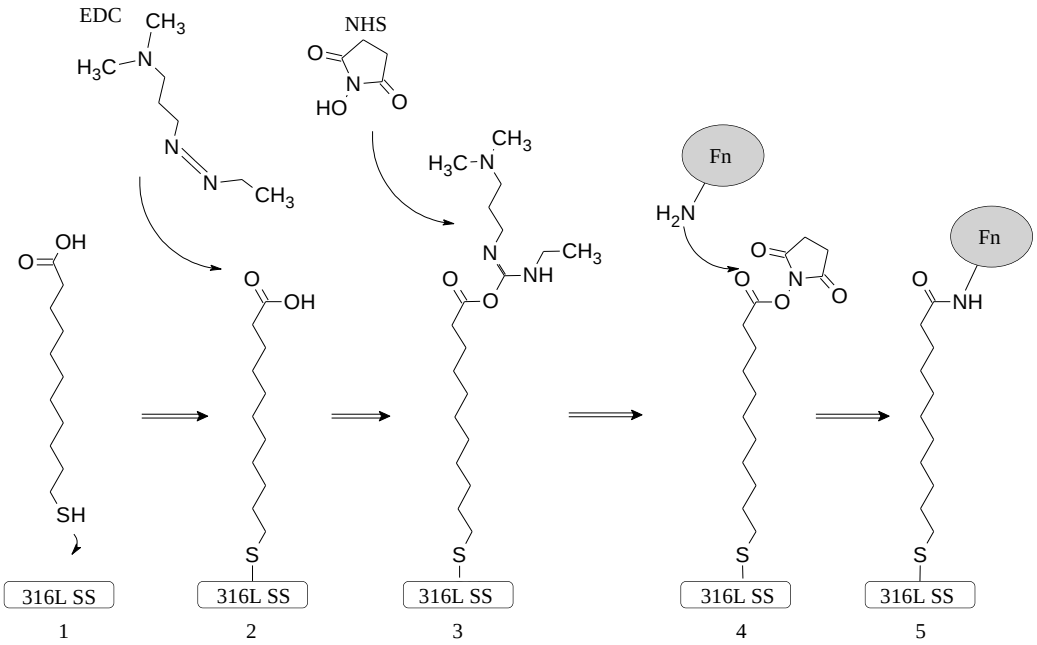

Figure 6.5 NHS/EDC covalent binding of proteins fibronectin (FN) to the COOH SAM on 316L SS.

In this reaction, EDC binds to the COOH SAM forms an intermediate complex with the COOH SAM. However, the formed complex is then easily replaced by NHS to form an ester on the COOH SAM surface (**Figure 6.5** steps 2 to 4) denoted NHS ester SAM.

The formation of an NHS ester SAM was necessary, because it was a reaction intermediate, that could easily be replaced by the amine groups from the protein to form a stable peptide bond on the 316L SS surface **Figure 6.5** step 5. As mentioned previously this chemistry can also be used to attach other amine containing molecules, including certain antibodies or medications or peptides. To validate the presence of NHS molecule covalently bonded to the COOH SAM surface, PM-IRRAS spectra were analyzed. The presences of the peaks representing NHS attachment are shown in **Figure 6.6**.

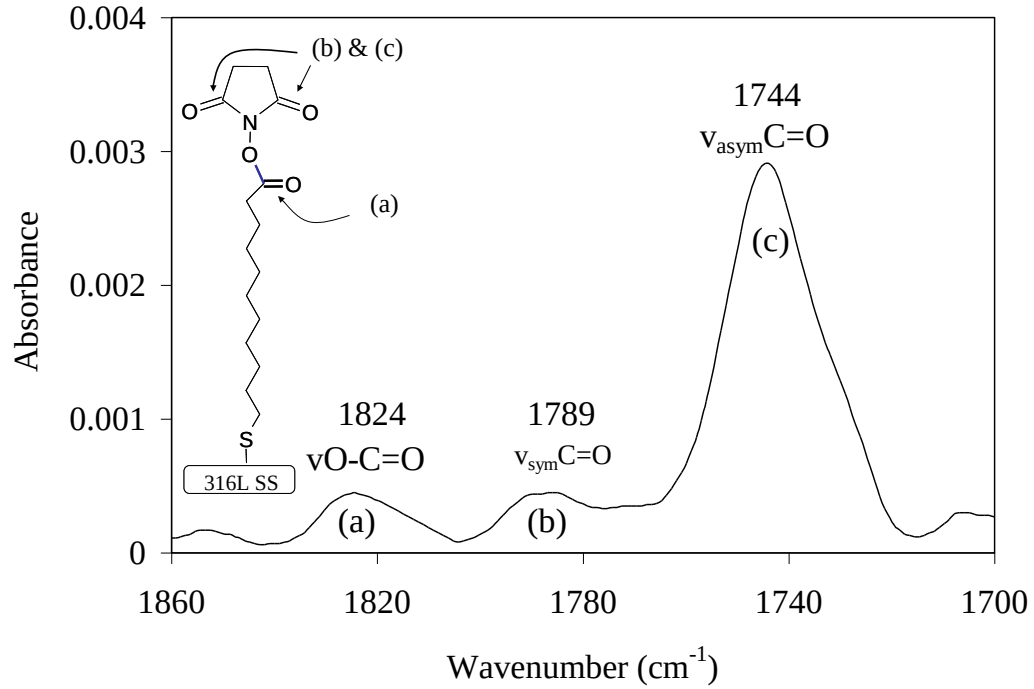

Figure 6.6 PM-IRRAS spectra of NHS SAM Ester on 316L SS after 2 hr immersion in 75 mM EDC and 15 mM NHS. Insert is the molecular schematic representing NHS ester SAM.

The peak frequently observed between 1814-1824 cm^{-1} is due to carbonyl stretch of the NHS as an ester formation on the surface, demonstrating that this is chemisorption rather than physisorption. The other peaks at 1744 cm^{-1} and 1789 cm^{-1} is asymmetric and symmetric carbonyl C=O stretching of the cyclic carbon ring from the NHS molecule.

The optimal soaking time for the COOH SAM reacting with NHS and EDC was determined to be around 2 hrs. The peak at approximately 1744 cm^{-1} was used to represent the quantity of NHS conjugation to the surface, and the peak at 1710 cm^{-1} (**Figure 6.7**) was used to represent un-reacted and free carboxylic acid of the COOH SAM. This reaction progression is clearly evident in **Figure 6.7.** The initial reaction was rapid as shown by a large increase the NHS ester formation peak. In conjunction, as time progressed over 2 hours, the peak around 1710 cm^{-1}, representing free carboxylic acid, was significantly diminished.

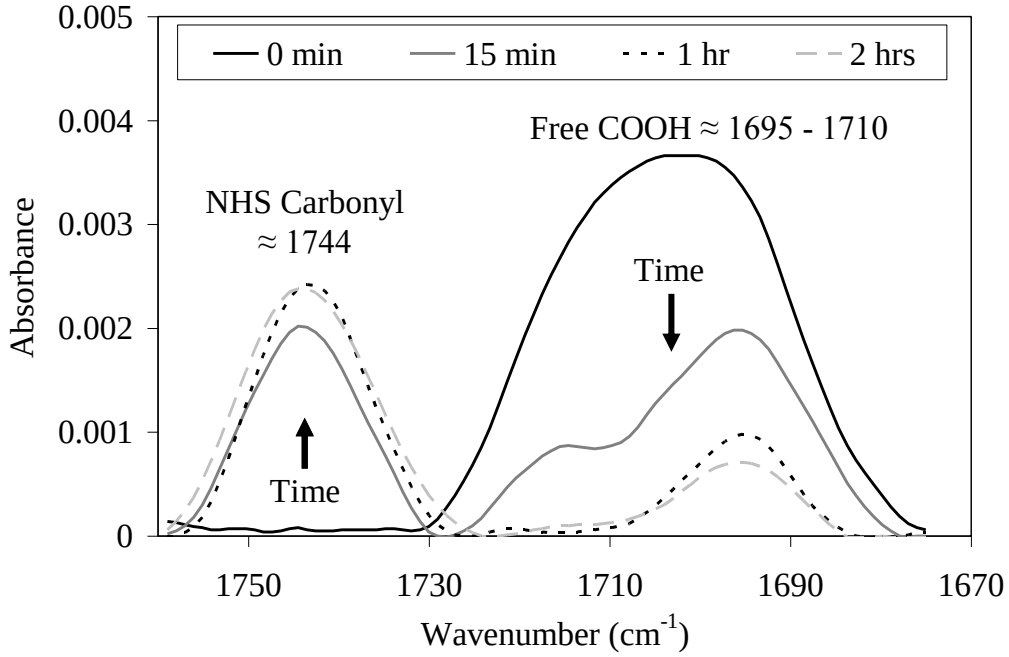

Figure 6.7 1600 cm^{-1} region PM-IRRAS spectra of NHS and EDC reaction on COOH SAM. The spectra was baselined at approximately 1730 cm^{-1} to distinguish between peaks.

To easily visualize the information shown in **Figure 6.7** the normalized integrated intensity (area) of those peaks as function of time is shown in **Figure 6.8**. It can be seen from the graph that a plateau of bound NHS is reached around 60 minutes and there is no statistical difference in the amount of NHS bound to the surface for increasing the reaction time. However given these operating conditions when building up these SAMs, this reaction was run for 120 minutes to increase confidence that the reaction had in fact fully gone to completion.

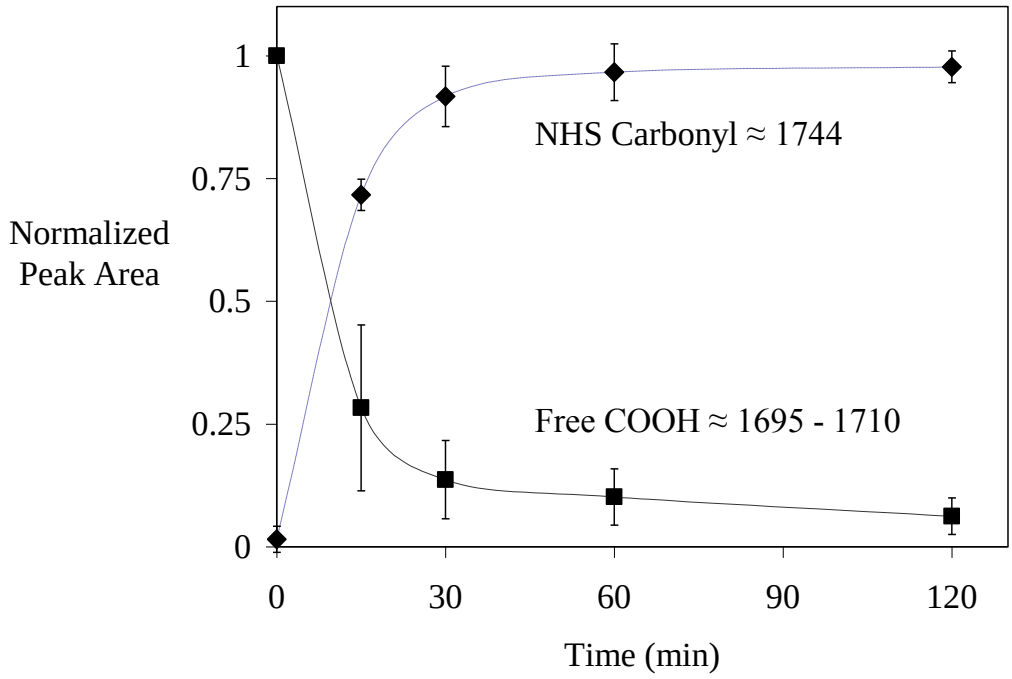

Figure 6.8 Normalized area of the NHS asymmetric carbonyl peak C=O at approximately 1740 cm^{-1} and the free unreacted COOH peak at approximately 1710 cm^{-1} as a function of time. The error bars represent ± 1 standard deviation from the mean, n=3.

6.3.4 Proof of Covalently Immobilized Fibronectin to COOH-SAMs

When a protein contacts the NHS ester, the NHS ester bond is broken and substituted with a more stable NH_2 amine from the protein, **Figure 6.5**. The advantage of this design as discussed previously is that the protein is now more firmly attached to the surface and robust to removal under shear flow compared to simply phsysisorbed protein. The protein removal tests were conducted exactly the same way as the BSA removal experiments for the NH_2 + glutaraldhyde SAMs (**Figure 6.4**); sonication in 0.1 M NaOH for 10 minutes. The results are presented in **Figure 6.9**.

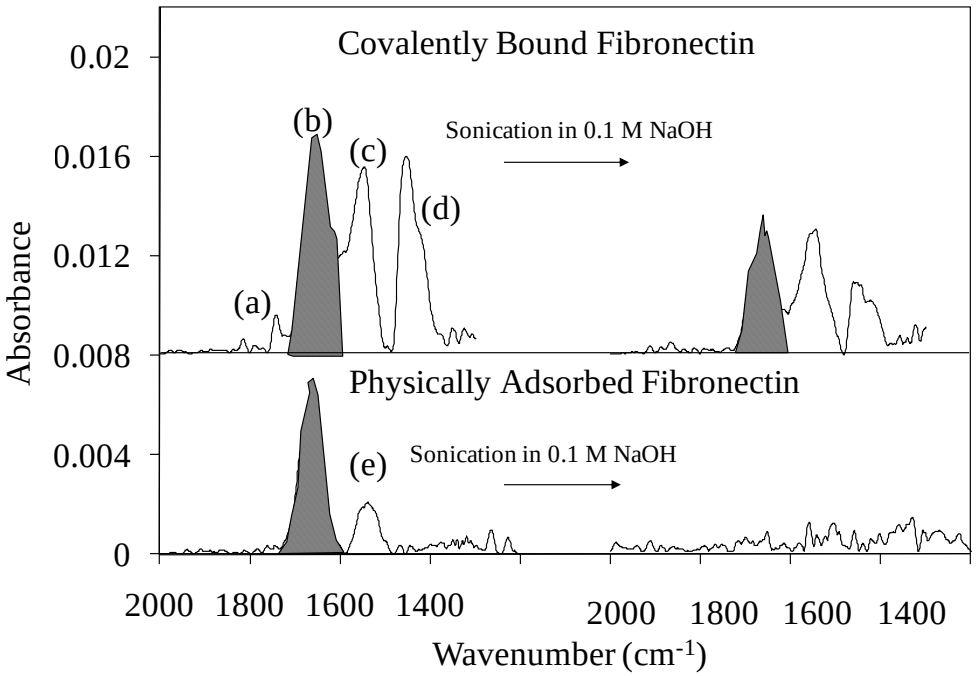

Figure 6.9 1600 cm^{-1} region PM-IRRAS spectra of (top) covalently bound FN to NHS ester SAM (bottom) physically adsorbed FN to bare 316L SS. (a) NHS ester peaks 1824 cm^{-1}, 1789 cm^{-1}, 1744 cm^{-1}. (b) Amide II 1600-1700 cm^{-1} (c) $\nu_{asym}COO^-$ 1542-1591 cm^{-1} with Amide II 1485-1580 cm^{-1} (d) $_{sym}COO^-$ with δCH_2 1456 cm^{-1} (e) only Amide II 1485-1580 cm^{-1}. Amide I peak is shaded to represent quantity of FN for visual effect.

The results of this experiment indicated that after 0.1 M NaOH sonication the NHS ester peak at 1744 cm^{-1} was completely removed (top plot). This was to be expected since NHS esters are particularly unstable in water over the long term and prone to hydrolysis. Using 0.1 M NaOH only sped up the process.

The major observation in **Figure 6.9** is that after sonication, physisorbed FN was completely removed from the 316L SS surface, while a significant amount of the FN covalently attached to the NHS SAM still remained on the 136L SS surface.316L SS The quantification of the amounts was made by the integrated intensity of the amide peaks in the PM-IRRAS spectra and presented in **Figure 6.10**.

48% of the FN remained on the covalently bound FN compared to 0.5% on the control p=0.006. Actually, the author of the thesis believes that even more than 48% of FN remained on the surface, since some of the FN identified before sonication may have been physisorbed FN that did not react with the NHS, or the FN was not in direct contact with the surface due to multiple layer buildup. Namely, the rinsing procedure performed before the 'before sonication' samples were analyzed was not able to remove all non-covalently attached FN, which was then identified by PM-IRRAS. However, these FN molecules were then easily removed by sonication in 0.1M NaOH.

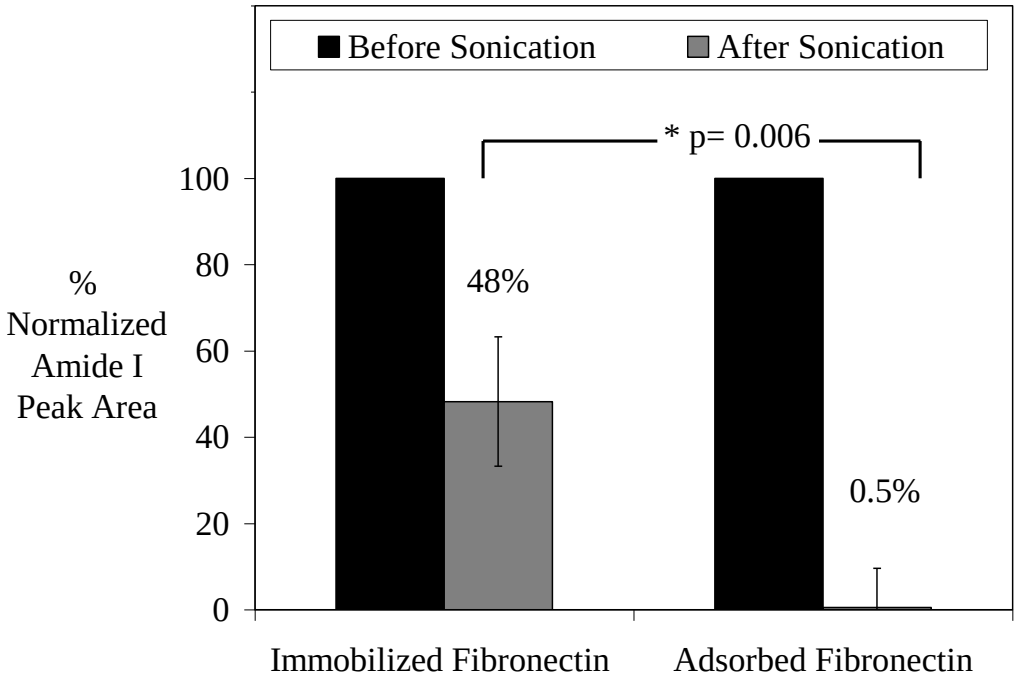

Figure 6.10 Normalized amide I peak area representing fibronectin. (left) immobilized FN on NHS ester SAM (right) adsorbed FN on bare 316L SS surface. Sonication was 0.1 M NaOH for 10 minutes, followed by dionized water and denatured enthanol rinsing. Error bars represent 95% confidence intervals, n=3.

These tests have demonstrated that NHS/EDC chemistry can efficiently be used to immobilize fibronectin to a stainless steel surface, and that the protein displayed superior surface stability compared to physically adsorbed fibronectin.

6.4 Endothelial Cell Attachment on Covalently Immobilized Fibronectin on COOH SAMs

The previous sections demonstrated that FN can be efficiently attached to the 316L SS surface using the novel electrochemical SAM-formation method developed by the thesis author. The final objective of the project was to demonstrate that such a modified 316L SS surface was a better substrate for endothelial cell (EC) attachment than the bare 316L SS surface, which is commonly used for coronary stents. Namely, FN plays a strong role in cell attachment and subsequent proliferation on substrates [161, 172] and our initial hypothesis was that the FN-modified 316L SS surface would be morel EC-biocompatible than the bare 316L SS surface. To investigate this, the FN-coated COOH-SAM 316L SS surface was tested for EC/surface interactions (cell attachment) and the results are presented in **Figure 6.11**.

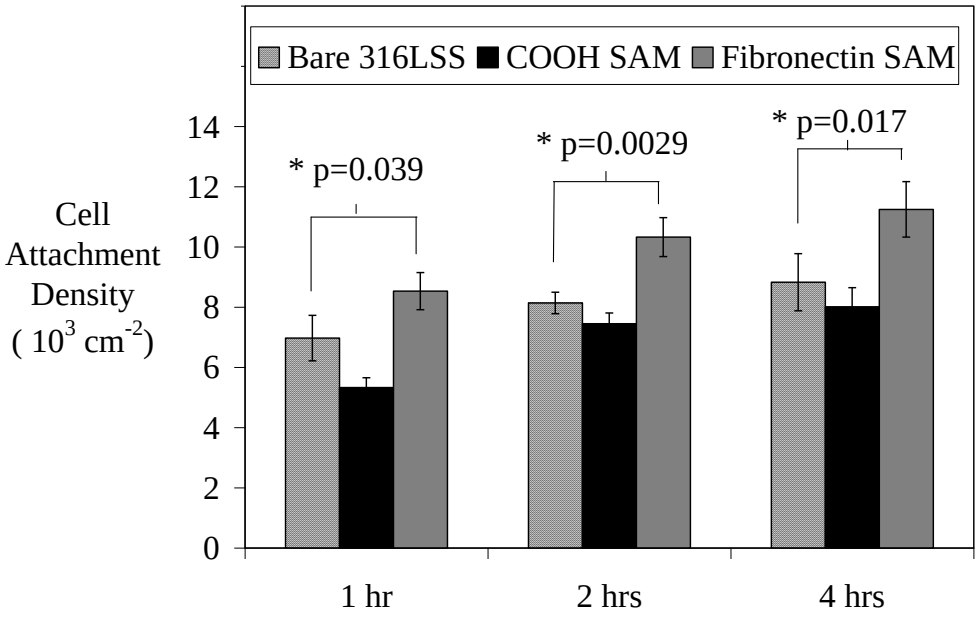

Figure 6.11 human umbilical vascular endothelial, HUVE, cell attachment onto 316L SS modified substrates for 1, 2 and 4 hrs of incubation. Initial incubation was 50,000 cells/cm^2: Error bars are ± 95% confidence interval, n=4. Fibronectin immobilized to the NHS ester SAM and COOH SAM.

The cell density was measured and compared between a control (bare 316L SS), and a COOH terminated SAM. The results of the experiment indicate the trend of increasing cell attachment with time on all substrates, demonstrating that none of the surfaces are cytotoxic. The FN COOH SAM surface showed approximately 22%, 21%, and 25% improvement in cell density compared to the bare 316L SS surface at 1, 2 and 4 hrs, respectively, at a significance of $p<0.05$ in all cases.

These results are similar to those observed by a laboratory colleague Nadia Afara who had an FN COOH SAM system developed on gold [181]. She observed EC attachment improvement of 20-30% on these substrates up to 4 hrs. As well, the results obtained here are also comparable; 20-50% improvement in endothelical cell attachment observed in a recently published paper, on the effects of endothelial cell attachment to anti-CD34 immobilized onto polycaprolactone spin coated stents. [195]. Relating back to **Figure 6.11**, the augmented cell attachment to the modified surfaces indicates that the immobilization of FN onto the COOH-modified 316L SS surface does not affect FN's structure and function sufficiently to inhibit integrin attachment to the RGD and PHSRN cell binding sequences [196, 197]. Therefore it is quite likely that the COOH SAM on 316L SS surface provided a suitable environment for the attainment of the elongated (open conformation) [198] of covalently bound FN, and it was a positive factor to influence endothelial cell attachment.

In conclusion, the results in **Figure 6.11** are quite promising since they demonstrate that the FN-modified 316L SS is indeed more biocompatible then the naked 316L SS surface, which is currently used in practice. However, due to the simplicity of in vitro cell testing environment, endothelial cell attachment tests can only demonstrate proof of concept. It is only after *in vivo* testing, the more realistic situation, can one really determine if FN-modified stents actively suppress restenosis.

CHAPTER 7: CONCLUSIONS

7.1 Thesis Summary and Conclusions

In this work the development of a new alkanethiol SAM formation procedure on 316L SS and the feasibility of enhancing endothelial cell attachment to a 316L stainless steel surface (stent) through irreversible immobilization of fibronectin was investigated. The following conclusions can be drawn from this work.

i. A novel electrochemical method to bind alkanethiol self-assembled monolayers (SAMs) of terminal groups NH_2, COOH or CH_3 to a stainless steel surface was developed.

ii. The alkanethiols SAMs displayed enhanced surface stability in a variety of solvents; as demonstrated by the SAMs withstanding sonication in 0.1 M NaOH, 0.16 M NaCl and ethanol for over 6 hrs.

iii. Polarization Modulation Infrared Reflection Absorption Spectroscopy, PM-IRRAS, was a valuable tool for identification and characterization of monolayer chemistry on the stainless steel surface.

iv. It was discovered that soaking a COOH SAM modified surface in selected weak acids was the solution to remove undesired metal/carboxylate complexes from the SAM, and make the SAM chemically reactive. To the author's knowledge this technique has not be suggested previously.

v. Glutaraldehyde was easily linked to NH_2 SAM modified surfaces to immobilize bovine serum albumin (BSA) and fibronectin (FN).

vi. N-hydroxysuccinimide (NHS) and 1-ethyl-3-[3dimethyl aminopropyl] carbodiimide (EDC) coupling agents were used on COOH SAM modified surfaces to immobilize FN as well.

vii. Immobilized proteins were considerably more stable on the 316L stainless steel surface than physically adsorbed proteins (which almost completely desorbed) after rigorous 0.1 M NaOH sonication.

viii. Endothelial cell attachment to the FN-modified 316L SS surface was enhanced by approximately 25% after 4 hrs of incubation compared to a bare 316L stainless steel surface, thus demonstrating the surface's higher biocompatibility for blood-contacting implants

ix. The procedures developed in this thesis have many applications. There are a wide range of biologically active organics; proteins, pharmaceuticals, polymers or antibodies that can be immobilized to a 316L SS stent surface using these procedures. Therefore the work provided here is an excellent starting block for future stent designs. In addition, the newly developed SAM-formation method can be used for a range of other biomedical and industrial applications that involve 316L stainless steels (bone implants, corrosion protection, sensors development, etc.)

It is the eventual hope of this author that a viable solution for minimizing in-stent restenosis is developed in the years to come. Investigation into novel stent designs such as the one proposed here will eventually lead to better understanding and therefore more effective cardiovascular devices to lower morbidity and mortality of patients suffering from cardiovascular diseases.

CHAPTER 8: REFERENCES

1. Johansen H., et al., *Diseases of the Circulatory System- Hospitalization and Mortality*. Health Reports, 2005. **17**(1): p. 49-52.
2. *The American Heart and Stroke Foundation: Heart Disease and Stroke Statistics 2008 Update*. 2008 [cited August 2008; Available from: http://www.americanheart.org/downloadable/heart/1200082005246HS_Stats%202008.final.pdf.
3. CDC Wonder. *Centers for Disease Control and Prevention*. 2005 [cited August 2008; Available from: http://wonder.cdc.gov/cmf-icd10.html.
4. Belanger A., *Population Projections for Canada Provinces and Territories*, in *Statistics Canada*. 2005.
5. Batchelor WB., et al., *Contemporary outcome trends in the elderly undergoing percutaneous coronary interventions: Results in 7,472 octogenarians.* Journal of American College of Cardiology, 2000. **36**: p. 723-730.
6. Ross R., *Atherosclerosis — An Inflammatory Disease.* New England Journal of Medicine, 1999. **340**(2): p. 115-126.
7. Hill R., et al., *Drug-eluting stents: an early systematic review to inform policy* European Heart Journal, 2004. **25**(11): p. 902-919.
8. Conte MS., et al., *Endothelial cell seeding influences lesion development following arterial injury in the cholesterol-fed rabbit.* Cardiovascular Research, 2002. **1**(53): p. 502-511.
9. Raman A., et al., *Formation of Self-Assembled Monolayers of Alkylphosphonic Acid on the Native Oxide Surface of SS316L*. Langmuir, 2006. **22**: p. 6469-6472.
10. Harm U., et al., *Novel protective coatings for steel based on a combination of self-assembled monolayers and conducting polymers.* Macromolecules Symposium, 2002.
11. Van Alsten., *Self-Assembled Monolayers on Engineering Metals: Structure, Derivatization and Utility.* Langmuir, 1999. **15**: p. 7605-7614.
12. Pellerite MJ., Dunbar TD., and Boardman LD., *Effects of Fluorination on Self-Assembled Monolayer Formation from Alkanephoshonic Acids on Aluminum: Kinetics and Structure.* Journal of Physical Chemistry B, 2003. **107**(42): p. 11726-11736.
13. Foster TT., et al., *Friection Force Microscopy of Alkylphosphonic Acid and Carboxylic Acids Adsorbed on the Native Oxide of Aluminum.* Langmuir, 2006. **22**: p. 9254-9259.
14. Raman A. and Gawalt ES., *Self-Assembled Monolayers of Alkanoic Acids on the Native Oxide Surface of 316LSS by Solution Deposition.* Langmuir, 2007. **23**: p. 2284-2288.
15. Shustak G., Domb AJ., and Mandler D., *n-Alkanoic Acid Monolayers on 316L Stainless Steel Promote the Adhesion of Electropolymerized Polypyrrole Films.* Langmuir, 2006. **22**: p. 5237-5240.
16. Shustak G., Domb AJ., and Mandler D., *Preparation and Characterization of n-Alkanoic Acid Self-Assembled Monolayers Adsorbed on 316L Stainless Steel.* Langmuir, 2004. **20**: p. 7499-7506.
17. Shustak G., et al., *Electrostatic Attachment of Gold and PLA Nanoparticles onto Aminoalkanoic Acid Self-Assembled Monolayers on 316L Stainless Steel.* Chemistry a European Journal, 2007. **13**: p. 6402-6407.

18. Bigelow W. and Pickett D., *Oleophobic monolayers films adsorbed from solution in non-polar liquids.* Journal of Colloid Science, 1946. **1**(6): p. 513-538.
19. Ruan CM., et al., *Creation and characterization of n-alkylthiol and n-alkylamine self-assembled monolayers on 316L stainless steel.* Thin Solid Films 2002(419): p. 95–104.
20. Mekhalif Z., et al., *Elaboration of Self-Assembled Monolayers of n-Alkanethiols of Nickel Polycrystalline Substrates: Time, Concentration and Solvent Effects.* Langmuir, 2003. **19**(3): p. 637-645.
21. Mekhalif Z., et al., *Self-Assembled Monolayers of n-Dodecanethiol on Electrochemically Modified Polycrystalline Nickel Surfaces.* Langmuir, 1997. **13**: p. 2285-2290.
22. Benji S., et al., *Electrochemical Self-Assembly of Alkanethiolate Molecules on Ni(111) and Polycrystalline Ni Surfaces.* Journal of Physical Chemistry B, 2005. **109**(49): p. 23450-23460.
23. Brukman MJ., et al., *Nanotribological Properties of Alkanephosphonic Acid Self-Assembled Monolayers on Aluminum Oxide: Effects of Fluorination and Substrate Crystallinity.* Langmuir, 2006. **22**: p. 3988-3998.
24. Gawalt ES., et al., *Bonding Organics to Ti Alloys: Facilitying Human Osteoblast Attachment and Spreading on Surgical Implant Materials.* Langmuir, 2003. **19**: p. 200-204.
25. Gawalt ES., et al., *Sefl-Assembly and Bonding of Alkanephosphonic Acids on the Native Oxide Surface of Titanium.* Langmuir, 2001. **17**: p. 5736-5738.
26. Sukenik CN., et al., *Modulation of cell adhesion by modification of titanium surfaces with covalently attached self-assembled monolayers.* Journal of Biomedical Materials Research, 1990. **24**: p. 1307-1323.
27. Volmer M., Stratmann M., and Viefhaus H., *Electrochemical and Electron Spectroscopic Investigations of Iron Surfaces Modified with Thiols.* Surface and Interface Analysis, 1990. **16**(27): p. 282.
28. Pavelko GF., *Reactions of thiols and organic disulfides with iron and its oxides.* Russian Chemical Bulletin International Edition, 2006. **55**(8): p. 1436-1439.
29. Petrovykh DY., et al., *Alkanethiols on Platinum: Multicomponent Self-Assembled Monolayers.* Langmuir, 2006. **22**: p. 2578-2587.
30. Yan L., et al., *Formation and reaction of interchain carboxylic anhydride groups on self-assembled monolayers on gold* Langmuir, 1997. **13**: p. 6704-6712.
31. Zamborini FP. and Crooks RM., *Corrosion Passivation of Gold by n-Alkanethiol Self-Assembled Monolayers: Effect of Chain Length and End Group.* Langmuir, 1998. **14**(12): p. 3279-3286.
32. Xiao Y., Ju H-X., and Chen H-Y., *Hydrogen peroxide sensor based on horseradish peroxidase-labeled Au colloids immobilized on gold electrode surface by cysteamine monolayer.* Analytica Chimica Acta 1999(391): p. 73-82.
33. Godin M., *Design of a Differential Cantilever-Based Sensor*, in *Department of Physics*. 2000, McGill: Montreal.
34. Hanson EL., et al., *Bonding Self-Assembled, Compact Organophosphonate Monolayers to Native Oxide Surface of Silicon.* Journal of Amermican Chemical Society, 2003. **125**: p. 16074-16080.

35. Briand E., et al., *Building of an immunosensor: How can the composition and structure of the thiol attachment layer affect the immunosensor efficiency?* Biosensors and Bioelectronics 2006. **22**: p. 440-448.
36. Jiang D., et al., *Covalently coupling the antibody on an amine-self-assembled gold surface to probe hyaluronan-binding protein with capacitance measurement.* Biosensors and Bioelectronics, 2003. **18**: p. 1183-1191.
37. Shervedani R. and Mozaffari S., *Preparation and electrochemical characterization of a new nanosensor based on self-assembled monolayer of cysteamine functionalized with phosphate groups.* Surface & Coatings Technology, 2005(198): p. 123-128.
38. Mahapatro A., et al., *The use of alkanethiol SAMs on 316L SS for coronary artery stent nanomedicine applications: an oxidative and in vitro stability study.* Cardiovascular Nanomedicine, 2006(2): p. 182-190.
39. Keselowsky BG., Collard DM., and Garcia AJ., *Surface chemistry modulates fibronectin conformation and directs integrin binding and specificity to control cell adhesion.* Journal of Biomedical Materials Research, 2003(66A): p. 247-259.
40. Cong P., Igari T., and Mori S., *Effects of film characteristics on frictional properties of carboxylic acid monolayers.* Tribology Letters, 2000. **9**(3-4): p. 175-179.
41. Tan YS., et al., *Effects of ring subsituents on the protective properties of self-assembled benzenethiols on copper.* Corrosion Science, 2006. **48**: p. 840-862.
42. Whelan CM., et al., *Corrosion inhibition by self-assembled monolayers for enhanced wire bonding on Cu surfaces.* Microelectronic Engineering, 2003. **70**(2-4): p. 551-557.
43. Kuhnle A., *Self-assembly of organic molecules at metal surfaces.* Current Opinions in Colloid & Interface Science, 2008. **14**(2): p. 157-168.
44. Smith RK., Lewis PA., and Weiss PS., *Patterning self-assembled monolayers.* Progress in Surface Science, 2004(75): p. 1-68.
45. Poirier GE., *Characterization of Organosulfur Molecular Monolayers on Au(111) using Scanning Tunneling Microscopy.* Chem. Rev. , 1997. **97**: p. 1117-1127.
46. Poirier GE., *Coverage-Dependent Phases and Phase Stability of Decanethiol on Au(111).* Langmuir, 1999. **15**: p. 1167-1175.
47. Kondoh H., et al., *Molecular processes of adsorption and desorption of alkanethiol monolayers on Au(111).* Journal of Chemical Physics, 1999. **111**(3): p. 1175-1184.
48. Gawalt E., *Patent: Modified Metal Compositions, process for preparing the same, and biomaterials resistant to surface cell adhesion*. 2006: US 2007/0077440 A1.
49. Mahapatro A., et al., *Surface Modification of Functional Self-Assembled Monolayers on 316L Stainless Steel via Lipase Catalysis.* Langmuir, 2006. **22**(3): p. 901-905.
50. Johnson DM., et al., *Drug Delivery from Therapeutic Self-Assembled Monolayers (T-SAMs) on 316L Stainless Steel.* Current Topics in Medicinal Chemistry, 2008. **8**(4): p. 281-289.
51. Zhang H., Romero C., and Baldelli S., *Preparation of Alkanethiol Monolayers on Mild Steel Surfaces Studied with Sum Frequency Generation and Electrochemistry.* Journal of Physical Chemistry B, 2005. **109**: p. 15520-15530.

52. Sinapi F., et al., *Assessment by XPS and electrochemical techniques of two molecular organosilane films prepared on stainless steel surface.* Surface and Interface Analysis, 2004. **36**: p. 1484-1490.
53. Muller R., et al., *Surface engineering of stainless steel materials by covalent collagen immobilzation to improve implant biocompatibility.* Biomaterials 2005. **26**: p. 6962-6972.
54. Minier M., et al., *Covalent Immobilization of Lysozyme on Stainless Steel. Interface Spectroscopic Characterization and Measurement of Enzymatic Activity.* Langmuir, 2005. **21**: p. 5957-5965.
55. Gawalt ES., *Patent: Modified Metal Compositions, process for preparing the same, and biomaterials resistant to surface cell adhesion*. 2006: US 2007/0077440 A1.
56. Domb AJ., et al., *Modified Conductive Surfaces Haiving Active Substances Attached Thereto*, C.I.P. Office, Editor. 2006: Canada.
57. Burkitt HG. and Young JW., *Wheater's Functional Histology*. 3rd. ed. 1993, Edinburgh: Churchill Livingstone.
58. Panza JA. and Cannon RO., eds. *Endothelium, Nitric Oxide and Atherosclerosis*. 1999, Futura Publishing Company Inc.: Armonk, NY.
59. Pearson JD., *Endothelial cell function and thrombosis.* Bailleres Best Pract Res Clin Haematol., 1999. **12**(3): p. 329-341.
60. Pober JS. and Cotran RS., *The Role of Endothelial Cells in Inflammation.* Transplantation, 1990. **50**(4): p. 537-544.
61. Zarins CK. and Taylor CA., eds. *Hemodynamic Factors in Atherosclerosis*. Vascular Surgery A Comprehensive Review 6th edition 2002, W.B. Saunders company Toronto. 105-114.
62. Cornwell TL, Boerth ANJ, and Lincoln TM, *Inhibition of smooth muscle cell growth by nitric oxide and activation of cAMP-dependent protein kinase by cGMP*. Cell Physiology, 1994. **267**(5): p. 1405-1413.
63. Schwartz SM., Campbell GR., and Campbell JH., *Replication of smooth muscle cells in vascular disease.* Circulation Research, 1986. **58**: p. 427-444.
64. Invitrogen. *Introduction to vascular biology*. August 2009]; Available from: http://www.invitrogen.com/site/us/en/home/Products-and-Services/Applications/Cell-Culture/primary_cell_culture/PCC-Misc/vascular-biology.html.
65. Ross R., *Atherosclerosis: An Inflammatory Disease: Review Article.* New England Journal of Medicine, 2007. **340**(2): p. 117-.
66. Nieuwland R., et al., *Cell-derived microparticles generated in patients during cardiopulmonary bypass are highly procoagulant.* Circulation 1997. **96**(10): p. 3534-3541.
67. Naghavi M. and Johnson MC., *A Paradigm Shift in Cardiology. The Discovery of Vulnerable Plaque*. 2008, Association of Eradication of Heart Attack: http://www.youtube.com/watch?v=a8Idk4EUYTs&feature=user.
68. Nucleus. *Coronary Artey Angioplast (Heart Stent).* 2008; Available from: http://www.youtube.com/watch?v=N7nghr9TpSU.

69. MFMER. *Coronary angioplasty and stenting: Opening clogged heart arteries*. 2009 August 17th 2009]; Available from: http://www.riversideonline.com/health_reference/Articles/HQ00485.cfm.
70. Nucleus_Medial_Art, *Coronary Stent Procedure*. 2009.
71. Leaf A., et al., *Do fish oils prevent restenosis after coronary angioplasty?* Circulation, 1994. **90**(5): p. 2247-2257.
72. Zierler RE. and S. DE., *Hemodynamics for the Vascular Surgeon*, in *Vascular Surgery: A Comprehensive Review*. 2002, W.B. Saunders Company: Toronto.
73. Dee KC., Puleo DA., and Bizios R., *An Introduction To Tissue Biomaterial Interactions*, J.W. Sons, Editor. 2002: Canada.
74. Harker LA., et al., *Homocystine-induced arteriosclerosis. The role of endothelial cell injury and platelet response in its genesis.* J Clinical Invest., 1976. **58**(3): p. 731-741.
75. Burt H and Hunter W, *Drug-Eluting stents: A multidisciplinary success story.* Advanced Drug Delivery Reviews 2006(58): p. 350-357.
76. Karas SP., et al., *Coronary intimal proliferation after balloon injury and stenting in swine: an animal model of restenosis.* J Am Coll Cardiol 1992(20): p. 467–74.
77. Campbell GR. and Campbell JH., *Recent Advances in Molecular Pathology: Smooth Muscle Phenotypic Changes in Arterial Wall Homeostasis: Implications for Pathogenesis of Atherosclerosis.* Experimental and Molecular Pathology, 1985(42): p. 139-162.
78. Toutouzas K., Colombo A., and Stefanadis C., *Inflammation and restenosis after percutaneous coronary interventions.* European Heart Journal, 2004. **24**(19): p. 1679-1687.
79. Kipshidze N., et al., *Role of the endothelium in modulating neointimal formation: Vasculoprotective approaches to attenuate restenosis after percutaneous coronary interventions.* j Am Coll Cardiol, 2004. **44**(4): p. 733-739.
80. Unknown, *Biographical Scetches Andreas Gruentzig*. 2008, Angioplasty.org.
81. Topol EJ., et al., *A Comparison of Directional Atherectomy with Coronary Angioplasty in Patients with Coronary Artery Disease.* New England Journal of Medicine, 1993. **329**: p. 221-227.
82. Holmes DR., et al., *Restenosis after precutaneous transluminal coronary angioplasty (PTCA): a report from the PTCA registry of the national heart, lung and blood institute.* American Journal of Cardiology, 1984. **15**(12): p. 77C-81C.
83. Serruys PW., et al., *A comparison of Balloon-Expandable-Stent Implantation with Balloon Angioplasty in Patients with Coronary Artery Disease.* New England Journal of Medicine, 1994. **331**: p. 489-495.
84. Fischman DL., et al., *A randomized comparison of coronary-stent placement and balloon angioplaty in the treatment of coronary artery disease.* New England Journal of Medicine, 1994(331): p. 496-501.
85. Spaulding C., et al., *A Pooled Analysis of Data Comparing Sirolimus-Eluting Stents with Bare-Metal Stents.* New England Journal of Medicine, 2007. **356**(10).
86. Stettler C., et al., *Outcomes associated with drug-eluting and bare metal stents: a collaborative network meta-analysis.* The Lancet, 2007. **370**(9591): p. 937-948.
87. Stoeckel D., Bonsignore C., and Duda S., *A survey of stent designs.* Min Invas Ther & Allied Technol 2002. **11**(4): p. 137-147.

88. Shih C., et al., *Stability of passivated 316L stainless steel oxide films for cardiovascular stents.* Journal of Biomedical Materials Research Part A, 2006. **67A**(4): p. 1320-1328.
89. Zhao H., et al., *Electrochemical polishing of 316L stainless steel slotted tube coronary stents.* Journal of Materials Science: Materials in Medicine, 2002. **13**: p. 911-916.
90. Aoki J., et al., *Endothelial Progenitor Cell Capture by Stents Coated With Antibody Against CD34* Clinical Research Interventional Cardiology, 2005(45): p. 1574-1579.
91. Kereiakes DJ., et al., *Usefulness of a Cobalt Chromium Coronary Stent Alloy.* American Journal of Cardiology, 2003(92): p. 463-466.
92. Ortolani P., et al., *Randomized Comparative Trial of a Thin-Strut Bare Metal Cobalt-Chromium Stent Versus a Sirolimus-Eluting Stent for Coronary Revascularization.* Catherization and Cardiovascular Intervention, 2007. **69**: p. 790-798
93. Barth KH., et al., *Paired Comparison of Vascular Wall Reactions to Palmaz Stents, Strecker Tantalum Stents, and Wallstents in Canine Iliac and Femoral Arteries* Circulation, 1996(93): p. 2161-2169.
94. Barth KH., et al., *Flexible Tantalum Stents Implanted in Aortas and Iliac Arteries: Effects in Normal Canines.* Radiology, 2000(175): p. 91-96.
95. Hijazi Z., et al., *A new platinum balloon-expandable stent (Angiostent) mounted on a high pressure balloon: acute and late results in an atherogenic swine model.* J Invas Cardiol 1995. **7**(5): p. 127-34.
96. Trost D., et al., *Three-dimensional MR angiography in imaging platinum alloy stents.* Journal of Magnetic Resonance Imaging 2004. **20**(6): p. 975-980.
97. Heublein B., et al., *Biocorrosion of magnesium alloys: a new principle in cardiovascular implant technology?* Heart, 2004. **89**(6): p. 651-6.
98. Di Mario C., et al., *Drug-Eluting Bioabsorbable Magnesium Stent.* Journal of Interventional Cardiology, 2004. **117**(6): p. 391-395.
99. Mania G., et al., *Coronary stents: A materials perspective.* Biomaterials 2007. **28**: p. 1689-1710.
100. Heintz C., et al., *Corroded Nitinol Wires in Explanted Aortic Endografts: An Important Mechanism of Failure?* J Endovasc Therapy, 2001. **8**: p. 248-253.
101. Han RO., et al., *Comparison of Self-Expanding and Balloon-Expandable Stents for the Reduction of Restenosis.* Am J Cardiology, 2001. **88**: p. 253-259.
102. Stoeckel D., Pelton A., and Duerig T., *Self-expanding nitinol stents: material and design considerations.* Eur Radiol 2004. **14**: p. 292-301.
103. Ryhanen J., *Biocompatibility evaluation of nickel-titanium shape memory metal alloy*, in *Faculty of Medicine*. 1999, University of Oulu.
104. Cragg AH., et al., *Nitinol intravascular stent: results of preclinical evaluation.* Radiology, 1993. **189**: p. 775-778.
105. Grenadier E., et al., *Self-expandable and higly flexible nitinol stent: immediate and long- term results in dogs.* Am Heart J, 1994. **128**: p. 870-878.
106. Sheth S., et al., *Subacute thrombosis and vascular injury resulting from slotted-tube nitinol and stainless steel stents in a rabbit carotid arter model.* Circulation, 1996(94): p. 1733-1740.

107. Zartner P., et al., *First Successful Implantation of a Biodegradable Metal Stent Into the Left Pulmonary Artery of a Preterm Baby.* Catherization and Cardiovascular Interventions, 2005. **66**: p. 590-594.
108. Waksman R., et al., *Safety and Efficacy of Bioabsorbably Magnesium Alloy Stents in Porcine Coronary Arteries.* Catherization and Cardiovascular Interventions, 2006. **68**: p. 607-617.
109. Harding SA., et al., *Long-term clinical safety and efficancy of NIROYAL vs. NIR intracoronary stents.* Catherization and Cardiovascular Intervention, 2001(54): p. 141-145.
110. von Dahl J., Haager PK., and Grube E., *Effect of gold coatings of coronary stents on neointimal proliferation following sten implantation.* American Journal of Cardiology, 2002. **89**: p. 801-805.
111. Menown I., Lowe R., and Penn I., *Review: Passive Stent Coatings in the Drug-Eluting Era.* Journal of Invasive cardiology 2005(17): p. 222-228.
112. Windecker S., et al., *Stent Coating With Titanium-Nitride-Oxide for Reduction of Neointimal Hyperplasia.* Circulation, 2001(104): p. 928-933.
113. Windecker S., et al., *Randomized Comparison of a Titanium-Nitride-Oxide–Coated Stent With a Stainless Steel Stent for Coronary Revascularization*
The TiNOX Trial Circulation, 2005(111): p. 2617-2622.
114. Haase J., et al., *Comparison of Stainless-Steel Stents Coated with Turbostratic Carbon and Uncoated Stents for Percutaneous Coronary Interventions.* Journal of Invasive cardiology, 2003. **15**(10): p. 562-565.
115. Morice MC., et al., *Direct stenting of de nono coronary stenoses with tacrolimus-eluting versus carbon-coated carbostents. The randomized JUPITER II trial.* EuroIntervention, 2006. **2**: p. 45-52.
116. Gutensohn K., et al., *In Vitro Analyses of Diamond-like Carbon Coated Stents: Reduction of Metal Ion Release, Platelet Activation and Thrombogenicity.* Thrombosis Research, 2000(99): p. 577-585.
117. Korkmaz ME., et al., *Carbon Coating of Stents Has No Effect on Imflammatory Response to Primary Stent Deployment.* Angiology, 2002(53).
118. Rzany A., Harder C., and Schaldach M., *Silicon Carbide as an Anti-Thrombogenic Stent Coating: An Example of a Science-Based Development Strategy.* Progress in Biomedical Research, 2000(5): p. 168-177.
119. Heublein B., Ozbek C., and Pethig K., *Silicon Carbide-Coated Stents: Clinical Experimence in Coronary Lesions With Increased Thrombotic Risk.* Journal of Endovascular Surgery, 1998(5): p. 32-41.
120. Amon M., Bolz A., and Schaldach M., *Improvement of stenting therapy with a silicon carbide coated tantalum stent.* Journal of Materials Science: Materials in Medicine, 1996(7): p. 273-278.
121. Bickel C., et al., *Substantial Reduction of Platelet Adhesion by Heparin-Coated Stents.* Journal of Interventional Cardiology, 2001. **14**(4).
122. FDA. *TAXUS™ Express²™ Paclitaxel-Eluting Coronary Stent System FDA Approved*
2004; Available from: http://www.fda.gov/cdrh/mda/docs/p030025.html.
123. Kothwala D., et al., *Paclitaxel Drug Delivery from Cardiovascular Stent.* Trends Biomaterials and Artifical Organs, 2006. **19**(2): p. 88-92.

124. Faxon DP., et al., *Low molecular weight heparin in prevention of restenosis after angioplasty: results of Enoxaparin Restenosis (ERA) trial.* Circulation, 1994. **90**: p. 908-914.
125. Cao W., et al., *Effects of rapamycin on growth factor-stimulated vascular smooth muscle cell DNA synthesis: inhibition of basic fibroblast growth factor and platelet-derived growth factor action and antagonism of rapamycin by FK506.* Transplantation, 1995(59): p. 390-395.
126. Stone GW., et al., *Safety and Efficacy of Sirolimus- and Paclitaxel-Eluting Coronary Stents.* New England Journal of Medicine, 2007. **356**: p. 998-1008.
127. Kastrati A., et al., *Analysis of 14 trials Comparing Sirolimus-Eluting Stents with Bare-Metal Stents.* New England Journal of Medicine, 2007. **356**: p. 1030-9.
128. Tu JV., et al., *Effectiveness and Safety of Drug-Eluting Stents in Ontario.* N Eng J Med, 2007(357): p. 1393-1402.
129. Joner M., et al., *Pathology of Drug-Eluting Stents in Humans.* Journal of American College of Cardiology, 2006. **48**(1): p. 193-202.
130. Wardeh AJ., et al., *ß-Particle–Emitting Radioactive Stent Implantation A Safety and Feasibility Study* Circulation, 1999. **100**(1684-1689).
131. Sheppard R. and Eisenberg MJ., *Intracoronary radiotherapy for restenosis.* New England Journal of Medicine, 2001(344): p. 295-297.
132. Kay IP. and Wardej AJ., *Radioactive stents delay but do not prevent in-stent neointimal hyperplasia.* Circulation, 2001. **103**: p. 14-17.
133. Shirotaa T., et al., *Fabrication of endothelial progenitor cell (EPC)-seeded intravascular stent devices and in vitro endothelialization on hybrid vascular tissue* Biomaterials, 2003. **24**(13): p. 2295-2302
134. Rotmans JI., et al., *In Vivo Cell Seeding With Anti-CD34 Antibodies Successfully Accelerates Endothelializations but Stimulates Intimal Hyperplasia in Procine Arteriovenous Expanded Polytetrafluoroethylen Grafts.* Circulation, 2005.
135. Consigny P., *Endothelial cell seeding on prosthetic surfaces.* J. Long Term Eff Med Implants, 2000. **10**(1-2): p. 79-95.
136. Scott NA., et al., *Clinical Investigation.* American Heart Journal, 1995. **129**(5): p. 860-865.
137. Topol EJ. and Serruys PW., *Frontiers in Interventional Cardiology* Circulation, 1998. **98**: p. 1802-1820.
138. Koren B., et al., *Efficient transduction and seeding of human endothelial cells onto metallic stents using bicistronic pseudo-typed retroviral vectors encoding vascular endothelial growth factor.* Cardiovasc Revasc Med, 2006. **7**(3): p. 173-178.
139. Whelan DM., et al., *Biocompatibility of phosphorylcholine coated stents in normal porcine coronary arteries. Heart*, 2000(83): p. 338-345.
140. Hårdhammar PA., et al., *Reduction in Thrombotic Events With Heparin-Coated Palmaz-Schatz Stents in Normal Porcine Coronary Arteries.* Circulation, 1996. **93**: p. 423-430.
141. Yoshioka T., et al., *Preparation of alginic acid layers on stainless-steel substrates for biomedical applications* Biomaterials, 2003. **24**(17): p. 2889-2894.

142. Suh KY., et al., *Characterization of chemisorbed hyaluronic acid directly immobilized on solid substrates* Journal of Biomedical Materials Research Part B: Applied Biomaterials, 2004 **72B**(2): p. 292-298.
143. Thierry B., et al., *Biodegradable membrane-covered stent from chitosanbased polymers.* Journal of Biomedical Materials Research Part A, 2005. **75A**(3): p. 556-566.
144. Blindt R, et al., *A Novel Drug-Eluting Stent Coated With an Integrin-Binding Cyclic Arg-Gly-Asp Peptide Inhibits Neointimal Hyperplasia by Recruiting Endothelial Progenitor Cells* Journal of the American College of Cardiology, 2006. **47**(9): p. 1786-1795
145. Kutryk MJ. and Kuliszewski MA., *In Vivo Endothelial Progenitor Cell Seeding for the Accelerated Endothelialization of Endovascular Devices.* . Presented at Transcatheter Cardiovascular Therapeutics 2003.
146. Kutryk M., Cottone R., and Maxwell R., *Medical Device with Coating That Promotose Endothelial Cell Adherence*. 2007: United States of America.
147. Orbus Medical Technology. *Endothelial Progenitor Cell (EPC) Capture Technology for the Prevention of In-stent Thrombosis and Restenosis*. 2004; Available from: http://www.orbusneich.com/genous/literature/Genous-Overview.pdf.
148. Feng Y. and Mrksich M., *The synergy Peptide PHSRN and the Adhesion Peptide RGD Mediate CEll Adhesion through a Common Mechanism.* Biochemistry, 2004. **43**(50): p. 15811-15821.
149. Geiger B., et al., *Transmembrane Extracellular Matrix-cytoskeleton crosstalk.* Nature Reviews, 2001. **2**: p. 793-805.
150. Schultz GS., Ladwig G., and Wysocki A., *Extracellular matrix: review of its roles in acute and chronic wounds.* Would Wide Wounds, 2005.
151. Mao Y. and Schwarzbauer JE., *Fibronectin fibrillogenesis, a cell-mediated matrix assembly process: Mini Review.* Matrix Biology, 2005(24): p. 389-399.
152. Carey DJ., *Control of Growth and Differentiation of Vascular Cells by Extracellular Matrix Proteins.* Annu. Rev. Physiol. , 1991(53): p. 161-177.
153. Sakai T., et al., *Plasma fibronectin supports neuronal survival and reduces brain injury following transient focal cerebral ischemia but is not essential for skin-wound healing and hemostasis*
Nature Medicine, 2001(7): p. 324-330.
154. Ni H., et al., *Plasma fibronectin promotes thrombus growth and stability in injured arterioles.* PNAS, 2002. **100**(5): p. 2415-2419.
155. Astrof S., Crowley D., and Hynes RO., *Multiple cardiovascular defects caused by the absence of alternateively spliced segments of fibronectin.* Developmental Biology, 2007(311): p. 11-24.
156. Allio AE. and McKeown-Longo P., *Extracellular matrix assembly of cellderived and plasma-derived fibronectins by substrate-attached fibroblast.* Journal of Cell Physiology, 1988(135): p. 459-466.
157. Darribere T. and Schwarzbauer JE., *Fibronectin matrix composition and organization can regulate cell migration during amphibian development.* Mechanisms of Development 2000(92): p. 239-250.

158. Mao Y. and Schwarzbauer JE., *Fibronectin fibrillogenesis, a cell-mediated matrix assembly process: Mini Review.* Matrix Biology 2005(24): p. 389-399.
159. Potts JR. and Campbell ID., *Fibronectin structure and assembly.* Current opions in Cell Biology, 1994. **6**: p. 648-655.
160. Schwarzbauer J., *Identification of the Fibronetin Sequences Required for Assembly of a Fibrillar Matrix.* The Journal of Cell Biology, 1991. **113**(6): p. 1463-1473.
161. Johansson S., et al., *Fibronectin-Integrin Interactions.* Frontiers in Bioscience, 1997(2): p. 126-146.
162. Schwarzbauer J. and Sechler J., *Fibronectin fibrillogenesis: a paradigm for extracellular matrix assembly.* Current opions in Cell Biology, 1999(11): p. 622-627.
163. RO, H., *Integrins: Versatility, Modulation and Signaling in Cell Adhesion.* Cell, 1992. **69**: p. 11-25.
164. Johansson S, et al., *Fibronectin-Integrin Interactions.* Frontiers in Bioscience, 1997(2): p. 126-146.
165. Williams E., et al., *Conformational States of Fibronectin.* The Journal of Biological Chemistry, 1982. **257**(24): p. 14973-14978.
166. Aguirre K., McCormick J., and Schwarzbauer J., *Fibronectin Self-associationI s Mediated by Complementary Sites within the Amino-terminal One-third of the Mole.* The Journal of Biological Chemistry, 1994. **269**(45): p. 27863-2786.
167. Johnson K., et al., *The compact Conformation of Fibronectin is Determined by Intramolecular Ionic Interactions.* The Journal of Cell Biology, 1999. **274**(22): p. 15473-15479.
168. Wierzbicka-Patynowski I. and Schwarzbauer J., *The ins and outs of fibronectin matrix assembly.* Journal of Cell Science, 2003. **116**: p. 3269-3276.
169. Mosher DF and Furcht LT, *Fibronectin: Review of its Structure and Possible Functions.* Journal of Investigative Dermatology, 1981(77): p. 175-180.
170. Magnuson MA. and Mosher DF., *Fibronectin: Structure, Assembly and Cardiovascular Implications.* Arteriosclerosis, Thrombosis, and Vascular Biology, 1998. **18**(9).
171. Manabe R., et al., *Modulation of cell-adhesive activity of fibronectin by the alternatively spliced EDA segment.* The Journal of Cell Biology, 1997(139): p. 295-307.
172. McKeown-Longo P. and Mosher DF., *Binding of Plasma Fibronectin to Cell Layers of Human Skin Fibroblasts.* The Journal of Cell Biology, 1983. **97**: p. 466-472.
173. Pavlishchuk VV. and Addison AW., *Conversion constants for redox potentials measured versus different reference electrodes in acetonitrile solutiosn at 25oC.* Inorganica Chimica Acta, 2000. **298**(1): p. 97-102.
174. Shavel A., Gaponik N., and Eychmuller A., *Covalent Linking of CdTe Nanocrystals to Amino- Functionalized Surfaces.* ChemPhysChem, 2005(6): p. 449-451.
175. Delvaux M. and Demoustier-Champagne S., *Immobilisation of glucose oxidase within metallic nanotubes arrays for application to enzyme biosensors.* Biosensors and Bioelectronics, 2003. **18**: p. 943-951.

176. Patel N., et al., *Immobilization of Protein Molecules onto Homogeneous and Mixed Carboxylate-Terminated Self-Assembled Monolayers.* Langmuir, 1997(13): p. 6485-6490.
177. Sun J-J., Fang H-Q., and Chen H-Y., *Immobilization of horseradish peroxidase on a self-assembled monolayer modified gold electrode for the detection of hydrogen peroxide.* Analyst, 1998(123): p. 1365-1366.
178. KISCC., *What is PM-IRRAS?*, N.W. University, Editor. 2009: Evanston, IL.
179. Zawisza I., et al., *Electrochemical, neutron reflectivity and in situ PM-FT-IRRAS studies of a monolayer of n-ocadecanol at a Au(111) electrode surface.* Electrochemica Acta, 2004. **49**: p. 3651-3664.
180. BioVision, *Quick Cell Proliferation Assay Kit II*, B.R. Products, Editor: 980 Linda Vista Avenue, Mountain View, CA.
181. Afara N., *Modification of a gold surface with mixed alkanethiol self-assembled monolayers and fibronectin: design of surfaces for controlled cell/surface interactions*, in *Chemical Engineering*. 2008, McGill: Montreal. p. 117.
182. Petrovic Z., *Modificiranje povrsina samoorganizirajucim monoslojevima organskih molekula*, in *Fakultet kumijkog inzenjerstva tehnologije*. 2008, Zagrebu.
183. Azzaroni O., Schilardi PL., and Salvarezza RC., *Metal electrodeposition on self-assembled monolayers: a versatile tool for pattern transfer on metal thin films.* Electrochemica Acta, 2003. **48**: p. 3107-3114.
184. Esplandiu M. and Hagenstrom H., *Functionalized self-assembled monolayers and their influence on silver electrodeposition.* Solid State Ionics 2002. **150**: p. 39-52.
185. Liakos IL., et al., *Comparative study of self-assembly of a range of monofunctional aliphatic molecules on magnetron-sputter aluminum.* Surface and Interface Analysis, 2004. **36**: p. 347-354.
186. Elzein T., Brogly M., and Schultz J., *Quantitative calculation of the orientation angles of adsorbed polyamides nanofilms.* Polymer 2003. **44**: p. 3649-3660.
187. Toda M., et al., *Complement activation on surfaces carrying amino groups.* Biomaterials, 2008. **29**: p. 407-417.
188. Frey B. and Corn R., *Covalent Attachment and Derivatization of Poly(L-lysine) Monolayers on Gold Surfaces As Characterized by Polarization-Modulation FT-IR Spectroscopy.* Anal. Chem. , 1996. **68**: p. 3187-3193.
189. Strathmann TJ. and Myneni SCB., *Speciation of aqueous Ni(II)-carboxylate and Ni(II)-fulvic acid solutions: Combined ATR-FTIR and XAFS analysis.* Geochemica et Cosmochmica Acta, 2004. **68**(17): p. 3441-3458.
190. Aramaki K. and Shimura T., *Self-assembled monolayers of carboxylate ions on passivated iron for preventing passive film breakdown.* Corrosion Science, 2003. **46**(2): p. 313-328.
191. Surble S., et al., *Synthesis of MIL-102, a Chromium Carboxylate Metal- Organic Framework, with Gas Sorption Analysis.* J Am Chem Soc., 2006. **128**: p. 14889-14896.
192. Jirousova J. and Davidek J., *Reactions of n-Hexanal with Glycine in Model Systems.* Z. Lebensm. Unters.-Forsch, 1975(157): p. 269-276.

193. Pradier C-M., et al., *Specific binding of avidin to biotin immobilised on modified gold surfaces Fourier transform infrared reflection absorption spectroscopy analysis.* Surface Science, 2002(502-503): p. 193-202.
194. Stuart B., ed. *Infrared Spectrsocpy: Fundmentals and Applications*. 2004, Jon Wiley & Sons Inc.: Chichester, West Sussex, England.
195. Yin M., et al., *Combinatorial coating of adhesive polypeptide and anti-CD34 antibody for improved endothelial cell adhesion and proliferation.* J Mater Sci: Mater Med, 2009(20): p. 1513-1523.
196. Cabaniss SE., Leenheer JA., and McVey IF., *Aqueous infrared carboxylate absorbances: Aliphatic di-acids.* Spectrochim Acta, 1998. **Part A 54**: p. 449-458.
197. Garcia AJ. and S. JE., *Distinct Activation States of a5b1 Integrin Show Differential Binding to RGD and Synergy Domains of Fibronectin* Biochemistry, 2002. **41**(29): p. 9063-9069.
198. Bergkvist M and Oscarsson S, *Surface-dependent conformations of human plasma fibronectin adsorbed to silica, mica and hydrophobic surfaces, studied with use of atomic force microscopy.* Journal Biomedical Materials Research, 2003(64A).

APPENDIX

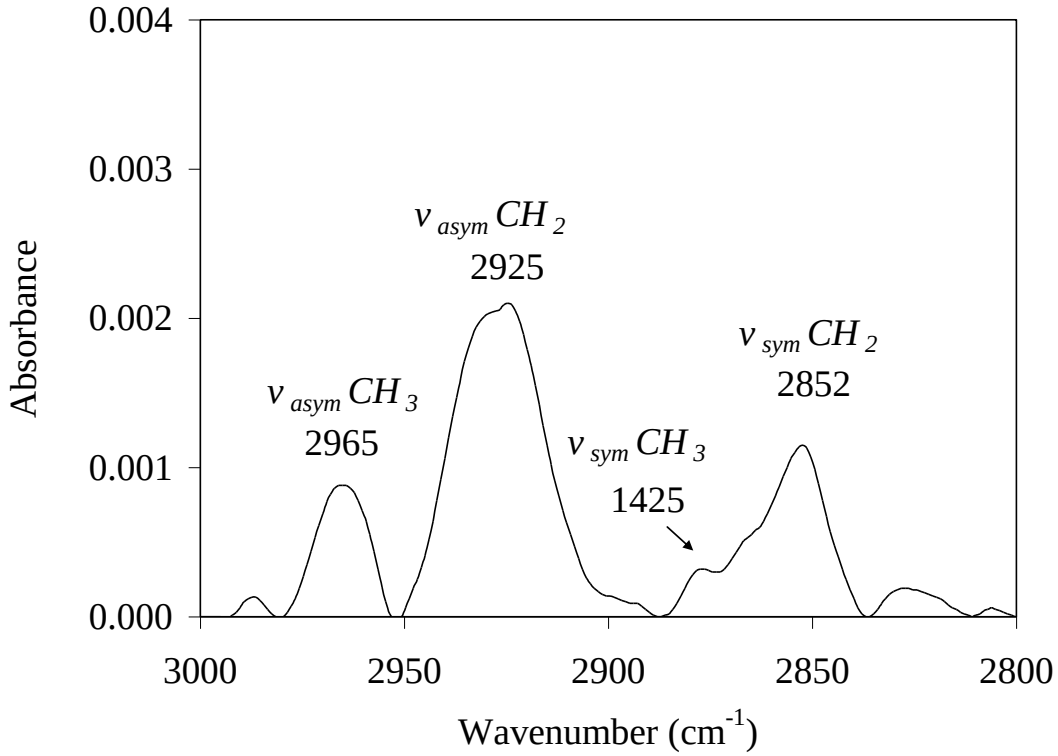

Figure A.1 PM-IRRAS spectra of palmitic acid SAM on 316L SS after 20 cycles of 0.1 mM palmitic acid in acetonitrile and 0.1 M tetrabutylammonium tetrafluoroborate, TBATFB (Shustak's Method)

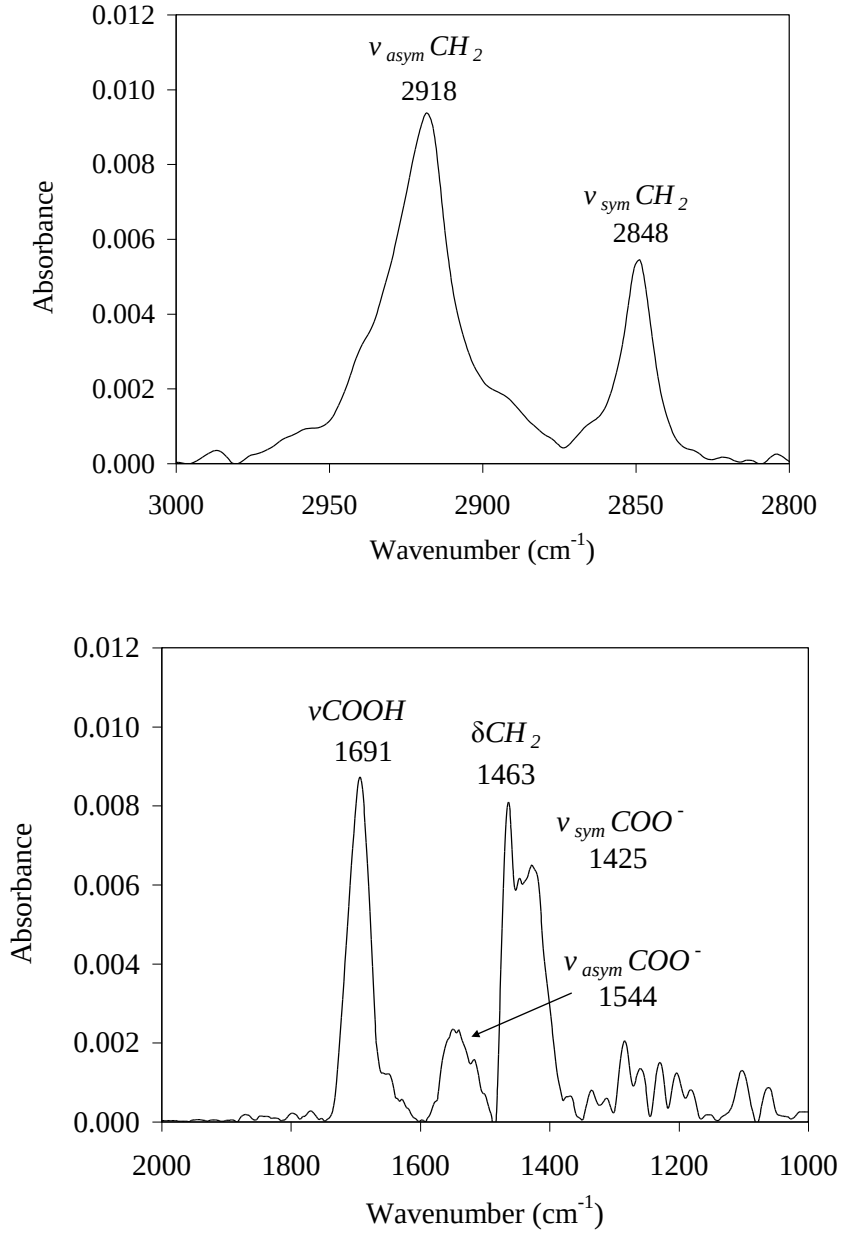

Figure A.2 PM-IRRAS of a 1 mM mercapto-undecanoic acid SAM on 316L stainless steel after 20 minutes at -1.2 V_{SCE} in 1.0 M $NaClO_4$ then immersion in the same solution for 24 hrs. This film has very aligned structure; however it was difficult to reproduce this film consistently. (top) 2900 cm^{-1} region (bottom) 1600 cm^{-1} region. (Ruan's method)

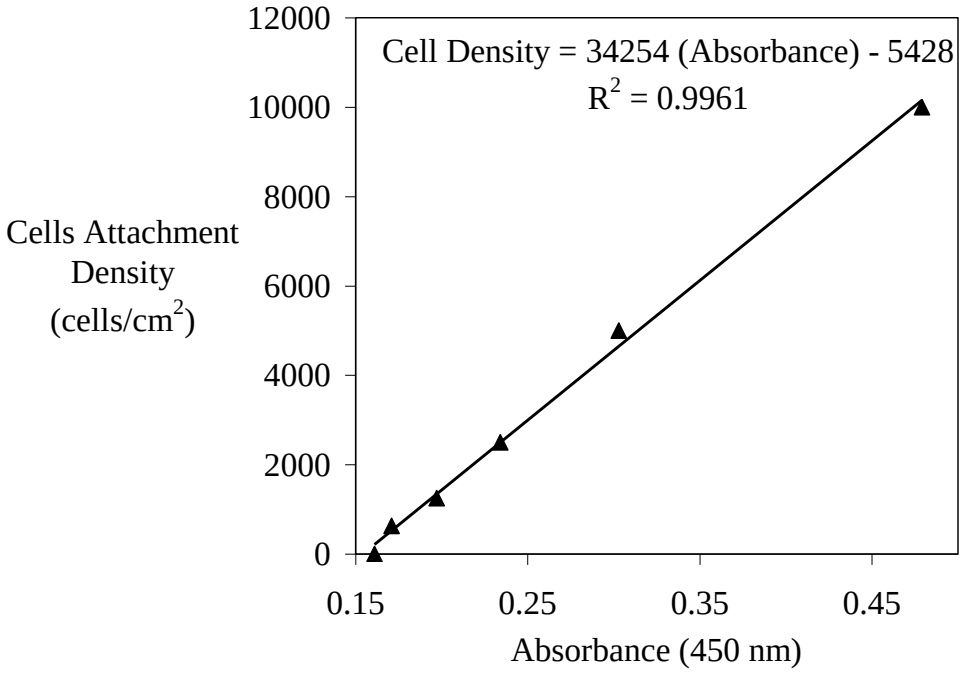

Figure A.3 Calibration curve, cell density (cells/cm^2) vs. absorbance at 250 nm